

## INFORMATION TO USERS

This manuscript has been reproduced from the microfilm master. UMI films the text directly from the original or copy submitted. Thus, some thesis and dissertation copies are in typewriter face, while others may be from any type of computer printer.

**The quality of this reproduction is dependent upon the quality of the copy submitted.** Broken or indistinct print, colored or poor quality illustrations and photographs, print bleedthrough, substandard margins, and improper alignment can adversely affect reproduction.

In the unlikely event that the author did not send UMI a complete manuscript and there are missing pages, these will be noted. Also, if unauthorized copyright material had to be removed, a note will indicate the deletion.

Oversize materials (e.g., maps, drawings, charts) are reproduced by sectioning the original, beginning at the upper left-hand corner and continuing from left to right in equal sections with small overlaps.

ProQuest Information and Learning  
300 North Zeeb Road, Ann Arbor, MI 48106-1346 USA  
800-521-0600

UMI<sup>®</sup>



CLARKSON UNIVERSITY

**Vibration Analysis and Reduction in  
Switched Reluctance Motors**

A Dissertation  
by  
**ZHANGJUN TANG**

Department of Electrical and Computer Engineering

Submitted in partial fulfillment of the requirements

for the degree of

**Doctor of Philosophy**

(Electrical and Computer Engineering)

September 2, 2002

Accepted by the Graduate School

9/03/02  
Date

A. Neil  
Dean

UMI Number: 3058571

UMI<sup>®</sup>

---

UMI Microform 3058571

Copyright 2002 by ProQuest Information and Learning Company.

All rights reserved. This microform edition is protected against  
unauthorized copying under Title 17, United States Code.

---

ProQuest Information and Learning Company  
300 North Zeeb Road  
P.O. Box 1346  
Ann Arbor, MI 48106-1346

The undersigned have examined the thesis/dissertation entitled **Vibration Analysis and Reduction in Switched Reluctance Motors** presented by **Mr. Zhangjun Tang**, a candidate for the degree of **Doctor of Philosophy** (Electrical and Computer Engineering), and hereby certify that it is worthy of acceptance.

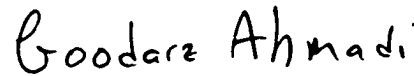
9/2/02

Date



Dr. Pragasen Pillay, Advisor

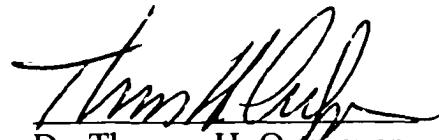
Examining Committee:



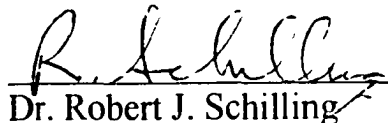
Dr. Goodarz Ahmadi



Dr. Ming-Cheng Cheng



Dr. Thomas H. Ortmeier



Dr. Robert J. Schilling

# Abstract

A detailed normal force vs. phase current and rotor position look-up table for a switched reluctance motor is constructed using Finite Element calculations. Subsequently, a normal force vs. stator acceleration transfer function is determined in this dissertation based on sinusoidal shaker excitation tests. A vibration prediction model of the SRM is built based on the transfer function and normal force look-up table. The model is verified by motor tests, which show acceptable accuracy. This now allows the possibility of using a transfer function model, such as this, for improved design of SRMs from vibration and acoustic noise points of view.

Simulation models based on Matlab/SIMULINK are developed in this dissertation, which can be used to simulate the transient phase current response, normal force and hence stator vibrations during accelerating, sudden change of torque and braking operations. An 8/6 SRM is used to experimentally validate the simulation results of both phase current and stator vibrations. The simulated phase currents are used in the previous described vibration prediction model to calculate the vibrations in different SRM operating conditions: constant speed running, accelerating, sudden change of torque and braking.

The effects of mountings on the vibrations in the SRM are investigated, using Finite Element calculations and impulse hammer test results. The calculated and test results are compared with each other to verify if the methods developed are valid in the research of SRM vibrations under various mounting conditions. Firstly, the finite element method is used to calculate the resonant frequencies for free vibrations and different mounting

conditions: free hanging, foot-mounted and face-mounted (with mounting feet and without mounting feet). Secondly, vibration tests are done with different mountings, and the results summarized in the form of mounting guidelines.

Some experimental methods other than sinusoidal shaker excitation tests are introduced in this dissertation, which include white noise shaker excitation tests and impulse hammer tests. The white noise shaker tests can be used to identify the mode shapes of the motor stator and locate the resonant frequencies. Practical measurements of mode shapes using this method are described. The 2<sup>nd</sup> and 3<sup>rd</sup> mode resonant frequencies and mode shapes for free vibration are measured and compared with FE results, which show good correlation. The impulse hammer tests are described and the advantages and disadvantages when compared with shaker excitation are discussed.

Techniques for noise reduction require knowledge of the modal frequencies, which depend on Young's modulus. This dissertation introduces a simple and nondestructive method for the measurement of Young's modulus, which is then used in a finite element program to determine the resonant frequencies of SRM stator vibration. The FE results are validated by impulse force hammer tests. Some other material properties like Poisson's ratio, winding effects and stator core lamination stacking factor are also examined.

## Acknowledgements

I wish to express my sincere gratitude to my advisor, Dr. Pragasen Pillay, for his valuable guidance, encouragement and continuous support during the course of completion of my Ph.D. program. My gratitude extends to Dr. Goodarz Ahmadi, Dr. Ming-Cheng Cheng, Dr. Thomas H. Ortmeyer, and Dr. Robert J. Schilling for their participation in serving on my examining committee and constructive suggestion.

My special thanks go to Dr. Avoki Omekanda of Delphi Research Labs for the financial and technical support of this research.

I would like to thank my friends in the Electric Machines and Power group at Clarkson University: Dr. Wei (William) Cai, Dr. Jianguo Liu, Dr. Kaiyan Jin, Mr. Liuping Chen, Mr. Yicheng Chen, Ms. Liang Ban and Mr. Naidu A. Singampalli for their friendship, which has made my time in the lab very enjoyable. Special thanks go to Mr. Timothy J. Humiston, who has always been around when I needed help. I have always enjoyed exchanging ideas with you.

I would also like to thank Dr. Cetin Cetinkaya and Mr. Chen Li from Mechanical Engineering Department of Clarkson University for their providing Young's Modulus measurement equipment.

Finally, my heartfelt thanks go to my wife Weixin (Wendy) Yan and my parents, sisters and brothers back in China, for their love and understanding, the encouragement and the sacrifice they have made during the entire course of my life. Without their support, nothing would have become true.



# Table of Contents

<b>List of Figures .....</b>	<b>xi</b>
<b>List of Tables.....</b>	<b>xvi</b>
<b>Chapter 1 Introduction .....</b>	<b>1</b>
1.1 Brief History of Switched Reluctance Motors .....	1
1.2 Operation Principles and Power Electronic Control of Switched Reluctance Motors.....	2
1.3 Advantages and Disadvantages of Switched Reluctance Motors.....	5
1.4 Current Research on Vibration and Acoustic Noise of Switched Reluctance Motors.....	7
1.5 Dissertation Overview .....	10
<b>Chapter 2 Prediction of Electromagnetic Forces in SRMs Operating at Steady State         and Transient Speeds .....</b>	<b>12</b>
2.1 Summary.....	12
2.2 Numerical Calculation of Normal Forces and Lookup Table Construction.....	13
2.2.1 Numerical Calculation of Normal Forces.....	13
2.2.2 Lookup Table Construction.....	16
2.3 Modeling and Simulation of Transient Vibrations.....	19
2.3.1 Introduction .....	19
2.3.2 SRM Dynamics .....	20

2.3.3 Simulation Models and Results .....	21
2.3.4 Experimental Validation.....	25
2.3.5 Braking and Sudden Change of Torque Operations.....	26
2.4 Radial Forces at Steady State Speed.....	29
2.4.1 Radial Force Calculated from Measured Phase Current .....	29
2.4.2 Radial Force Calculated from Simulated Phase Current.....	31
2.5 Radial Forces during Transients.....	32
2.6 Conclusions .....	33

### **Chapter 3 Transfer Function Identification, Vibration Prediction and Experimental**

<b>Validation .....</b>	<b>35</b>
3.1 Summary.....	35
3.2 Introduction .....	35
3.3 Transfer Function Determination .....	37
3.3.1 Sinusoidal Excitation Method .....	37
3.3.1.1 Frequency Response Function (FRF) of SRM Vibrations .....	37
3.3.1.2 Free Vibration of Viscous Damping — Damping Ratio	
Measurement .....	39
3.3.1.3 Test Setup and Procedure .....	44
3.3.1.4 Test Results .....	46
3.3.1.5 Damping Ratio Measurement.....	46
3.3.1.6 Gain Relative to the Second Mode.....	48
3.3.1.7 Final Transfer Function .....	49

3.3.2	Transfer Function Modeling: Simulation and Verification .....	50
3.3.2.1	Simulation.....	50
3.3.2.2	Verification .....	53
3.4	Vibration Prediction Model.....	55
3.5	Vibration Prediction Results.....	56
3.5.1	Running Motor Test and its Results .....	56
3.5.2	Transient Vibration Prediction .....	63
3.6	Conclusions .....	64
<b>Chapter 4</b>	<b>Analysis of Mounting Effects on Vibrations of SRMs .....</b>	<b>66</b>
4.1	Summary.....	66
4.2	Introduction .....	66
4.3	Finite Element Calculations .....	67
4.4	Vibration Tests under Different Mounting Conditions .....	76
4.4.1	Test Setup and Procedure .....	76
4.4.2	Test Results .....	77
4.5	Mounting Effects on Vibrations of SRMs.....	79
4.6	Conclusions .....	82
<b>Chapter 5</b>	<b>SRM Vibration Measurements .....</b>	<b>83</b>
5.1	Summary.....	83
5.2	Mode Shapes Identification with White Noise Shaker Tests .....	84
5.2.1	Test Setup .....	84

5.2.2 Test Results .....	86
5.3 Wide Band Excitation Experiments — Impulse Hammer Excitation Method.....	88
5.3.1 Introduction .....	88
5.3.2 Impulse Hammer Excitation Theory, Setup and Procedure .....	90
5.3.2.1 Hammer Excitation Theory .....	90
5.3.2.2 Hammer Excitation Setup.....	91
5.3.2.3 Hammer Excitation Procedure.....	92
5.3.3 Impulse Hammer Experimental Results .....	93
5.3.3.1 Impulse Force and Acceleration Response in the Time Domain .....	93
5.3.3.2 Impulse Force and Acceleration Response in the Frequency Domain .....	94
5.3.3.3 Transfer Function Calculation.....	95
5.3.4 Comparisons between Different Test Methods and FE Calculations.....	96
5.4 Measurement of Young’s Modulus for the Switched Reluctance Motor .....	97
5.4.1 Introduction .....	97
5.4.2 Development of the Method .....	98
5.4.3 Test Setup .....	100
5.4.4 Test Results .....	102
5.4.5 Correlation with FEA Results and Vibration Tests .....	104
5.4.5.1 Equivalent Mass Density Determination.....	104
5.4.5.2 FE Calculation Results .....	106
5.4.5.3 Experimental Validation.....	108
5.4.6 Comparisons.....	110

5.5 Conclusions .....	112
<b>Chapter 6 Conclusions and Future Work.....</b>	<b>113</b>
6.1 Conclusions .....	113
6.2 Future Work.....	115
6.2.1 Acoustic Noise Prediction and Measurement.....	115
6.2.2 Vibration Reduction Approaches in SRM and Design Sensitivities.....	117
<b>References.....</b>	<b>120</b>
<b>Appendices .....</b>	<b>128</b>
Appendix A Dimensions and Material Properties for the 8/6 4kW SRM.....	128
Appendix B ANSYS Code for Electromagnetic Analysis for the SRM .....	131
Appendix C Moment of Inertia Calculation for the 8/6 SRM Rotor.....	149
Appendix D Phase Winding Resistance Measurement for the 8/6 SRM.....	151
Appendix E Matlab Code Used in SRM Operation Simulation Model .....	152
Appendix F Equivalent Mass Density Calculation: Matlab Code.....	154
Appendix G ANSYS Code for Resonant Frequency Determination .....	155

# List of Figures

Fig.1.1 Schematic of Switched Reluctance Laminations All with Two Poles Per Phase.....	3
Fig.1.2 Power Converter for Single Phase and Two Phase Motors with the Asymmetric Half-bridge.....	4
Fig.2.1 Finite Element Meshing for Electromagnetic Analysis .....	14
Fig.2.2 Flux Linkage Plot.....	15
Fig.2.3 Force Plot .....	15,16
Fig.2.4 Plot of Normal Force vs. Phase Current & Rotor Position (0~25A, 0~30°).....	17
Fig.2.5 2-D View of Normal Force vs. Phase Current & Rotor Position.....	17,18
Fig.2.6 Normal Force vs. Phase Current & Rotor Position (0~25A, 0~60°).....	18
Fig.2.7 Simulation Model for SRM — Look-up Table Method .....	21,22
Fig.2.8 Flux Linkage vs. Phase Current and Rotor Position .....	22,23
Fig.2.9 Torque vs. Rotor Position and Phase Current .....	23
Fig.2.10 Simulated Transient Phase Current, Rotor Speed, Flux Linkage and Torque (Accelerating).....	24
Fig.2.11(a,b,c) Measured Transient Stator Vibration and Phase Current.....	25,26
Fig.2.12 Simulation Model for Sudden Load Change and Braking Operations .....	27
Fig.2.13 Simulation Results of Phase Current, Rotor Speed, Flux-linkage and Torque under Different Operating Conditions: Accelerating, Sudden Change of Load and Braking .....	28

Fig.2.14 Measured SRM Phase Current at 1450RPM.....	29
Fig.2.15 Normal Force Calculated from Look-up Table.....	30
Fig.2.16 FFT Analysis Results of Normal Force .....	30
Fig.2.17 Simulated Phase Current and Rotor Position (start-up) .....	31
Fig.2.18 Simulated Normal Force and its FFT (start-up).....	32
Fig.2.19 Simulated Radial Force and its FFT (start-up, sudden change of load and braking).....	33
Fig.3.1 Flow Chart of Vibration Prediction Modeling and Verification.....	36
Fig.3.2 A Spring-mass-damper System.....	38
Fig.3.3 Test Setup of Sinusoidal Excitation Method.....	45
Fig.3.4 Locations of Force Transducer and Accelerometers.....	45
Fig.3.5 Measured Force and Acceleration Signals and their Magnitude Spectra.....	47
Fig.3.6 Damped Response at the Resonant Frequency .....	48
Fig.3.7 Simulation Block.....	50
Fig.3.8 Frequency and Phase Responses of the Transfer Function.....	51
Fig.3.9 Simulated Responses of the Transfer Function at Resonant, Low and High Frequencies.....	52,53
Fig.3.10 Measured Low Frequency and High Frequency Responses .....	54
Fig.3.11 Transient Vibration Simulation from Normal Force to Stator Acceleration...55	
Fig.3.12 Test Setup of Running SRM Acceleration Experiment .....	57
Fig.3.13 Measured Acceleration Response in Time & Frequency Domains at a Speed of 1450RPM.....	58

Fig.3.14 Input Normal Force and Output Acceleration Using the Vibration Prediction Model and Measured Current .....	58
Fig.3.15 Measured Transient Stator Vibration and Phase Current during Power-off...	59
Fig.3.16 3-D View of Acceleration Spectra at Different Speeds .....	60
Fig.3.17 Speed-Magnitude View of Acceleration Responses .....	61
Fig.3.18 Frequency-Magnitude View of Acceleration Responses .....	62
Fig.3.19 Comparison of Measured and Simulated Stator Vibration during Accelerating.....	64
Fig.3.20 Simulated Stator Acceleration vs. Motor Speed .....	64
Fig.4.1 Free Vibration FE Model and Mode Shapes.....	68
Fig.4.2 Foot-mounted FE Model and Mode Shapes.....	69,70
Fig.4.3 Face-mounted FE Model and Mode Shapes (with mounting feet) .....	71,72
Fig.4.4 Face-mounted FE Model and Mode Shapes (without mounting feet) .....	73
Fig.4.5 Some Complicated Mode Shapes.....	74,75
Fig.4.6 Test Setup of Impulse Force Hammer Excitation Experiment .....	76
Fig.4.7 Impulse Force and Acceleration Response (free vibration) .....	77
Fig.4.8 Impulse Force and Acceleration Response (foot-mounted without rubber cushions).....	78
Fig.4.9 Impulse Force and Acceleration Response (foot-mounted with rubber cushions).....	79
Fig.4.10 Effect of Cushions on the Vibration.....	81



Fig.5.1 White Noise Shaker Excitation Experiment .....	85
Fig.5.2 Force Spectrum, Acceleration Spectrum and Transfer Function .....	86
Fig.5.3 Magnitude Responses at Different Points at the Resonant Frequency of 1346Hz .....	87
Fig.5.4 Comparison of Ideal and Measured Mode Shapes.....	87
Fig.5.5 Modal Hammer Impact Force Waveform and Spectrum .....	89
Fig.5.6 Block Diagram of Modal Hammer Excitation Experiment .....	92
Fig.5.7 Measured Time Domain Waveforms of Force and Acceleration .....	94
Fig.5.8 Frequency Domain Analysis of Measured Force and Acceleration.....	95
Fig.5.9 Transfer Function Calculation of Force to Acceleration.....	96
Fig.5.10 Block Diagram of Ultrasonic Method.....	99
Fig.5.11 Stator of the Prototype SRM.....	101
Fig.5.12 Young's Modulus Measurement.....	101
Fig.5.13 Travel Time of Ultrasonic Signal inside the Stator Core Lamination .....	103
Fig.5.14 One Turn of the Coil .....	106
Fig.5.15 FE Basic Area, Mesh and 2 <sup>nd</sup> Mode Shapes (with measured Young's modulus).....	107
Fig. 5.16 Force Hammer Test Result: Force Impulse and Stator Acceleration.....	109
Fig.6.1 Flow Chart of SRM Acoustic Noise Analysis .....	116
Fig.A.1 Stator Dimensions of a 4kW SRM with 8/6 Poles and 4 Phases .....	128
Fig.A.2 Rotor Dimensions of a 4kW SRM with 8/6 Poles and 4 Phases.....	129

Fig.C.1 Moment of Inertia Calculation .....	149
---	-----

## List of Tables

Table 3.1 Parameters for the 2 <sup>nd</sup> and 3 <sup>rd</sup> Order Vibration Transfer Functions .....	50
Table 4.1 Comparisons of FE Results under Different Mounting Conditions .....	75
Table 4.2 Comparisons of FE and Experimental Results.....	79
Table 5.1 Comparisons of Different Test Methods .....	96
Table 5.2 Measured Young's Modulus .....	102
Table 5.3 Effect of Young's Modulus on the Resonant Frequencies of the 2 <sup>nd</sup> Mode Shapes.....	108
Table D.1 Measurement of Phase Winding Resistance.....	151

# Chapter 1

## Introduction

### 1.1 Brief History of Switched Reluctance Motors

In a magnetic circuit, a magnetically salient rotor that is free to move, will move to a position of minimum reluctance to the flux flow. This phenomenon has been known ever since the first experiments on electromagnetism. The operating principle of Switched Reluctance Motors (SRMs) is based on that principle.

The first relevant invention of the SRM can be traced to 1838, with W. H. Taylor's patent of an "Electromagnetic Engine" in the United States. The engine was composed of a wooden wheel, seven pieces of soft iron equally spaced around the periphery were mounted on its surface. The wheel rotated freely in a framework mounted with four electromagnets. The electromagnets were connected to a battery through a mechanical switching system on the shaft of the wheel, so that excitation of an electromagnet would attract the closest piece of soft iron, driving the wheel and energizing the next electromagnet in sequence to continue the rotation. This "Engine" and other subsequent similar inventions were soon replaced by the DC machine and the AC induction machine.

Almost 140 years later, with the development of power electronics technology, the electronic switch could replace the original mechanical one of the early reluctance motors. Patented in 1972 [1], the Switched Reluctance Motor did not become prominent in research and development until after Lawrenson's seminal paper of 1980 [2]. In the

early 80's, many companies and groups exploited commercial interests, among them the best known is *TASC Drives*, who manufactured a range of general-purpose variable-speed switched reluctance drives for industrial applications. In 1993 T.J.E. Miller from Glasgow University, UK, published the first complete book of Switched Reluctance Motor design "Switched Reluctance Motors and their Control" [3]. He is also the founder of SRM design software PC-SRD.

## **1.2 Operation Principles and Power Electronic Control of Switched Reluctance Motors**

Schematic representations of the lamination patterns of single phase, two phase and three phase switched reluctance motors are shown in Fig.1.1. In each of the motors shown in Fig.1.1 a coil is wound around each stator pole and is connected, usually in series with the coil on the diametrically opposite stator pole to form a phase winding. The reluctance of the flux path between the two diametrically opposite stator poles varies as a pair of rotor poles rotates into and out of alignment. Since inductance is inversely proportional to reluctance, the inductance of a phase winding is a maximum when the rotor is in the aligned position and a minimum when the rotor is in the unaligned position. A pulse of positive torque is produced if current flows in a phase winding as the inductance of that phase winding is increasing. A negative torque contribution is avoided if the current is reduced to zero before the inductance starts to decrease again. The rotor speed can be varied by changing the frequency of the phase current pulses while retaining synchronism with the rotor position.

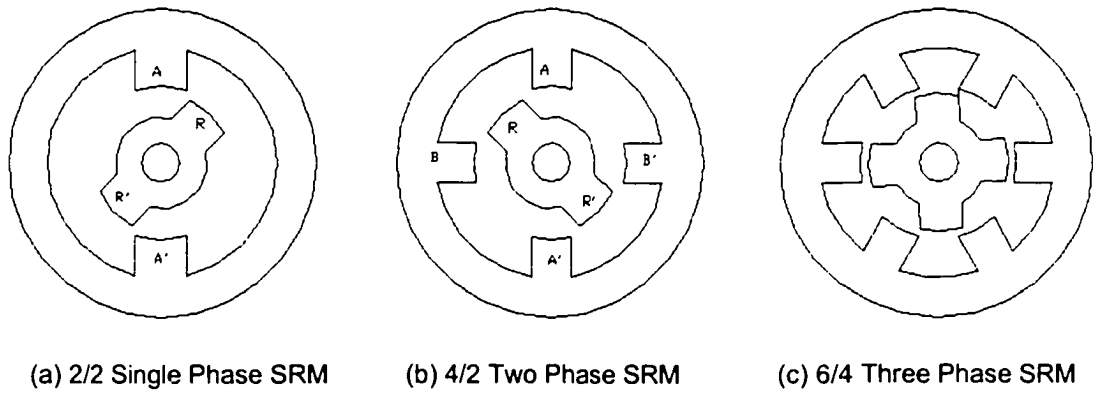


Fig.1.1 Schematic of Switched Reluctance Laminations All with Two Poles Per Phase

The absence of permanent magnets or coils on the rotor means that torque is produced purely by the saliency of the rotor laminations. The torque produced is the same irrespective of the direction of the flux through the rotor, and hence the direction of current flow in the stator phase windings is not important. The need for unipolar phase current in the reluctance motor results in simpler and more reliable power converter circuits.

Unlike induction motors or DC motors the reluctance motor cannot run directly from an AC or DC supply. A certain amount of control and power electronics must be present. The power converter, which is the electronic commutator, controls the phase currents to produce continuous motion. The control circuit monitors the current and position feedback to produce the correct switching signals for the power converter to match the demands placed on the drive by the user. The purpose of the power converter circuit is to provide some means of increasing and decreasing the supply of current to the phase winding. Many different power converter circuits have been proposed for the switched reluctance motor [6-13]. By far the most common is the asymmetric half-bridge, shown in Fig.1.2 for a single-phase and a two-phase motor. Each asymmetric

half-bridge has three main modes of operation. The first, a positive voltage loop, occurs when both switching devices associated with a phase winding are turned on. The supply voltage is connected across the phase winding and the current in the phase winding increases rapidly, supplying energy to the motor. The second mode of operation is a zero voltage loop. This occurs if either of the two switching devices is turned off while current is flowing in a phase winding. In this case the current continues to flow through the other switching device and one diode. Energy is either taken from or returned to the DC supply. The voltage across the phase winding during this time is equal to the sum of the on-state voltages of the two semiconductor devices. This voltage is very small compared to the supply voltage and so the current in the phase winding decays very slowly.

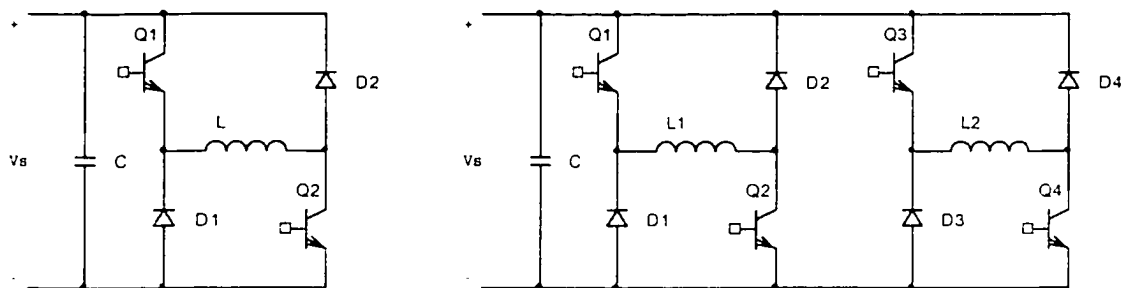


Fig.1.2 Power Converter for Single Phase and Two Phase Motors with the Asymmetric Half-bridge

The final mode of operation is a negative voltage loop. Both the switching devices are turned off. The current is forced to flow through both freewheeling diodes. The current in the phase winding decreases rapidly as energy is returned from the motor to the supply. The asymmetric half-bridge thus offers three very flexible modes for current control. The zero voltage loops is very important in minimizing the current ripple at any given switching frequency. The zero voltage loops also tend to reduce the power flow to and from the motor during chopping by providing a path for motor current to flow

without either taking energy from or returning it to the supply capacitors. The major advantage with this circuit is that all the available supply voltage can be used to control the current in the phase windings. As each phase winding is connected to its own asymmetric half-bridge there is no restriction on the number of phase windings. However, as there are two switches per phase winding it is best suited to motors with low phase numbers.

### **1.3 Advantages and Disadvantages of Switched Reluctance Motors [39,55]**

The difficulty in understanding the switched reluctance motor stems from its *Double Saliency*: neither the rotor nor the stator has a smooth cylindrical surface at the air-gap, but both members have salient poles or teeth. Both the stator and the rotor are stacked with laminations. There are neither windings nor permanent magnets on the rotor. A stator phase consists of concentrated windings on opposite poles. Because of these features, the switched reluctance motor has the following advantages and disadvantages.

Advantages:

- (1) There is no winding on the rotor, hence a lower manufacturing cost; the motor can run at very high speeds without rotor mechanical distortion; easy to accelerate and decelerate because of lower moment of inertia.
- (2) The concentrated windings can be easily mounted onto salient stator poles; the heating due to the copper losses in the stator windings is easy to remove because of the cooling effects of the salient structure; there is no permanent magnet on the rotor hence a higher temperature rise is allowed.



- (3) The output torque and efficiency of the SRM are high over a wide speed and power range, and starting torque is also high; easy to control; can operate at regenerating state.
- (4) The brushless structure of SRMs leads to applications requiring explosion proof equipment; can be used in dangerous environments.
- (5) The torque is independent of the direction of the phase currents. The drive can be operated in all four quadrants by controlling the turn-on, turn-off and conduction angles. It is possible to reduce the number of power switches hence lower the price of the drive system. The main power electronic switches can be less than 2 per phase, even only one per phase.
- (6) The open-circuit voltage of the phase windings is negligible; shoot-through problems can be avoided, which raises the fault tolerance of SRM drives.

Disadvantages:

- (1) Torque ripple is high (typically  $\pm 15\%$ ) due to the doubly salient structure and the pulsed current excitation with forced commutations.
- (2) The variation of the strong radial electromagnetic forces between stator and rotor produces a large vibration, which results in serious acoustic noise at the moment of switch-off. Other factors such as the blade effects of the salient rotor also results in vibration and acoustic noise.
- (3) Unlike other conventional motors, the SRM cannot run without a power electronic converter, and the drive requires rotor position information. One or more large capacitors are essential for a stable DC link.
- (4) The number of terminals increases with an increase on the phase number of the

SRM, resulting in more cables.

#### **1.4 Current Research on Vibration and Acoustic Noise of Switched Reluctance Motors**

During the 1980's a small number of commercial SRM products — and an even larger number of laboratory prototypes — gave rise to a widespread perception that the SRM is “inherently noisy”. Along with this perception was the related impression that the SRM has inherently high torque ripple.

The first systematic study of SRM noise was published by Cameron [21]. A series of carefully designed experiments were developed and one source is determined to be dominant: the ovalizing deformation of the stator due to its radial magnetic attraction to the rotor, in particular when the frequency of deformation coincides with that of a natural mechanical resonance of the stator. Since then, more and more attention has been paid to the vibration issues in SRMs, including the origin of vibration, vibration calculation methods, vibration tests and the *experimental determination of acoustic noise*, noise reduction techniques, etc.

It is essential to determine the resonant frequencies of the motor stator to determine its noise performance. The resonant frequencies can be obtained by analytical calculation, numerical computation (finite element method) and/or experimental techniques. Analytical calculation is the fastest way. Contributions for this include Girgis and Verma [26], who developed a general frequency equation for all modes of vibration. Cai, Pillay and Omekanda [34] developed two simplified formulae for the 2<sup>nd</sup> order resonant frequency and one more sophisticated formula for higher orders, the effect

of the length of the stator lamination was also considered. C.Yongxiao *et al.* [41] presented a method of calculating resonant frequencies of SRM stators based on energy principles, good agreement was obtained by comparing with experimental results.

The Finite Element method has been widely used in the study of SRMs, including modeling of electromagnetic characteristics [24][42] and the calculation of vibration [23][31][32][43]. Besbes *et al.* [44] studied the influence of the stator geometry upon the vibratory behavior of the SRM, which showed the importance of stator yoke thickness on vibration reduction. Cai, Pillay and Reichert [46] summarized the theory and practice of the electromagnetic force calculations in SRMs, including electric torque and radial force calculations. A 2-D FE model is built in this dissertation to calculate the radial force between rotor and stator poles. Several 3-D models are built for the resonant frequency calculations for two motors, one 5hp 8/6 SRM and one square motor designed for use in vehicle braking. The FE calculation of the electromagnetic force in SRMs is not fundamentally different to other motors. The FE models for vibration calculations are mostly borrowed from those of mechanical engineering. Thus one factor is neglected: nobody has ever considered the special structure of motor laminations, which has a different Young's modulus value from steel because of its laminated feature. This will be discussed in the dissertation.

Experimental measurements of vibrations are essential for the research of SRM vibrations. Sinusoidal shaker excitation [27][28][35] and impulse force hammer excitation [43] have been tried by different researchers.

Cai, Pillay and Tang [47] investigated the impact of stator windings and end-bells on resonant frequencies and mode shapes of SRMs. The Influence of mounting on the

vibration of motors other than SRMs has also been investigated [48]. However its effects on the vibration of SRMs have never been discussed, although it is a very important issue in industrial applications. This will be addressed in the dissertation.

The accurate prediction of vibration in SRMs is essential for the designing of quieter motors. Anwar and Husain [45] presented an analytical method for calculating the radial force and predicting the acoustic noise in SRMs. A more sophisticated prediction model is introduced in this dissertation, which will make it possible for SRM designers to improve their designs.

The simulation of SRM operation, like phase current, can be seen in several papers [2][37][38]. PSpice and Matlab/SIMULINK have been used, with acceptable results. Both linear and non-linear models were used in these papers. The phase current waveform after reaching steady state as well as the start-up transient speed were shown in these papers, while the transient phase current was not described, which will be done in this dissertation. The operation of braking (regenerating) will also be introduced. The normal force between rotor pole and stator pole caused by transient currents is then calculated, hence the transient vibration is predicted.

The approaches to solve the vibration and noise problem in SRMs are clearly far from exhausted. There is nothing to prove that the SRM cannot be made to have acceptably smooth torque and quiet [23]. This dissertation will investigate further the vibration and acoustic noise problem in Switched Reluctance Motors.

## 1.5 Dissertation Overview

This dissertation focuses on the analysis and reduction of vibration and hence noise in switched reluctance motors. It provides some guidelines for motor designers from vibration and acoustic noise points of view. The goal is to provide practical ways for the motor designers to reduce the vibration and acoustic noise in SRMs during the design process, which will be very important for the industrial commercialization of SRMs.

1. A detailed normal force vs. phase current and rotor position look-up table is constructed using Finite Element calculations. A normal force vs. stator acceleration transfer function is determined in this dissertation based on sinusoidal shaker excitation tests. A vibration prediction model of the SRM is built based on the transfer function and normal force look-up table. The model is then verified by a running motor test, which shows good accuracy. This now allows the possibility of using a transfer function model such as this for improved design of SRMs from vibration and acoustic noise points of view.
2. Simulation models based on Matlab/SIMULINK are developed in this dissertation, which can be used to simulate the transient phase current response, normal force and hence stator vibrations during accelerating, sudden changes of torque and also braking. An 8/6 SRM is used to experimentally validate the simulation results of both phase current and stator vibrations.
3. The effects of mountings on the vibrations in the SRM are investigated, using Finite Element calculations and impulse hammer test results. The calculated and test results are compared with each other to verify if the methods are valid in the research of SRM vibrations under various mounting conditions. Firstly,

the finite element method is used to calculate the resonant frequencies for free vibrations and different mounting conditions. Secondly, vibration tests are done with different mountings: free hanging, foot-mounted on a plate with rubber cushions and foot-mounted on a plate without rubber cushions, and the results summarized in the form of guidelines for mountings.

4. Some experimental methods other than sinusoidal shaker excitation tests are introduced in this dissertation, which include white noise shaker excitation tests and impulse hammer tests. The white noise shaker tests can be used to identify the mode shapes of the motor stator and locate the resonant frequencies. Practical measurements of mode shapes are also introduced using white noise shaker excitation. The 2<sup>nd</sup> and 3<sup>rd</sup> mode resonant frequencies and mode shapes for free vibration are measured and compared with FE results. The impulse hammer tests are described, the advantages and disadvantages compared with shaker excitation are discussed. Techniques for noise reduction require knowledge of the modal frequencies, which depend on Young's modulus. This dissertation introduces a simple and nondestructive method for the measurement of Young's modulus, which is then used in a finite element program to determine the resonant frequencies of SRM stator vibration. The FE results are validated by impulse force hammer tests, which show good accuracy.
5. Some conclusions are drawn with a summary of contributions in the dissertation. Suggestions for future work are made.

## Chapter 2

# Prediction of Electromagnetic Forces in SRMs Operating at Steady State and Transient Speeds

### 2.1 Summary

The normal force between SRM stator poles and rotor poles causes an attraction and thus an ovalization of the stator, which is the main cause of SRM vibration and acoustic noise [21]. The normal force in the SRM is very difficult to measure from experiment. The normal force cannot be easily and accurately modeled mathematically because of the double saliency of the stator and rotor poles, as well as the highly saturated nature of the flux density during SRM operations. Hence a Finite Element package (ANSYS) is used in this chapter to calculate the normal force in SRMs.

Simulation models based on Matlab/SIMULINK are developed in this chapter, which can be used to simulate the transient phase current response, normal force and hence stator vibrations at start-up, sudden change of torque and braking operations. An 8/6 SRM is used to experimentally validate the simulation results of both phase current and stator vibrations, with good accuracy.

## **2.2 Numerical Calculation of Normal Forces and Look-up Table Construction**

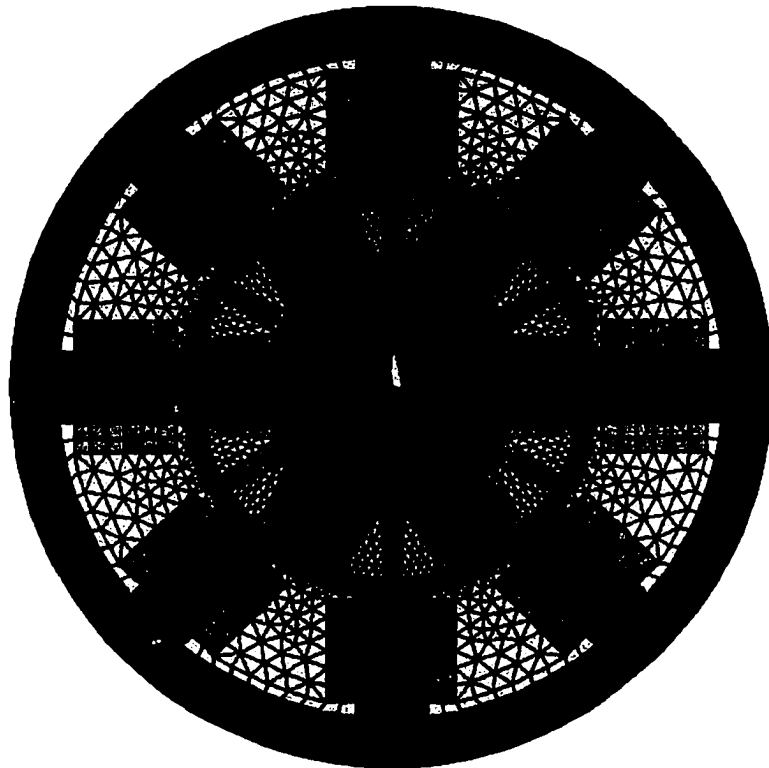
### **2.2.1 Numerical Calculation of Normal Forces**

A 2-D ANSYS model is used for the electromagnetic finite element analysis. A 4kW 8/6 SRM with four phases is used in this dissertation. The mechanical dimensions and material properties are listed in Appendix A. The ANSYS code is listed in Appendix B. Fig.2.1 shows the meshing of the elements for the model. Fig.2.1(a) is the meshing for the entire model and (b) is the zoomed view of the air gap area.

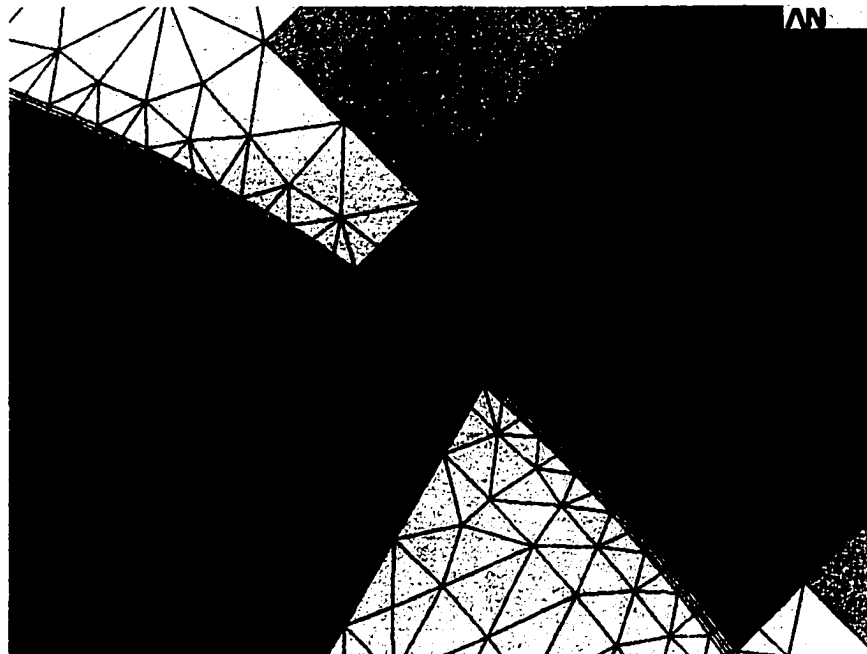
Shown in Fig.2.2 is the flux linkage plot of the motor (rotor is  $5^\circ$  away from the aligned position). Static force calculations are carried out for 31 positions from aligned to unaligned (from  $0^\circ$  to  $30^\circ$ , in steps of  $1^\circ$ ), and at each position, 25 different currents (from 1A to 25A, in steps of 1A) are applied to the windings. At each position and current, the normal force and tangential force (which leads to torque) are calculated and a table of force vs. rotor position and phase current is constructed.

Fig.2.3 shows the force plot of the SRM. Fig.2.3(a) shows the force plot of the entire motor and Fig.2.3(b) is the zoomed view of the pole area. It is very clear that the normal force dominates the tangential force, and the force concentrates on the stator pole – rotor pole area.





(a) Meshing of the Model



(b) Zoomed View of Air Gap Area

Fig.2.1 Finite Element Meshing for Electromagnetic Analysis

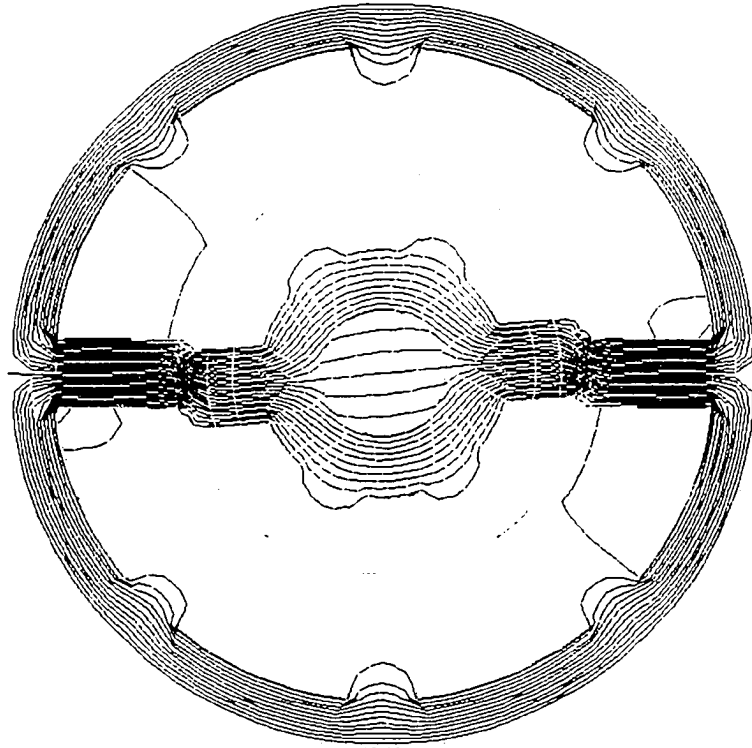
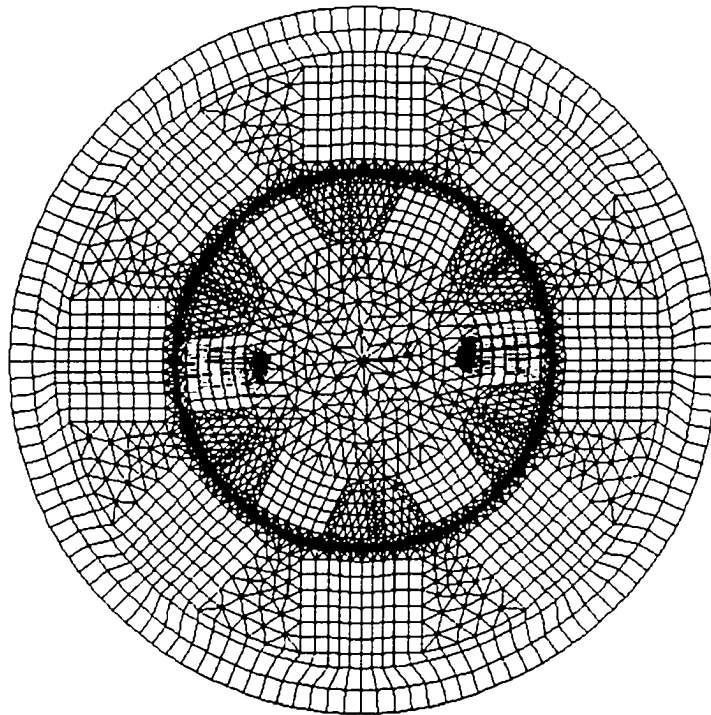
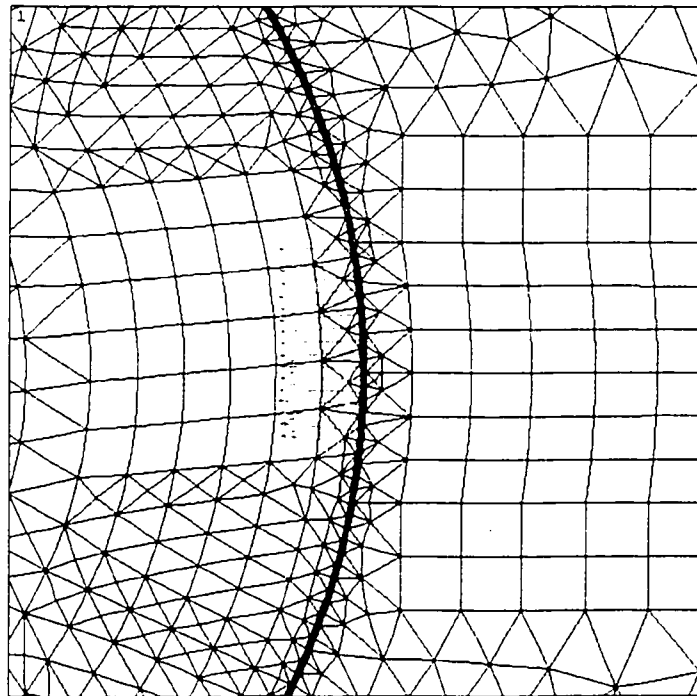


Fig.2.2 Flux Linkage Plot



(a) Force Plot of the Entire Motor



(b) Zoomed View of Force Acting in the Pole Area

Fig.2.3 Force Plot

### 2.2.2 Look-up Table Construction

Fig.2.4 is a plot of the Normal Force vs. Phase Current & Rotor Position, and Fig.2.5 is a 2-D View of this table. The force table is expanded from  $30^\circ$  to  $60^\circ$ , as shown in Fig.2.6.

This Normal Force vs. Phase Current & Rotor Position look-up table can now be used to obtain the actual normal force acting on the stator, for an arbitrary phase current waveform, once turn-on and turn-off angles are known. This will be used to determine the force harmonics and hence to calculate the vibration resulting from the normal forces.

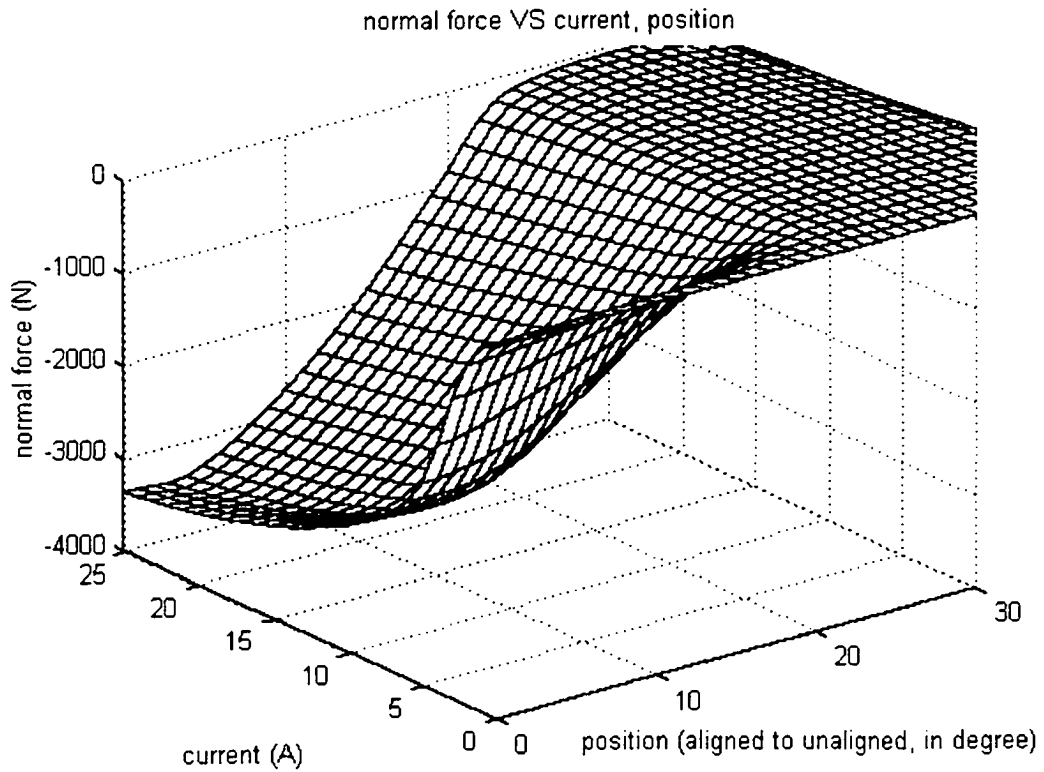
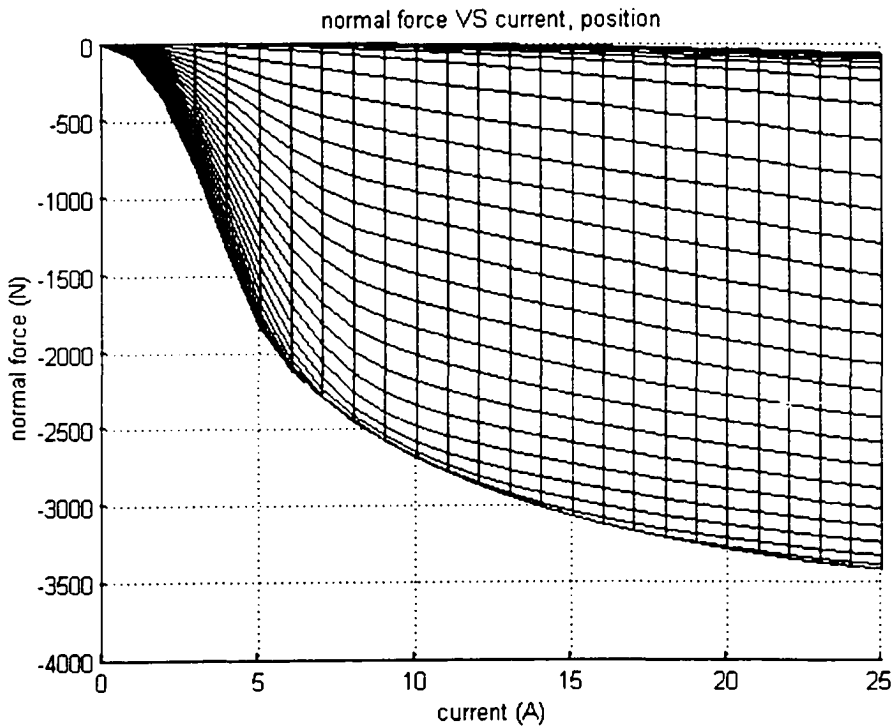


Fig.2.4 Plot of Normal Force vs. Phase Current & Rotor Position (0~25A, 0~30°)



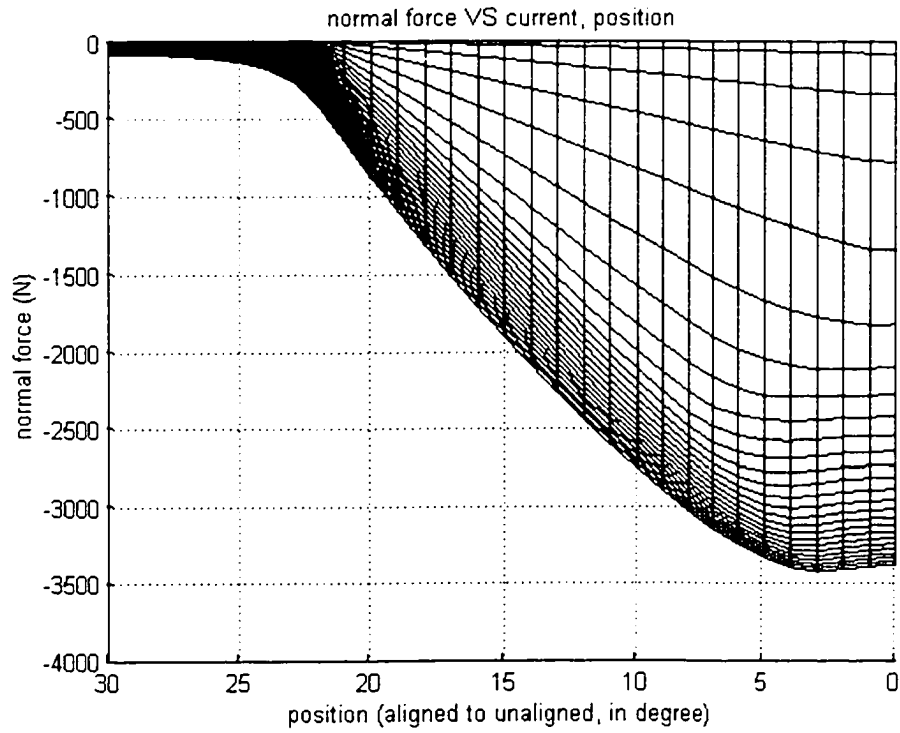


Fig.2.5 2-D View of Normal Force vs. Phase Current & Rotor Position

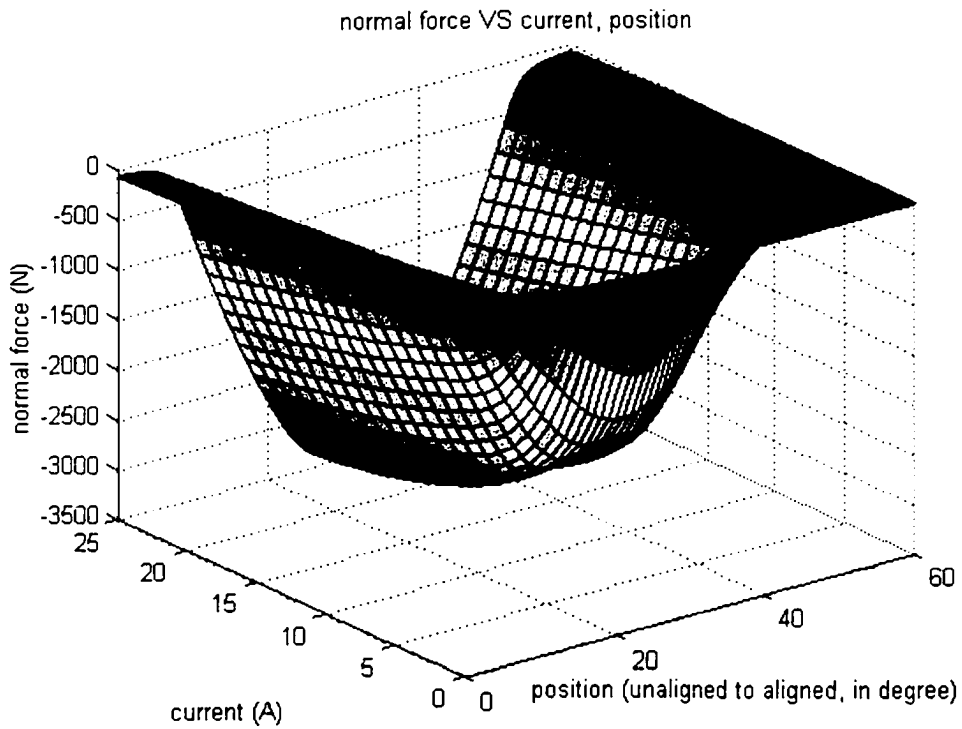


Fig.2.6 Normal Force vs. Phase Current & Rotor Position (0~25A, 0~60°)

## **2.3 Modeling and Simulation of Transient Vibrations**

### **2.3.1 Introduction**

The subject of vibrations in Switched Reluctance Motors has attracted recent attention including vibration tests [21][35], modal analysis [31], resonant frequency calculation [34], etc. However the transient vibration during start-up, braking or sudden change of torque remains unknown. In some circumstances, the transient vibration is more important than the steady state value, because the SRM is running in the transient state most of the time, for example with the application of the SRM as a brake motor in the automobile. So it is very important to analyze the transient vibration of SRMs as well as the constant speed vibrations.

The simulation of SRM operation, like phase current, can be seen in several papers [2][37][38]. PSpice and Matlab/SIMULINK have been used, with acceptable results. Both linear and non-linear models were used in those papers. The phase current waveform after reaching steady state as well as during start-up were shown. The operation of braking (regenerating) will also be introduced. The normal force between rotor pole and stator pole caused by transient currents is then calculated, hence the transient vibration is predicted.

An 8/6 5hp SRM is then used for experimental validation of the simulation results. Both phase current and stator vibration are measured, with acceptable accuracy.

### 2.3.2 SRM Dynamics

The governing equations of the SRM are described below.

Electromagnetic equation:

$$\frac{d\Psi}{dt} = v - Ri \quad (2-1)$$

Where  $\psi$  is the flux linked by the phase winding,  $v$  is the terminal voltage,  $i$  and  $R$  are phase current and phase winding resistance respectively.

Mechanical equation:

$$T = T_l + k_\omega \omega + J \frac{d\omega}{dt} \quad (2-2)$$

$$\omega = \frac{d\theta}{dt} \quad (2-3)$$

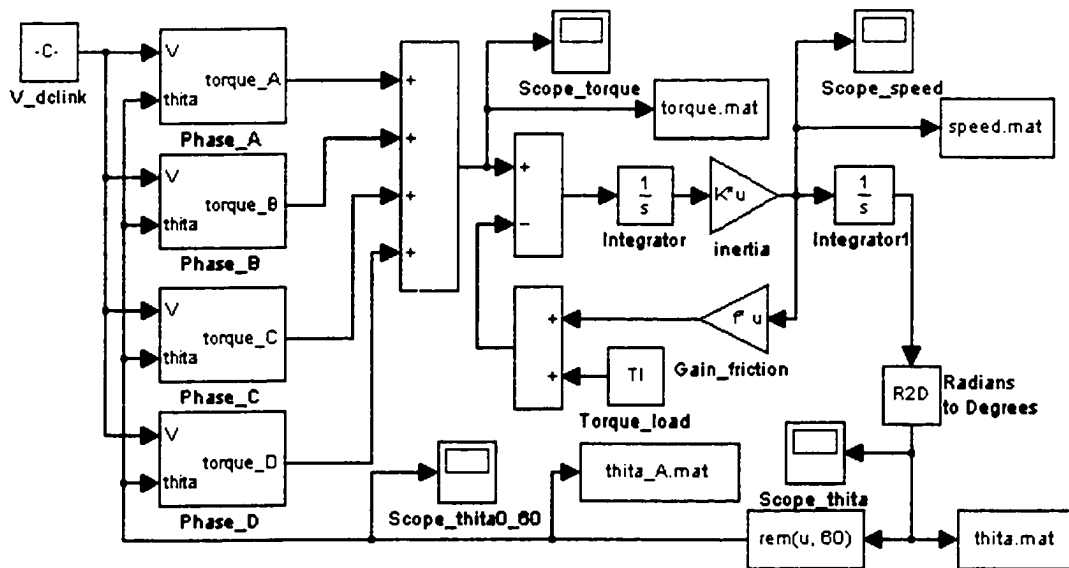
Where  $T$  is the electric torque,  $T_l$  is the load torque,  $k_\omega$  is the machine friction coefficient,  $J$  is the moment of inertia of the rotor,  $\omega$  is the rotor speed.

The moment of inertia  $J$  of the rotor is calculated in Appendix C, with  $J = 0.00522(kg \cdot m^2)$ . The phase winding resistance  $R$  is measured, which is shown in Appendix D, with  $R=0.741316(\Omega)$ .

### 2.3.3 Simulation Models and Results

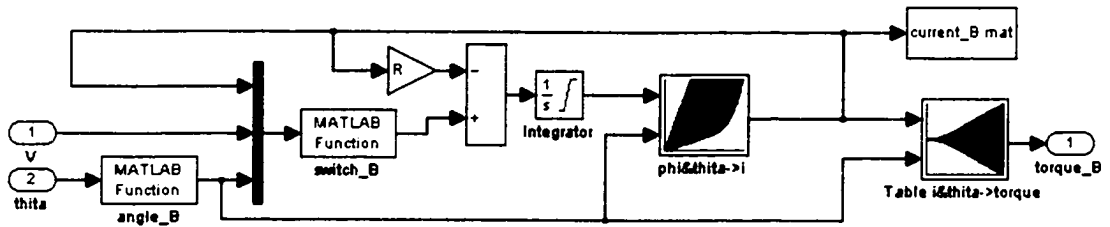
Instead of using a linear model of the SRM, two look-up tables are used in this simulation. One is flux linkage vs. rotor position and phase current look-up table; the other is phase current and rotor position vs. torque look-up table. The simulation model is shown in Fig.2.7. Fig.2.7(a) shows the entire model, (b) is the sub-system for each phase, which includes two look-up tables and is used to calculate the electric torque. Matlab codes for “Matlab Function angle\_B” and “Matlab Function switch\_B” included in Fig.2.7(b) are listed in Appendix E.

The data for the first look-up table can be from FEM calculations (if the motor is in the design stage), or from experimental test results (if the prototype exists). In this dissertation the data is from experimental tests. Fig.2.8 shows the flux linkage vs. phase current and rotor position table.



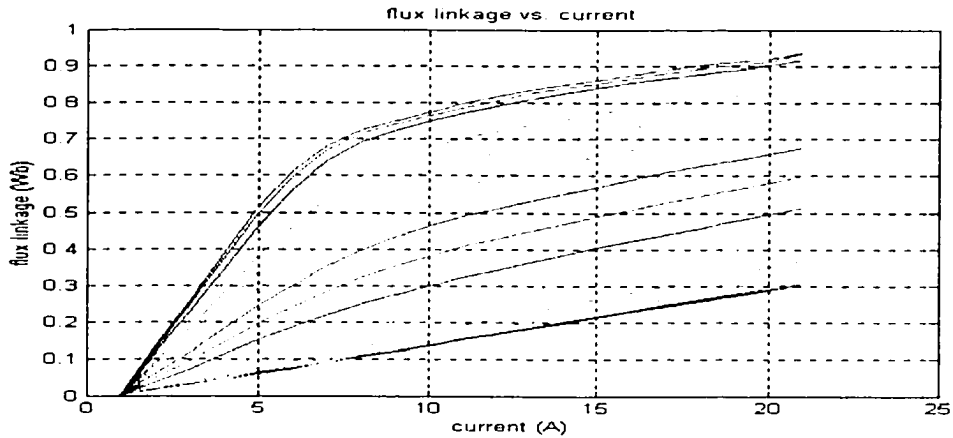
(a) Entire Model



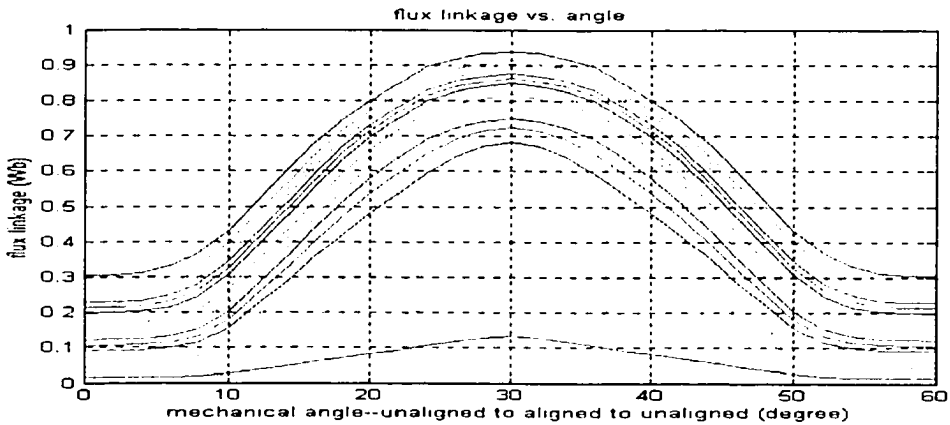


(b) Simulation Block for One Phase

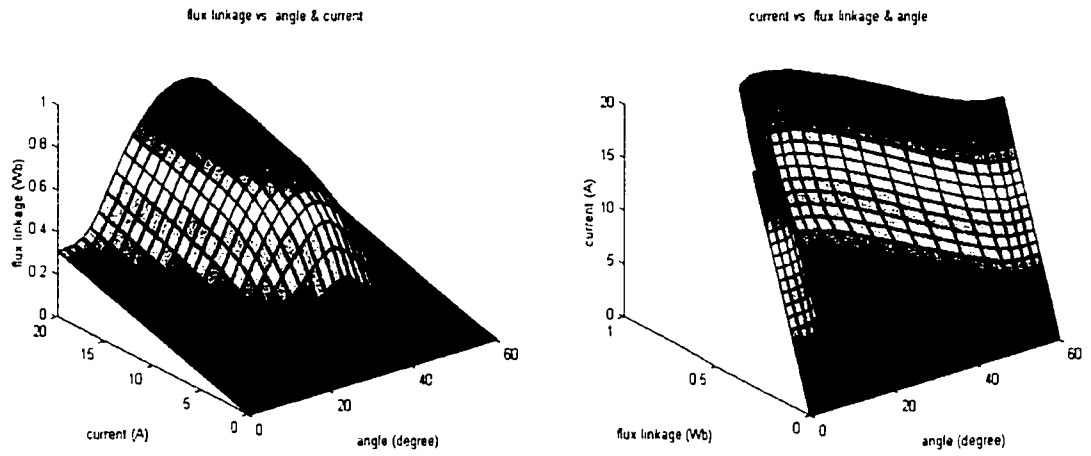
Fig.2.7 Simulation Model for SRM — Look-up Table Method



(a) Flux-linkage vs. Current at Different Rotor Positions



(b) Flux-Linkage vs. Rotor Position at Different Currents



(c) 3-D View of Flux-linkage vs. Current & Rotor Position

Fig.2.8 Flux Linkage vs. Phase Current and Rotor Position

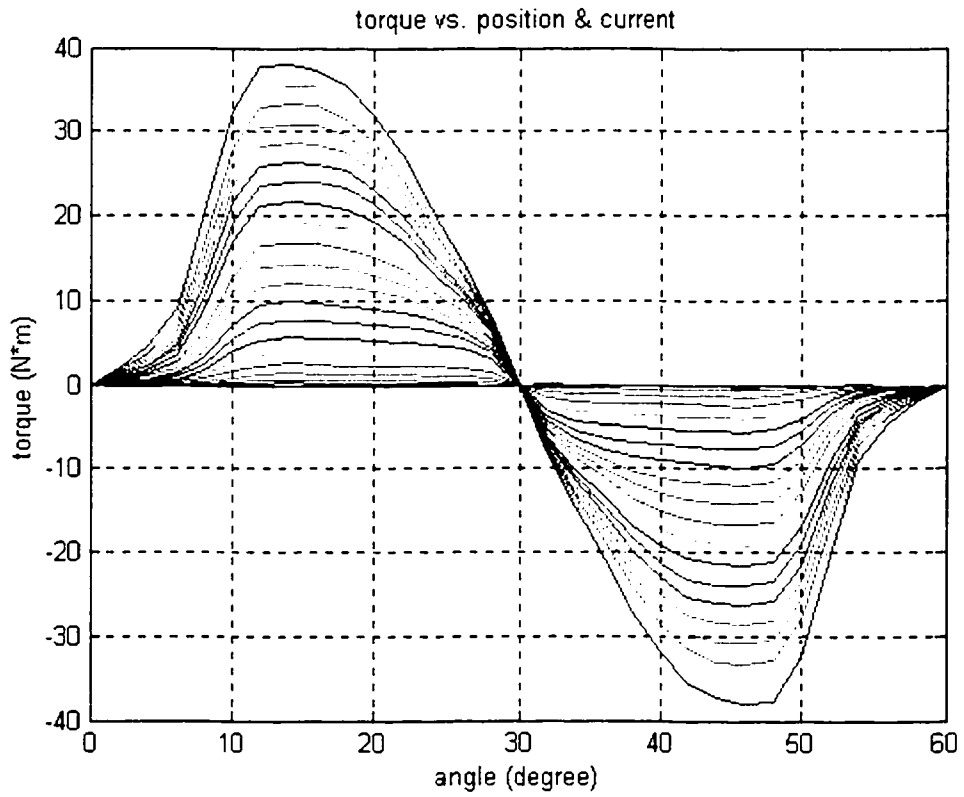


Fig.2.9 Torque vs. Rotor Position and Phase Current

The torque vs. rotor position and phase current look-up table can also be from FEM calculations or experimental test. Again the data used in this chapter is from experimental tests. It is shown in Fig.2.9.

Fig.2.10 shows the simulated results of phase current, flux linkage, transient speed and total torque. It is for no-load operation at full speed of 1700rpm, with turn-on angle at  $7^\circ$  and turn-off angle at  $22.5^\circ$ .

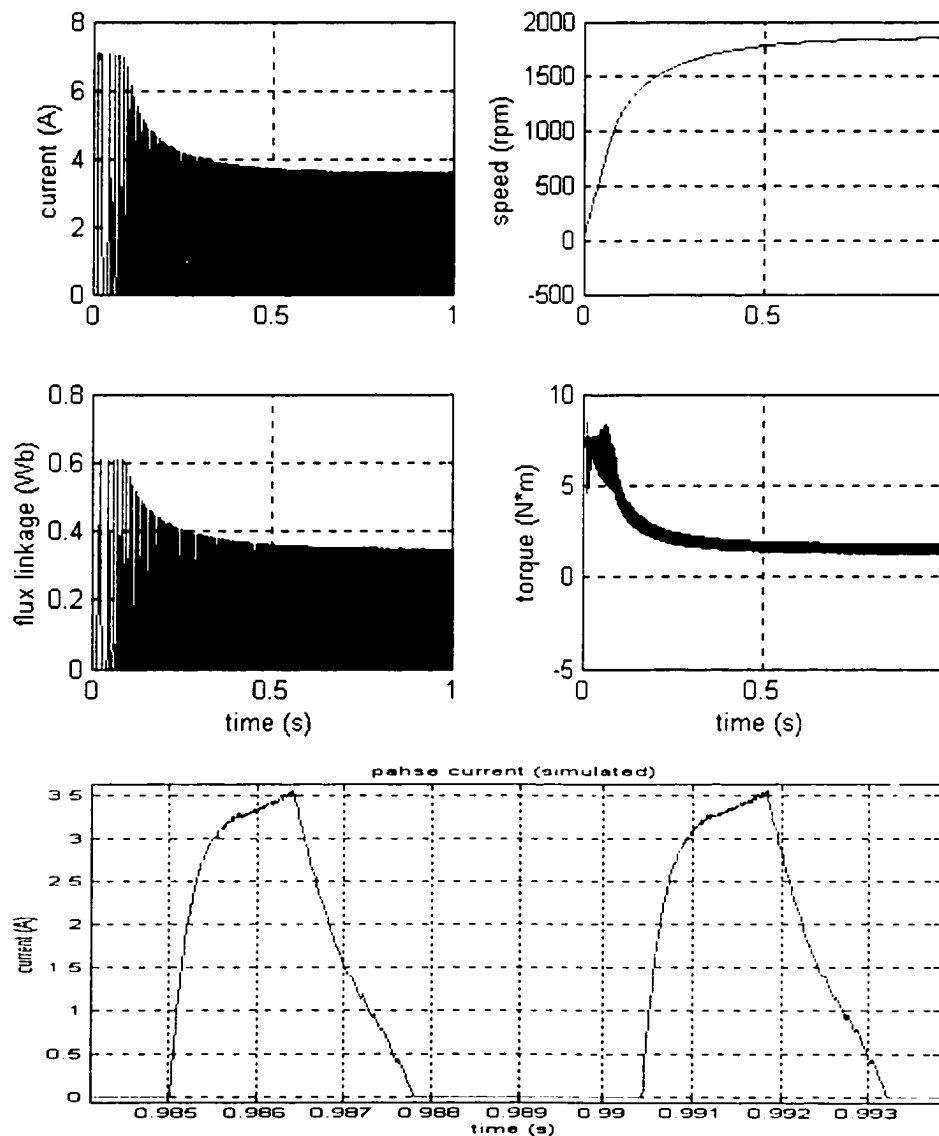
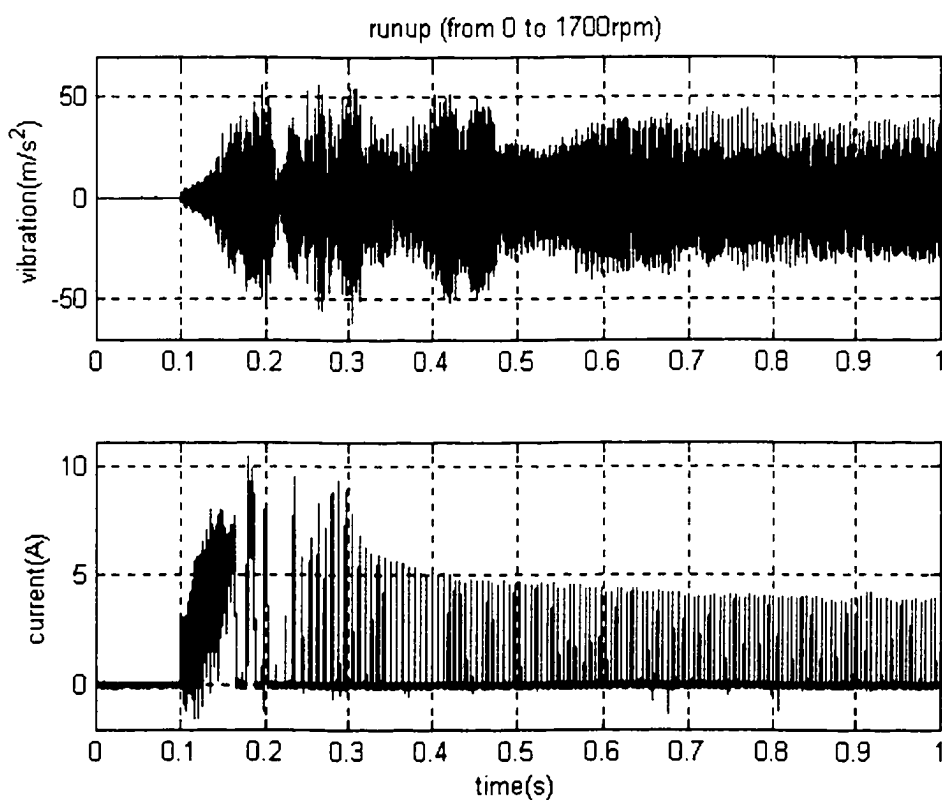


Fig.2.10 Simulated Transient Phase Current, Rotor Speed, Flux Linkage and Torque (Accelerating)

### 2.3.4 Experimental Validation

An 8/6 4kW SRM is used for experiment. The transient stator vibration and phase current are measured, as shown in Fig.2.11. Fig.2.11(a) shows the measured transient stator acceleration during start-up, (b) is the phase current, (c) is the zoomed view of phase current.

The measured phase current is close enough to the simulated one, especially when the SRM reaches steady state. The phase current during start-up is not exactly the same as the simulated one, that is believed to be because of different control technique used in the commercial drive (the exact technique is unknown).



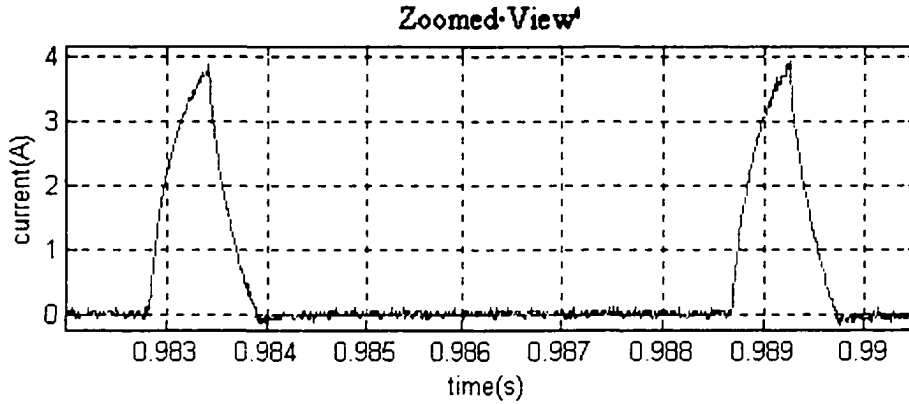


Fig.2.11(a, b, c) Measured Transient Stator Vibration and Phase Current

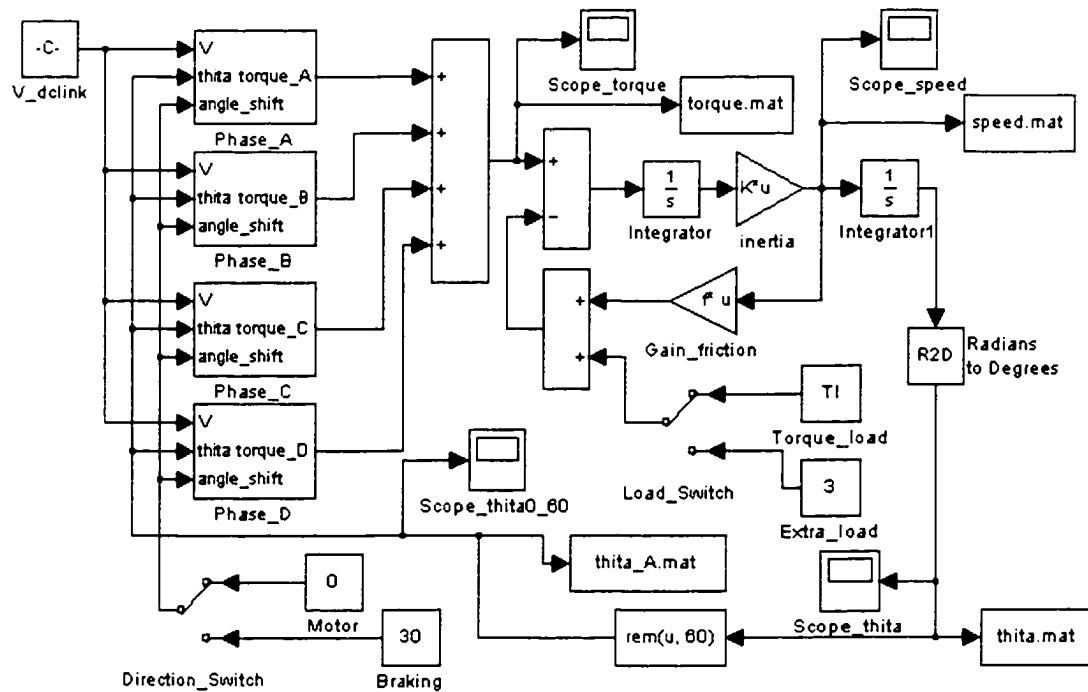
### 2.3.5 Braking and Sudden Change of Torque Operations

In industrial applications, SRMs do not always run at constant speed. In most cases, the speed and torque change. It is necessary to analyze SRM operations under the condition of sudden change of torque (speed) and even changing from motoring to generating (braking).

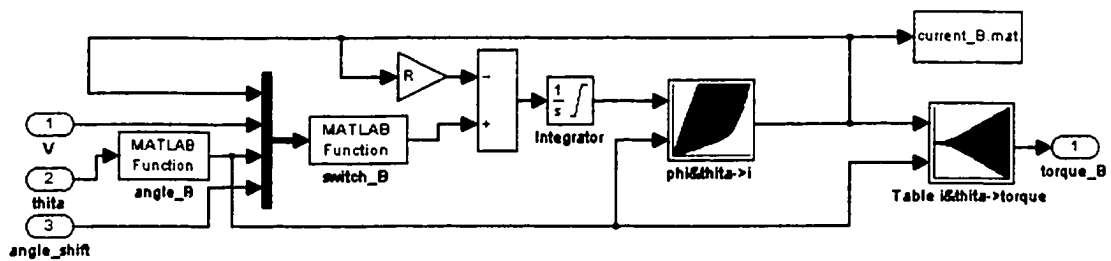
The simulation model shown in Fig.2.7 is good for simulating the SRM's start-up from zero to full speed, then remains constant. By adding two "switches", one called "Direction switch", the other called "Extra load switch", the model will be able to simulate the operation with a change of load, and braking. This new model is shown in Fig.2.12.

The SRM can be easily operated with regenerative braking, in which the turn-on angle  $\theta_{on}$  is increased to make most of the phase current appear in the  $\frac{\partial L}{\partial \theta} < 0$  area. It is still one of the APC (Angular Position Control) modes. During braking, the direction of electromagnetic torque is opposite to the rotor rotation. The mechanical energy in the

rotor is transformed to electrical energy, which will feed back to the power source through power electronics [39].



(a) Entire Model



(b) Sub-system for One Phase

Fig.2.12 Simulation Model for Sudden Load Change and Braking Operations

Fig.2.13 shows the simulation results of phase current, rotor speed, flux-linkage and torque under different operating conditions: start-up, sudden change of load and braking. The simulation model shown in Fig.2.12 is capable of simulation all these operations.

The simulation consists of the motor starting up from 0 to 0.25 seconds, then an additional torque is added (the turn-on and turn-off angles are kept the same) from 0.25 to 0.5 seconds. At 0.5 seconds the turn-on and turn-off angles are shifted by  $30^\circ$  so that the motor is operating in braking condition, until the speed reduces to be 0 rpm again. Finally at 0.85 second the SRM is returned to motoring operation and back to start up.

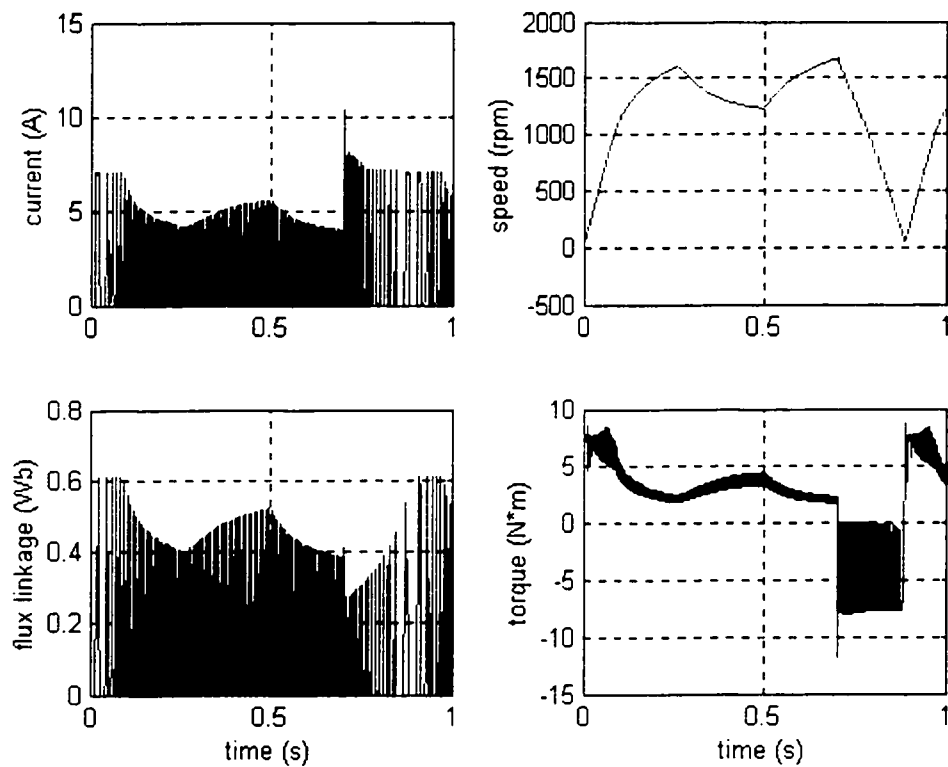


Fig.2.13 Simulation Results of Phase Current, Rotor Speed, Flux-linkage and Torque under Different Operating Conditions: Accelerating, Sudden Change of Load and Braking

## 2.4 Radial Forces at Steady State Speed

### 2.4.1 Radial Force Calculated from Measured Phase Current

Fig.2.14 shows the recorded phase current waveform of the SRM at 1450RPM (no-load). With the known turn-on and turn-off angles, this current waveform can be used in the previous lookup table to calculate the normal force acting on the stator poles, as shown in Fig.2.15.

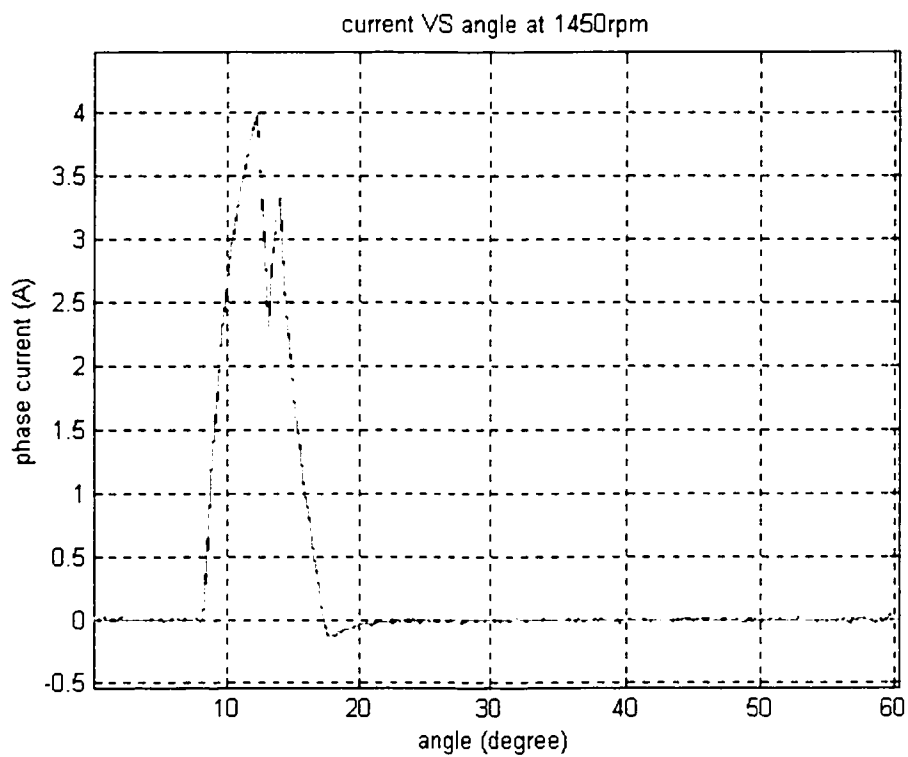


Fig.2.14 Measured SRM Phase Current at 1450RPM



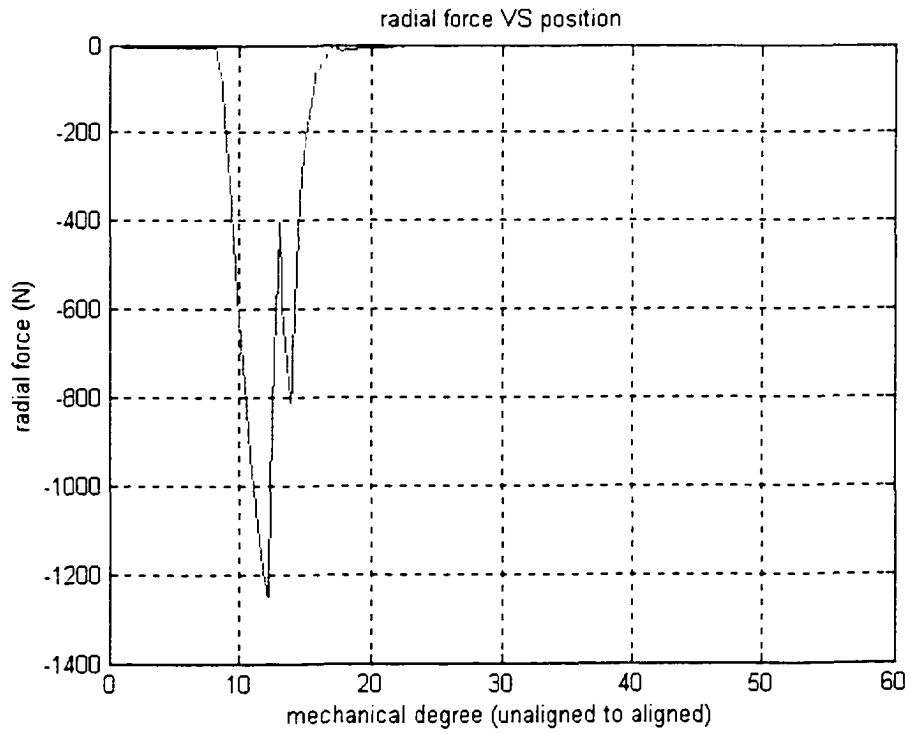


Fig.2.15 Normal Force Calculated from Look-up Table

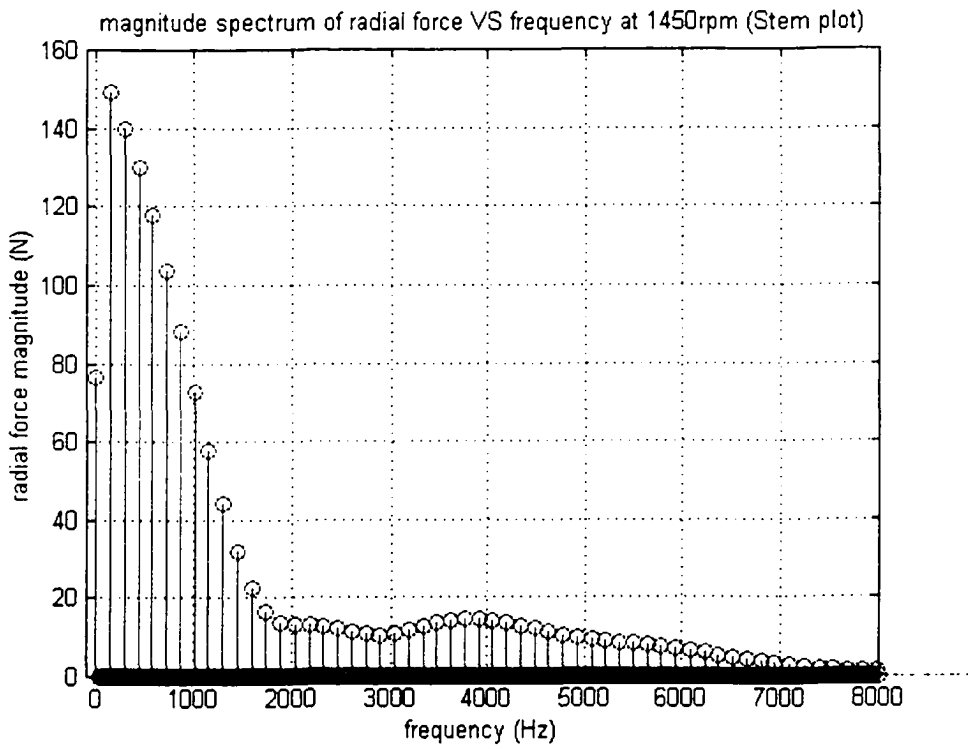


Fig.2.16 FFT Analysis Results of Normal Force

An FFT operation is carried out for the above normal force as shown in Fig.2.16. It has a DC component, fundamental and harmonics. The frequency of the fundamental is:

$$f_1 = \frac{1450RPM}{60sec/min} \times 6 poles = 145resolution/sec = 145Hz .$$

The normal force magnitudes

of all the harmonics are shown in this figure together with the frequencies. This result can be then used as input in the simulation model described in the next chapter; thus the output will be the simulated acceleration response.

## 2.4.2 Radial Force Calculated from Simulated Phase Current

Fig.2.17 shows the simulated phase current and rotor position. Notice that the rotor position is limited to be from 0 to 60°, which is required for the radial force calculations.

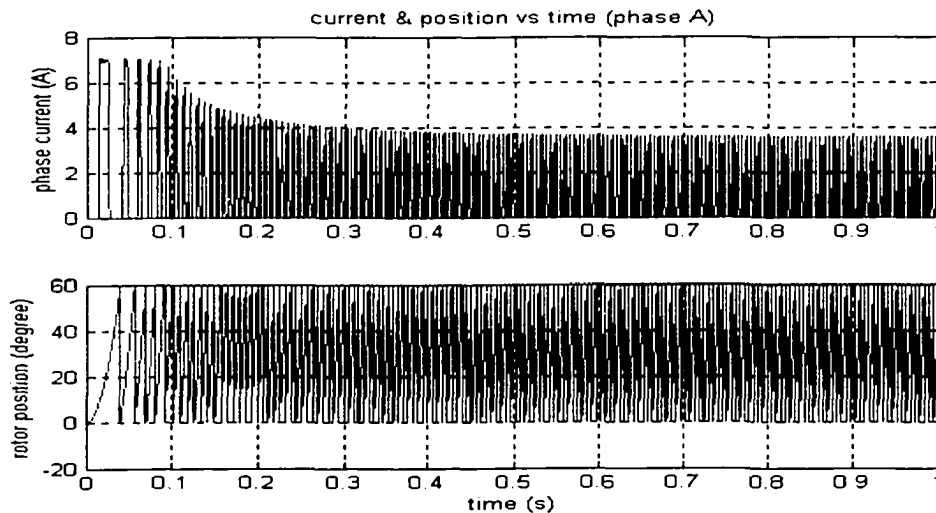


Fig.2.17 Simulated Phase Current and Rotor Position (start-up)

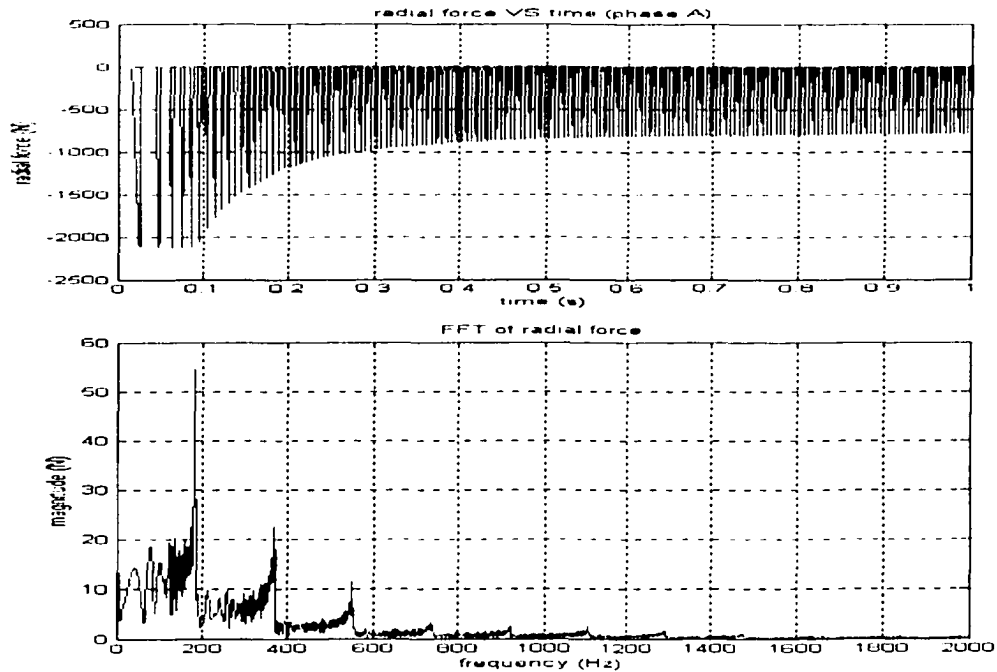


Fig.2.18 Simulated Normal Force and its FFT (start-up)

Fig.2.18 shows the calculated radial force (normal force) from look-up table technique, and its FFT. This radial force will be used later in the simulation model to predict the transient stator acceleration.

## 2.5 Radial Forces during Transients

Fig.2.19 shows the radial force and its FFT, using the same technique as described in the previous section. Compared with Fig.2.18, which shows the radial force and its FFT during motor acceleration, the radial force shown in Fig.2.19 is much more complicated, due to the change in different operating conditions. The FFT results shows that there higher levels of harmonics in the radial force in addition to new force harmonics when the operating conditions are changing, which means there are more opportunities to excite the resonant frequency of the motor stator.

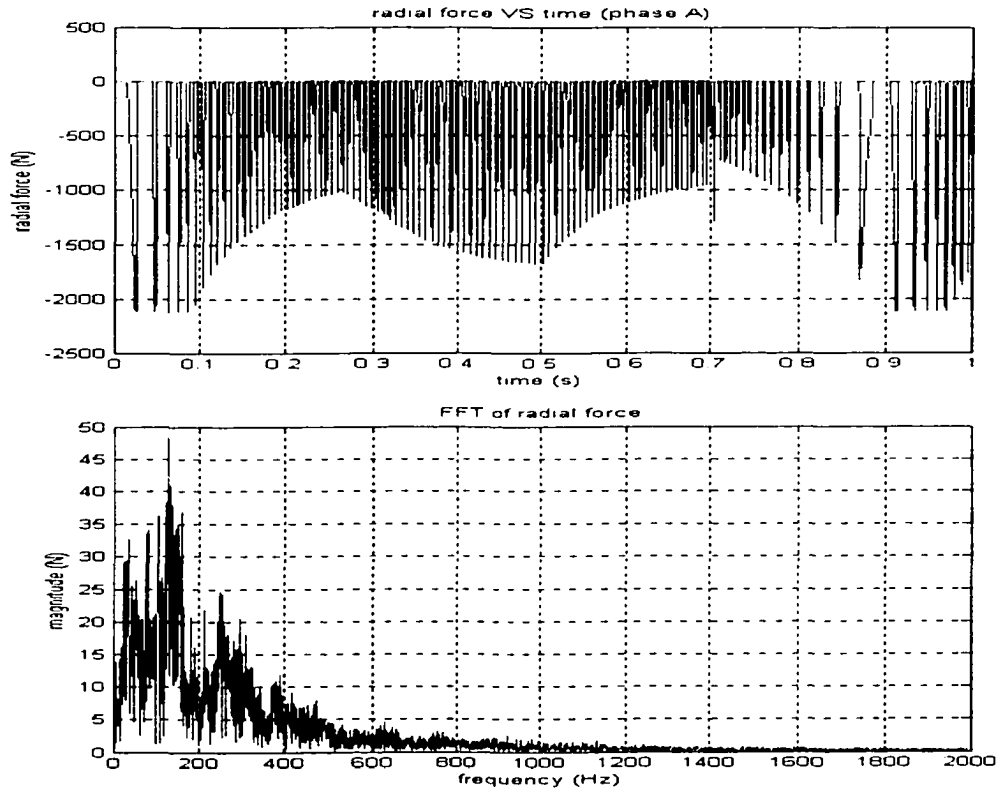


Fig.2.19 Simulated Radial Force and its FFT (start-up, sudden change of load and braking)

## 2.6 Conclusions

A detailed look-up table of normal force vs. phase current, turn-on and turn-off angles is built in this chapter, using the results from Finite Element calculations. This look-up table is ready to be used to obtain the actual normal force acting on the stator, for an arbitrary phase current waveform, once turn-on and turn-off angles are known. This will be used to determine the force harmonics and hence to calculate the vibration resulting from the normal forces.

The simulation models for SRM transient operations are presented in this chapter, with results of phase current, transient speed, flux linkage and total torque. The

accelerating, sudden change of torque and braking operations of the SRM are described, together with the stator vibration associated with each operating condition.

The method of calculating normal forces between stator pole and rotor pole is introduced in this chapter. Normal forces during constant running speed, acceleration, sudden change of torque and braking operations are calculated. Those normal forces are ready to be used in the vibration prediction model to predict steady state and transient vibrations, which will be discussed in the next chapter.

## Chapter 3

# Transfer Function Identification, Vibration Prediction and Experimental Validation

### 3.1 Summary

A vibration prediction model of normal force to stator vibration for the Switched Reluctance Motor is constructed in this chapter. Sinusoidal shaker excitation tests for vibration measurement are used for measuring crucial parameters like modal frequency and damping ratio of the transfer function. A vibration prediction model based on the transfer function is built in Matlab/SIMULINK. SRM stator vibrations are predicted for constant speed, accelerating, sudden change of torque and braking operations. The model is then verified by comparing the experimental results with simulated results, with acceptable accuracy.

### 3.2 Introduction

It is already accepted that the vibrations in SRMs are caused primarily by the ovalizing deformation of the stator lamination stack due to its radial magnetic attraction to the rotor [21, 23]. Currently there is work being done on the determination of resonant frequencies [31, 34], mode shapes [22, 25, 32] and testing [26, 27, 28, 35]. However the prediction of vibration deserves some attention.

This chapter will make it possible to predict the vibration in the SRM, using the vibration transfer function obtained from sinusoidal shaker excitation tests, together with a normal force look-up table from Finite Element calculations described in Chapter 2.

Fig.3.1 shows the flow chart for vibration prediction modeling and verification. The final goal is to compare the predicted and measured acceleration. As can be seen from the flow chart, there are two paths, one for the predicted acceleration and the other for the measured acceleration.

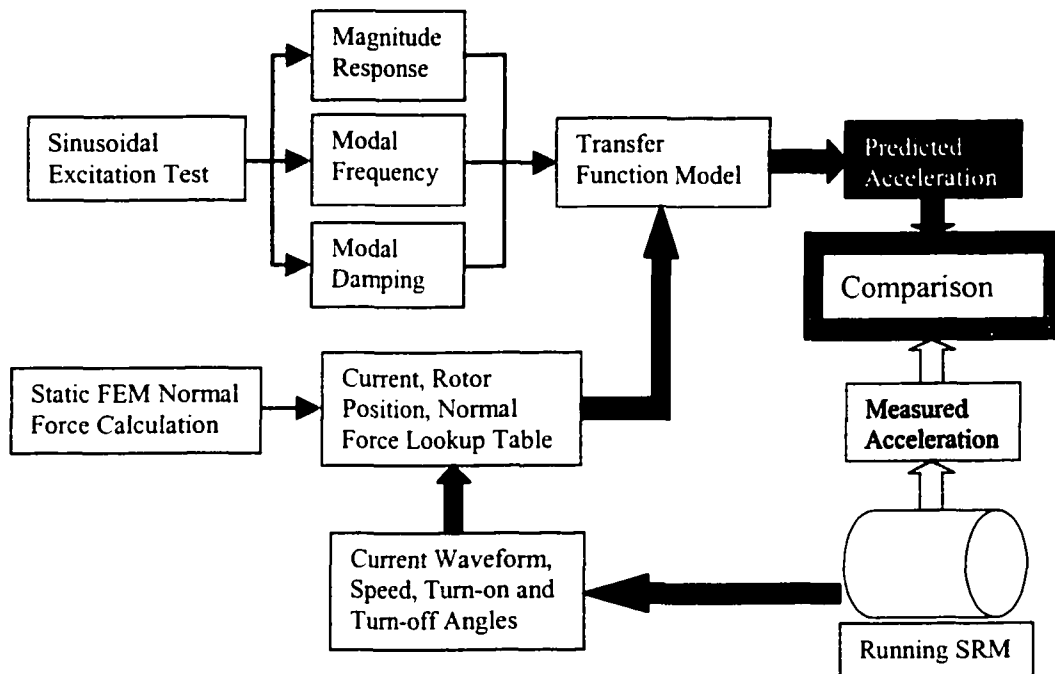


Fig.3.1 Flow Chart of Vibration Prediction Modeling and Verification

The most important and difficult path is the “Predicted Acceleration”, where a lot of work has to be done, this requires sinusoidal shaker tests, parameter determination, transfer function modeling, FEM normal force calculation, look-up table construction, running SRM current and acceleration measurements, etc. Firstly, sinusoidal shaker tests are done for SRM vibrations. Three parameters are needed for the transfer function

model at each resonant frequency, and they are then used to construct the transfer function model in SIMULINK. Secondly, intensive FEM calculations are done using ANSYS to construct a look-up table of SRM phase current, rotor position and normal force (which is done in Chapter 2). Next, the phase current waveform, motor speed, turn-on and turn-off angles of the running SRM are recorded and then used in the look-up table constructed in the previous step. If the motor is not available, simulated currents from  $\psi$ -i data can be used. The actual normal force applied to the stator-rotor pole is calculated while the SRM is running at different speeds and different operating conditions. Finally, the calculated normal force data is used in the transfer function to predict the acceleration and hence noise.

For the measured acceleration path, several accelerometers are mounted directly on the outer case of the stator. The motor is running and acceleration spectra are recorded at different motor speeds and operating conditions. This is compared with the predicted acceleration with acceptable results.

### **3.3 Transfer Function Determination**

#### **3.3.1 Sinusoidal Excitation Method**

##### **3.3.1.1 Frequency Response Function (FRF) of SRM Vibrations**

From a vibration point of view, the SRM is a complicated Multidegree of Freedom (MDOF) system [33, 36]. However it can be represented as the linear superposition of a finite number of Single Degree of Freedom (SDOF) systems.

Fig.3.2 is the model for a force acting on a viscously damped spring-mass system. The equation of motion can be obtained using Newton's second law:



$$m\ddot{x} + c\dot{x} + kx = F(t) \quad (3-1)$$

Perform s-transformation to the above equation:

$$s^2 mX(s) + scX(s) + kX(s) = F(s) \quad (3-2)$$

From:

$$\omega_n = \sqrt{\frac{k}{m}} = \text{undamped natural frequency,}$$

$$\zeta = \frac{c}{2m\omega_n} = \frac{c}{2\sqrt{mk}} = \text{Damping ratio; } \frac{c}{m} = 2\zeta\omega_n \quad (3-3)$$

$$s^2 X(s) + s \frac{c}{m} X(s) + \frac{k}{m} X(s) = \frac{1}{m} F(s) \quad (3-4)$$

$$s^2 X(s) + 2\zeta\omega_n sX(s) + \omega_n^2 X(s) = \frac{1}{m} F(s) \quad (3-5)$$

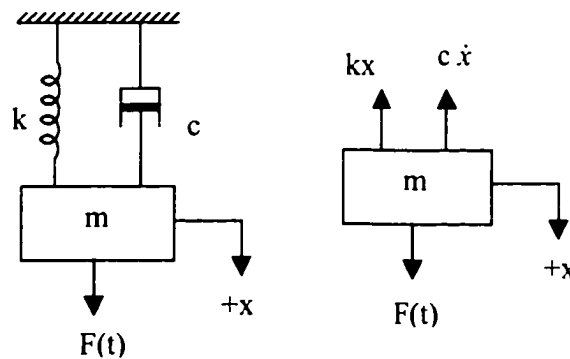


Fig.3.2 A Spring-mass-damper System

So the displacement response (Compliance) of the system is:

$$X(s) = \frac{F(s)}{m} \frac{1}{s^2 + 2\zeta\omega_n s + \omega_n^2} \quad (3-6)$$

$$\text{Velocity response (Mobility) is: } V(s) = sX(s) = \frac{F(s)}{m} \frac{s}{s^2 + 2\zeta\omega_n s + \omega_n^2} \quad (3-7)$$

Acceleration response (Accelerance) is:

$$a(s) = s^2 X(s) = \frac{F(s)}{m} \frac{s^2}{s^2 + 2\zeta\omega_n s + \omega_n^2} \quad (3-8)$$

So the transfer function from force to acceleration is:

$$H(s) = \frac{a(s)}{F(s)} = \frac{1}{m} \frac{s^2}{s^2 + 2\zeta\omega_n s + \omega_n^2} \quad (3-9)$$

For the stator of the SRM, the transfer function can be written as:

$$H(s) = \frac{a(s)}{F(s)} \cong \sum_i A_i \frac{s^2}{s^2 + 2\zeta_i\omega_{ni}s + \omega_{ni}^2} \quad (3-10)$$

Where  $\omega_{ni}$  is the resonant natural frequency of mode  $i$ ,  $\zeta_i$  is the damping ratio of mode  $i$ ,  $A_i$  is the gain relative to mode  $i$ , and  $s$  is the Laplace's variable.

It can be stated that the transfer function of the stator vibrations and the forces acting on the stator is composed of a sum of the second order high-pass filters.

### 3.3.1.2 Free Vibration of Viscous Damping — Damping Ratio Measurement

The motion of free vibration of the Single Degree of Freedom (SODF) system with non-zero initial condition can be expressed as  $m\ddot{x} + c\dot{x} + kx = 0$ . To solve this equation, we can assume a solution of the form of  $x(t) = Ce^{rt}$ , where  $C$  and  $r$  are undetermined constants. Inserting this function into the motion equation leads to the characteristic equation  $mr^2 + cr + k = 0$ . The roots of which are:

$$r_{1,2} = \frac{-c \pm \sqrt{c^2 - 4mk}}{2m} = -\frac{c}{2m} \pm \sqrt{\left(\frac{c}{2m}\right)^2 - \frac{k}{m}} \quad (3-11)$$

The roots give two solutions to the motion equation:  $x_1(t) = C_1 e^{r_1 t}$  and  $x_2(t) = C_2 e^{r_2 t}$ . Thus the general solution is given by the combination of the two solutions  $x_1(t)$  and  $x_2(t)$ :

$$x(t) = C_1 e^{r_1 t} + C_2 e^{r_2 t} = C_1 e^{\left\{-\frac{c}{2m} + \sqrt{\left(\frac{c}{2m}\right)^2 - \frac{k}{m}}\right\}t} + C_2 e^{\left\{-\frac{c}{2m} - \sqrt{\left(\frac{c}{2m}\right)^2 - \frac{k}{m}}\right\}t} \quad (3-12)$$

Where  $C_1$  and  $C_2$  are arbitrary constants to be determined from the initial conditions of the system.

The Critical Damping  $c_c$  is defined as the value of the damping constant  $c$  for which the radical in the root equation becomes zero:  $\left(\frac{c_c}{2m}\right)^2 - \frac{k}{m} = 0$  or  $c_c = 2m\sqrt{\frac{k}{m}}$

$= 2\sqrt{km} = 2m\omega_n$ . For any damped system, the damping ratio  $\zeta$  is defined as the ratio of the damping constant to the critical damping constant:  $\zeta = \frac{c}{c_c}$ . We can also write

$\frac{c}{2m} = \frac{c}{c_c} \cdot \frac{c_c}{2m} = \zeta\omega_n$  and hence  $r_{1,2} = \left(-\zeta \pm \sqrt{\zeta^2 - 1}\right)\omega_n$ . Thus the solution can be

written as:

$$x(t) = C_1 e^{\left(-\zeta + \sqrt{\zeta^2 - 1}\right)\omega_n t} + C_2 e^{\left(-\zeta - \sqrt{\zeta^2 - 1}\right)\omega_n t} \quad (3-13)$$

The nature of the roots  $r_1$  and  $r_2$  and hence the behavior of the solution depends on the magnitude of damping.

It can be seen that the case of  $\zeta = 0$  leads to the undamped vibration, which is not of interest here. The system is Underdamped for  $\zeta < 1$  (or  $c < c_c$  or  $\frac{c}{2m} < \sqrt{\frac{k}{m}}$ ), Critically Damped for  $\zeta = 1$  (or  $c = c_c$  or  $\frac{c}{2m} = \sqrt{\frac{k}{m}}$ ), and Overdamped for  $\zeta > 1$  (or  $c > c_c$  or  $\frac{c}{2m} > \sqrt{\frac{k}{m}}$ ). Since the Underdamped System is the only case that leads to an oscillatory motion, it is the most important case in the study of mechanical vibrations of SRMs.

For the underdamped condition,  $(\zeta^2 - 1)$  is negative and the roots  $r_1$  and  $r_2$  can be expressed as  $r_1 = (-\zeta + i\sqrt{1-\zeta^2})\omega_n$  and  $r_2 = (-\zeta - i\sqrt{1-\zeta^2})\omega_n$ , and the solution can be written in different forms:

$$\begin{aligned}
x(t) &= C_1 e^{(-\zeta + i\sqrt{1-\zeta^2})\omega_n t} + C_2 e^{(-\zeta - i\sqrt{1-\zeta^2})\omega_n t} \\
&= e^{-\zeta\omega_n t} \left\{ C_1 e^{i\sqrt{1-\zeta^2}\omega_n t} + C_2 e^{-i\sqrt{1-\zeta^2}\omega_n t} \right\} \\
&= e^{-\zeta\omega_n t} \left\{ (C_1 + C_2) \cos \sqrt{1-\zeta^2} \omega_n t + i(C_1 - C_2) \sin \sqrt{1-\zeta^2} \omega_n t \right\} \\
&= e^{-\zeta\omega_n t} \left\{ C'_1 \cos \sqrt{1-\zeta^2} \omega_n t + C'_2 \sin \sqrt{1-\zeta^2} \omega_n t \right\} \\
&= X e^{-\zeta\omega_n t} \sin \left( \sqrt{1-\zeta^2} \omega_n t + \phi \right) \\
&= X_0 e^{-\zeta\omega_n t} \cos \left( \sqrt{1-\zeta^2} \omega_n t - \phi_0 \right) \tag{3-14}
\end{aligned}$$

Where  $(C'_1, C'_2)$ ,  $(X, \phi)$  and  $(X_0, \phi_0)$  are arbitrary constants to be determined from the initial conditions.

For the initial conditions  $x(t = 0) = x_0$  and  $\dot{x}(t = 0) = \dot{x}_0$ ,  $C'_1$  and  $C'_2$  can be found:

$$C'_1 = x_0 \text{ and } C'_2 = \frac{\dot{x}_0 + \zeta \omega_n x_0}{\sqrt{1 - \zeta^2} \omega_n}, \text{ and hence the solution becomes:}$$

$$x(t) = e^{-\zeta \omega_n t} \left\{ x_0 \cos \sqrt{1 - \zeta^2} \omega_n t + \frac{\dot{x}_0 + \zeta \omega_n x_0}{\sqrt{1 - \zeta^2} \omega_n} \sin \sqrt{1 - \zeta^2} \omega_n t \right\} \quad (3-15)$$

The constants  $(X, \phi)$  and  $(X_0, \phi_0)$  can be expressed as:

$$X = X_0 = \sqrt{(C'_1)^2 + (C'_2)^2}, \quad \phi = \tan^{-1} \left( \frac{C'_1}{C'_2} \right), \quad \phi_0 = \tan^{-1} \left( -\frac{C'_2}{C'_1} \right).$$

The motion described by the solution is damped harmonic motion of angular frequency  $\sqrt{1 - \zeta^2} \omega_n$ , but because of the factor  $e^{-\zeta \omega_n t}$ , the amplitude decreases exponentially with time. The quantity  $\omega_d = \sqrt{1 - \zeta^2} \omega_n$  is called the Frequency of Damped Vibration. It can be seen that the frequency of damped vibration  $\omega_d$  is always less than the undamped natural frequency  $\omega_n$ .

The logarithmic decrement represents the rate at which the amplitude of a free damped vibration decreases. It is defined as the natural logarithm of the ratio of any two successive amplitudes. Let  $t_1$  and  $t_2$  denote the times corresponding to two consecutive amplitudes (displacements), measured one cycle apart for an underdamped system. The ratio can be formed as:

$$\frac{x_1}{x_2} = \frac{X_0 e^{-\zeta \omega_n t_1 \cos(\omega_d t_1 - \phi_0)}}{X_0 e^{-\zeta \omega_n t_2 \cos(\omega_d t_2 - \phi_0)}} \quad (3-16)$$

But  $t_2 = t_1 + \tau_d$  where  $\tau_d = 2\pi/\omega_d$  is the period of damped vibration. Hence  $\cos(\omega_d t_2 - \phi_0) = \cos(2\pi + \omega_d t_1 - \phi_0) = \cos(\omega_d t_1 - \phi_0)$ , and the ratio can be rewritten as

$$\frac{x_1}{x_2} = \frac{e^{-\zeta\omega_n t_1}}{e^{-\zeta\omega_n(t_1+\tau_d)}} = e^{\zeta\omega_n \tau_d}. \text{ The logarithmic decrement } \delta \text{ can be obtained as:}$$

$$\delta = \ln \frac{x_1}{x_2} = \zeta\omega_n \tau_d = \zeta\omega_n \frac{2\pi}{\sqrt{1-\zeta^2}\omega_n} = \frac{2\pi\zeta}{\sqrt{1-\zeta^2}} = \frac{2\pi}{\omega_d} \cdot \frac{c}{2m} \quad (3-17)$$

For small damping, it can be approximated as  $\delta \cong 2\pi\zeta$  if  $\zeta \ll 1$ .

The logarithmic decrement is dimensionless and is actually another form of the dimensionless damping ratio  $\zeta$ . Once  $\delta$  is known,  $\zeta$  can be found by solving equation

$$\zeta = \frac{\delta}{\sqrt{(2\pi)^2 + \delta^2}}, \text{ or it can be approximated as } \zeta \cong \frac{\delta}{2\pi} \text{ if } \delta \ll 2\pi \text{ or } \zeta \ll 1.$$

If the damping in the given system is not known, it can be determined experimentally by measuring any two consecutive displacements  $x_1$  and  $x_2$ . By taking the natural logarithm of the ratio of  $x_1$  and  $x_2$ ,  $\delta$  is obtained. By using the above equation, the damping ratio  $\zeta$  can be computed. In fact, the damping ratio  $\zeta$  can also be found by measuring two displacements separated by any number of complete cycles.

If  $x_1$  and  $x_{m+1}$  are the amplitudes corresponding to times  $t_1$  and  $t_{m+1} = t_1 + m\tau_d$ ,

where  $m$  is an integer,  $\frac{x_1}{x_{m+1}} = \frac{x_1}{x_2} \cdot \frac{x_2}{x_3} \cdot \frac{x_3}{x_4} \dots \frac{x_m}{x_{m+1}}$ . Any two consecutive displacements

separated by one cycle satisfy the equation  $\frac{x_j}{x_{j+1}} = e^{\zeta\omega_n \tau_d}$ . So  $\frac{x_1}{x_{m+1}} = \left(e^{\zeta\omega_n \tau_d}\right)^m = e^{m\zeta\omega_n \tau_d}$

and  $\delta = \frac{1}{m} \ln\left(\frac{x_1}{x_{m+1}}\right)$ , which can be substituted into the damping ratio equation to obtain the viscous damping ratio  $\zeta$ .

### 3.3.1.3 Test Setup and Procedure

The Sinusoidal Excitation Method is used to measure the parameters of the transfer function for each resonant frequency. The test setup of this method is shown in Fig.3.3. The SRM is suspended via four elastic ropes through its mounting holes to a solid bench, to establish a so-called free-free condition. A Signal Generator (Tektronix TM503, 3MHz) can supply sinusoidal signals of different frequencies to the Power Amplifier (B&K 2706). A shaker (B&K 4809) is driven by the sinusoidal signals and excites the SRM hanging above. A force transducer is stud-mounted onto the body frame (through a threaded hole) and connected to the shaker by the stinger. The shaker is placed directly on the ground where the reaction force will be absorbed. Accelerometers are screwed onto the body frame of several different locations to pick up the acceleration. Force and acceleration outputs are recorded in a storage oscilloscope (LeCroy 9304AM, QUAD 200MHz, 100MS/s) through a coupler (Kistler 5134), and then used in a MATLAB program for data processing.

The frequency of the sinusoidal signal output from the signal generator is adjustable. The frequency of the signal is changed until the predominant motion of the frame body is due to the desired mode of vibration, that is, in this experiment, the second mode vibration. Firstly, the so-called Wide Band sweeps are performed. Watching the response signal on an oscilloscope (or listening to the sound), a rise in the amplitude of

response is detected where a Narrow Band sweep is performed, using smaller frequency changes, in order to identify the frequency of the mode more accurately. The frequency of this mode is located when the response signal on the oscilloscope at this point is higher than either side. The shaker is shut down and the decaying waveforms of force and acceleration are recorded.

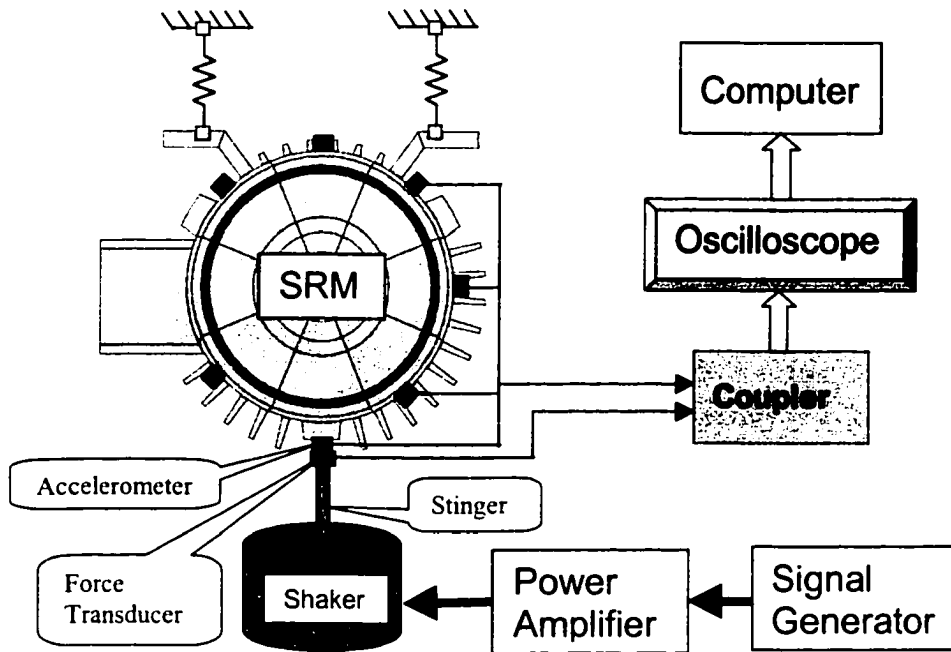


Fig.3.3 Test Setup of Sinusoidal Excitation Method

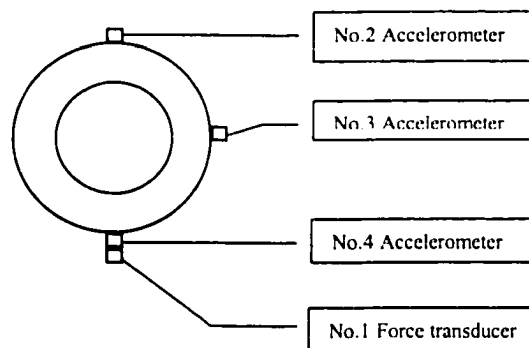


Fig.3.4 Locations of Force Transducer and Accelerometers



For identification of modal transfer functions, there is only one force transducer and three accelerometers. They are screwed into the SRM stator in the locations shown in Fig.3.4.

#### **3.3.1.4 Test Results**

The first objective here is to locate the resonant frequency, that is, to excite the undamped or normal modes of the stator, one at a time. The shaker is attached to the stator, and is driven with a sinusoidal signal equal in frequency to the natural frequency of the mode to be excited. Fig.3.5 shows the identified frequency of the second mode of vibration.

From Fig.3.5 it can be seen that the resonant frequency for the second mode of stator with end-bells is 1316.5Hz.

#### **3.3.1.5 Damping Ratio Measurement**

When a so-called “pure” mode is excited, the damping ratio of the stator at the modal frequency can be measured from the envelope of the damped sinusoidal response. The shaker is shut off to simulate a damped response of the stator at the frequency of the tested resonant mode. Ideally the stator should exhibit a damped sinusoidal response at all points, with a single frequency of vibration being the frequency of the excited mode. Fig.3.6 shows the recorded damped sinusoidal force and acceleration responses after the shaker was shut off during excitation of the second mode.

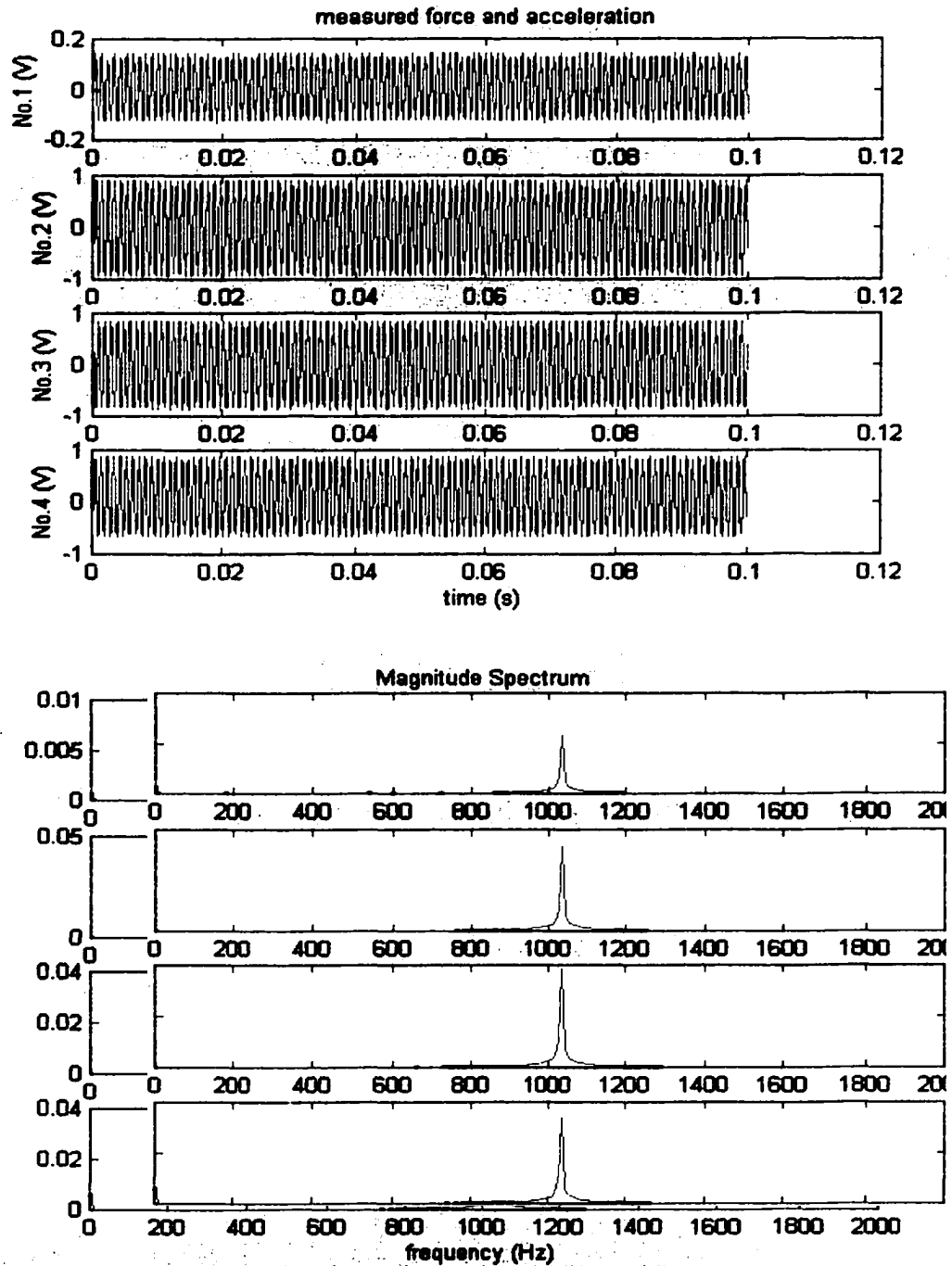


Fig.3.5 Measured Force and Acceleration Signals and their Magnitude Spectra

From Fig.3.6 the damping ratio of the second mode is calculated.

$$\text{Logarithmic decrement: } \delta = \frac{1}{N} \ln \frac{x_k}{x_{k+N}} = \frac{1}{15} \ln \frac{7.19235}{1.7602} = 0.09384 \quad (3-18)$$

$$\text{The damping ratio: } \zeta_2 = \frac{\delta}{\sqrt{(2\pi)^2 + \delta^2}} \approx \frac{\delta}{2\pi} = \frac{0.09384}{2\pi} \approx 0.0156 \quad (3-19)$$

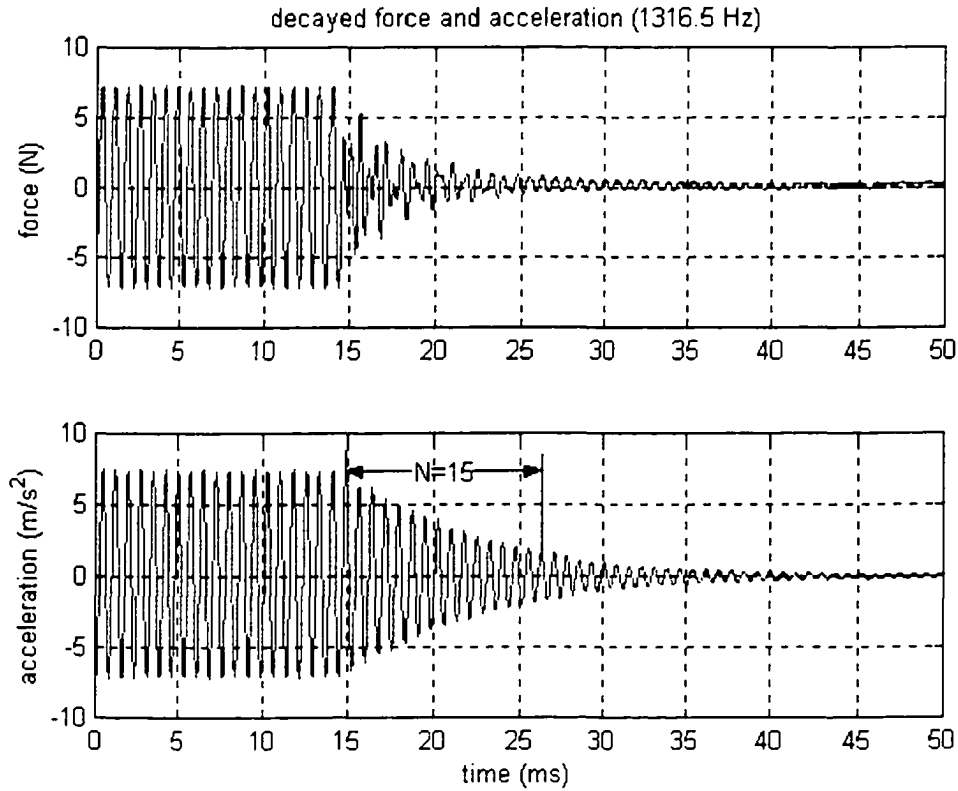


Fig.3.6 Damped Response at the Resonant Frequency

### 3.3.1.6 Gain Relative to the Second Mode

From the transfer function  $H_2(s) = \frac{a_2(s)}{F_2(s)} = A_2 \frac{s^2}{s^2 + 2\zeta_2\omega_{n2}s + \omega_{n2}^2}$  :

$$|H_2(j\omega)| = A_2 \left| \frac{(j\omega)^2}{(j\omega)^2 + 2\zeta_2\omega_{n2}(j\omega) + \omega_{n2}^2} \right|$$

$$\begin{aligned}
&= A_2 \left| \frac{-\omega^2}{(\omega_{n_2}^2 - \omega^2) + 2\zeta_2 \omega_{n_2} \omega j} \right| \\
&= A_2 \frac{\omega^2}{\sqrt{(\omega_{n_2}^2 - \omega^2)^2 + (2\zeta_2 \omega_{n_2} \omega)^2}} \quad (3-20)
\end{aligned}$$

At the resonant frequency,

$$|H_2(j\omega_{n_2})| = A_2 \frac{\omega_{n_2}^2}{\sqrt{(\omega_{n_2}^2 - \omega_{n_2}^2)^2 + (2\zeta_2 \omega_{n_2} \omega_{n_2})^2}} = \frac{A_2}{2\zeta_2} \quad (3-21)$$

From Fig.3.6 the amplitude of the force is 7.1747N (the sensitivity of the force transducer is 0.940mV/lbf (1lbf = 4.4498N), and the coupler gain is 100), and the amplitude of acceleration is 7.2607 m/s<sup>2</sup> (the sensitivity of the accelerometers is

10.00mV/g, and the coupler gain is 100). So  $|H_2(j\omega_{n_2})| = \frac{a_2(j\omega_{n_2})}{F_2(j\omega_{n_2})}$

$$= \frac{7.2607 \text{ m/s}^2}{7.1747 \text{ N}} = 1.012 \text{ kg}^{-1}.$$

So the gain relative to the second mode is:

$$A_2 = 2\zeta_2 |H_2(j\omega_{n_2})| = 2 \times 0.0156 \times 1.012 \text{ kg}^{-1} = 0.0315744 \text{ kg}^{-1}.$$

Finally, the transfer function for the second mode of the SRM stator can be written as:

$$H_2(s) = A_2 \frac{s^2}{s^2 + 2\zeta_2 \omega_{n_2} s + \omega_{n_2}^2}, \quad \text{where } A_2 = 0.0315744 \text{ kg}^{-1}, \quad \zeta_2 = 0.0156,$$

$\omega_{n_2} = 2\pi f_2 = 2\pi \times 1316.5 \text{ rad/s}$ , and s is the Laplace's variable.

Similarly, the transfer function of the other resonant frequencies can be obtained.

The results of the 2<sup>nd</sup> and 3<sup>rd</sup> mode resonant frequencies are listed in Table 3.1.

Table 3.1 Parameters for the 2<sup>nd</sup> and 3<sup>rd</sup> Order Vibration Transfer Functions

Mode Number	Frequency (Hz)	Damping Ratio ( $\zeta$ )	Gain A ( $\text{kg}^{-1}$ )
2	1316.5	0.0156	0.0315744
3	2480.2	0.0241	0.0054461

### 3.3.2 Transfer Function Modeling: Simulation and Verification

#### 3.3.2.1 Simulation

Fig.3.7 shows the simulation block. The input is a sinusoidal signal, whose frequency can be changed to simulate the force signal of different frequencies.

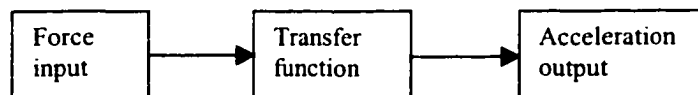


Fig.3.7 Simulation Block

Fig.3.8 shows the frequency and phase responses of the second mode transfer function. It can be seen that it is a high-pass filter.

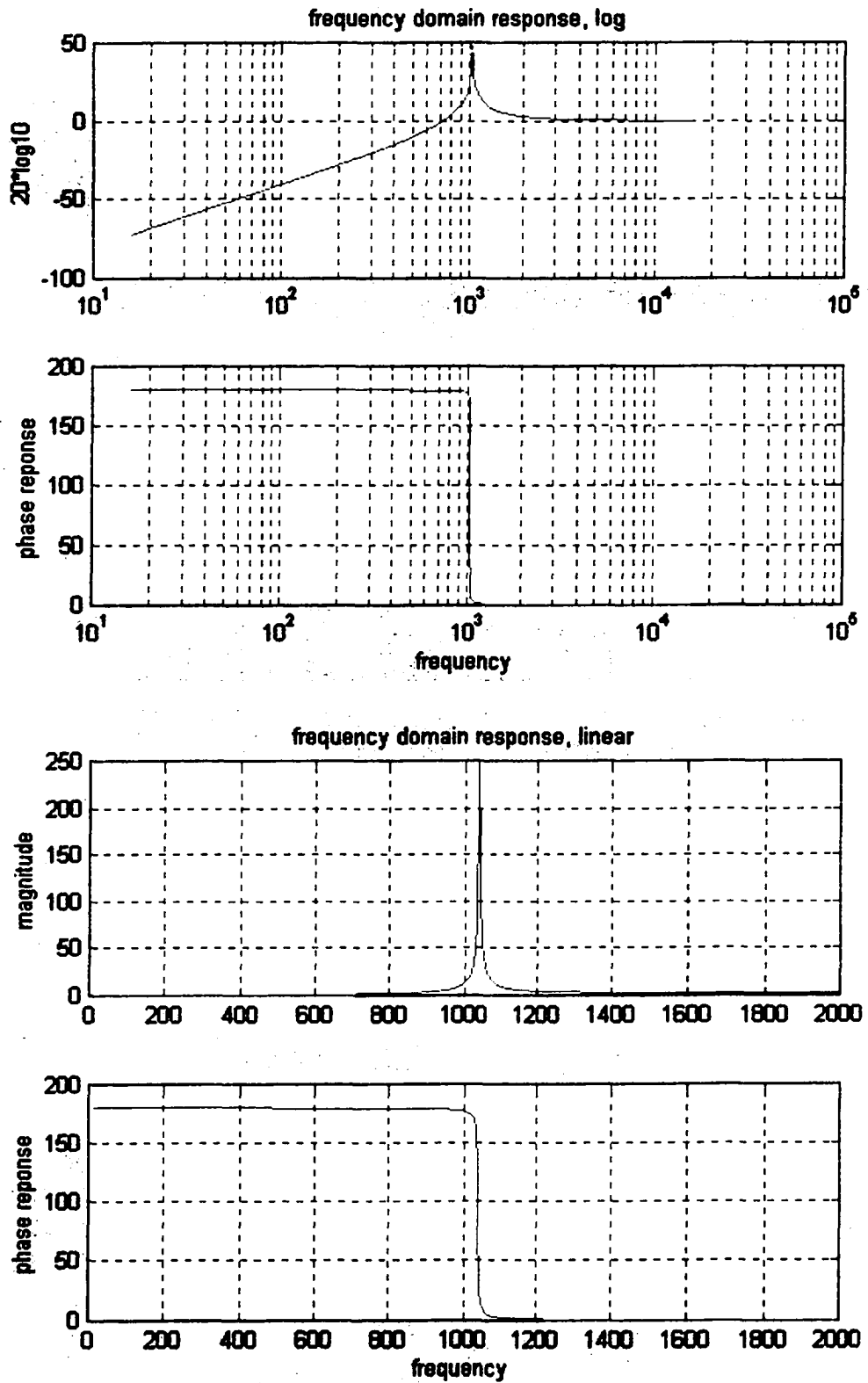
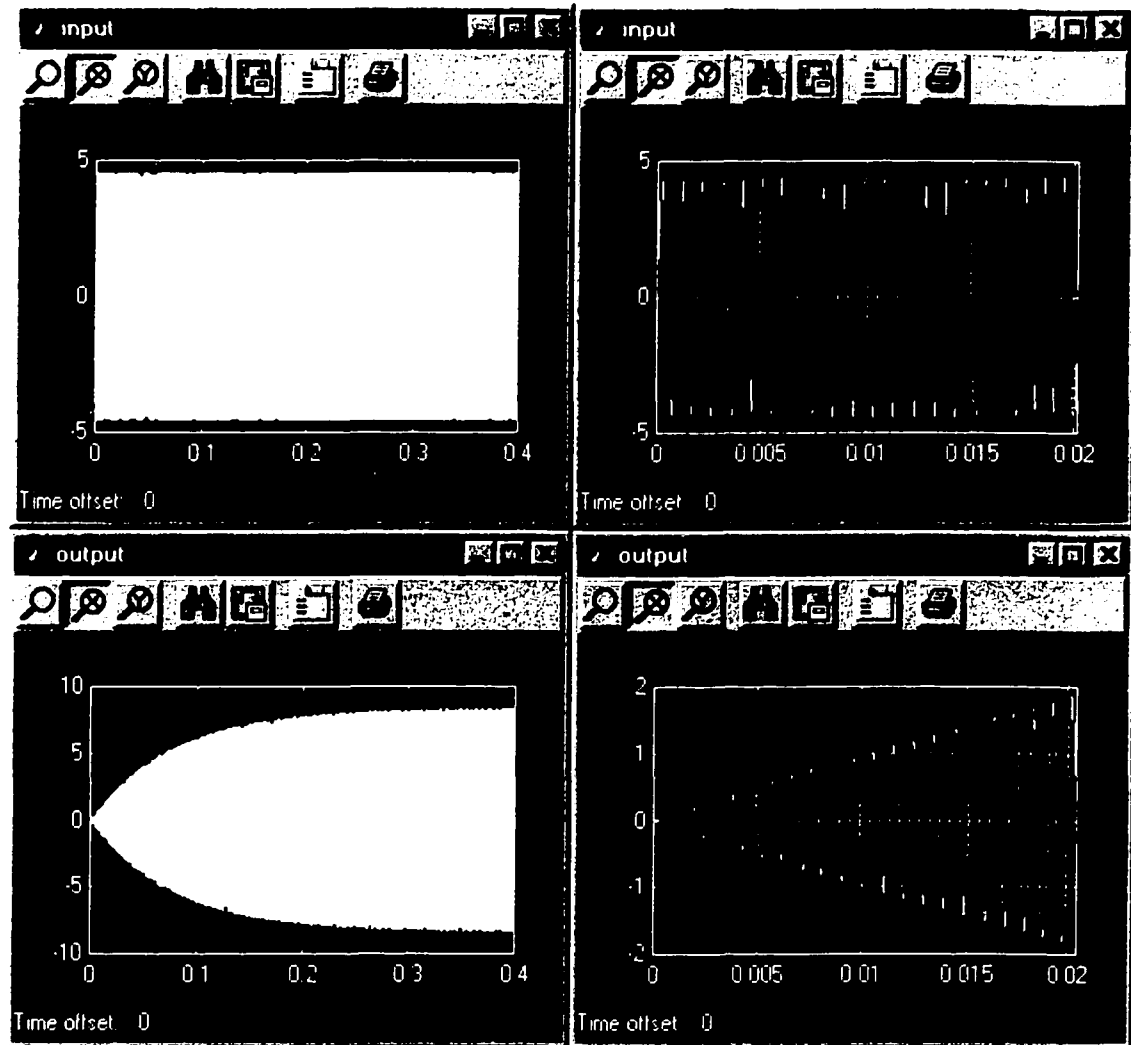
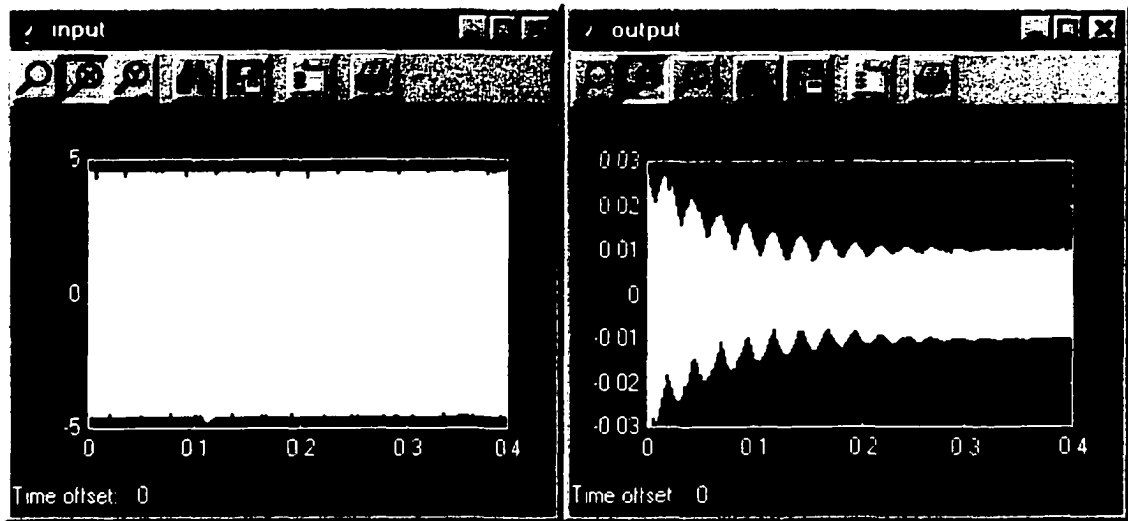


Fig.3.8 Frequency and Phase Response of the Transfer Function

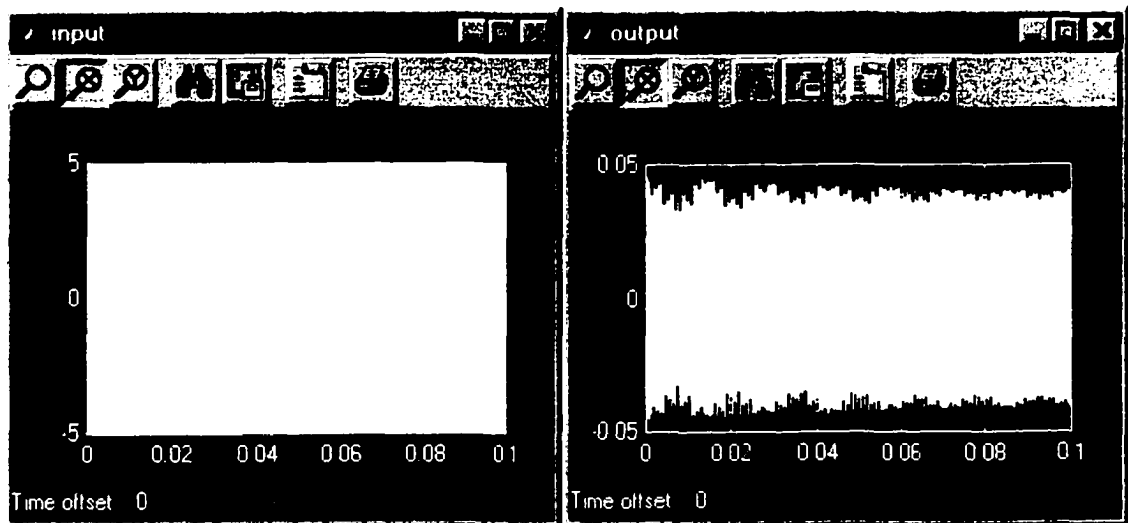
For the input signal at resonant frequency, the simulated output is shown in Fig.3.9(a). Fig.3.9(b) and (c) are simulated outputs for low frequency and high frequency inputs respectively.



(a) Response at the Resonant Frequency ( $f = 1316.5\text{Hz}$ )



(b) Responses at Low Frequency ( $f = 500$  Hz)



(c) Responses at High Frequency ( $f = 5000$  Hz)

Fig.3.9 Simulated Responses of the Transfer Function at Resonant, Low and High Frequencies

### 3.3.2.2 Verification

At low frequencies, the actual acceleration measured from the stator body is much lower than that at high frequencies, which is shown in Fig.3.10. This confirms the hypothesis that the transfer function has a high pass filter response.



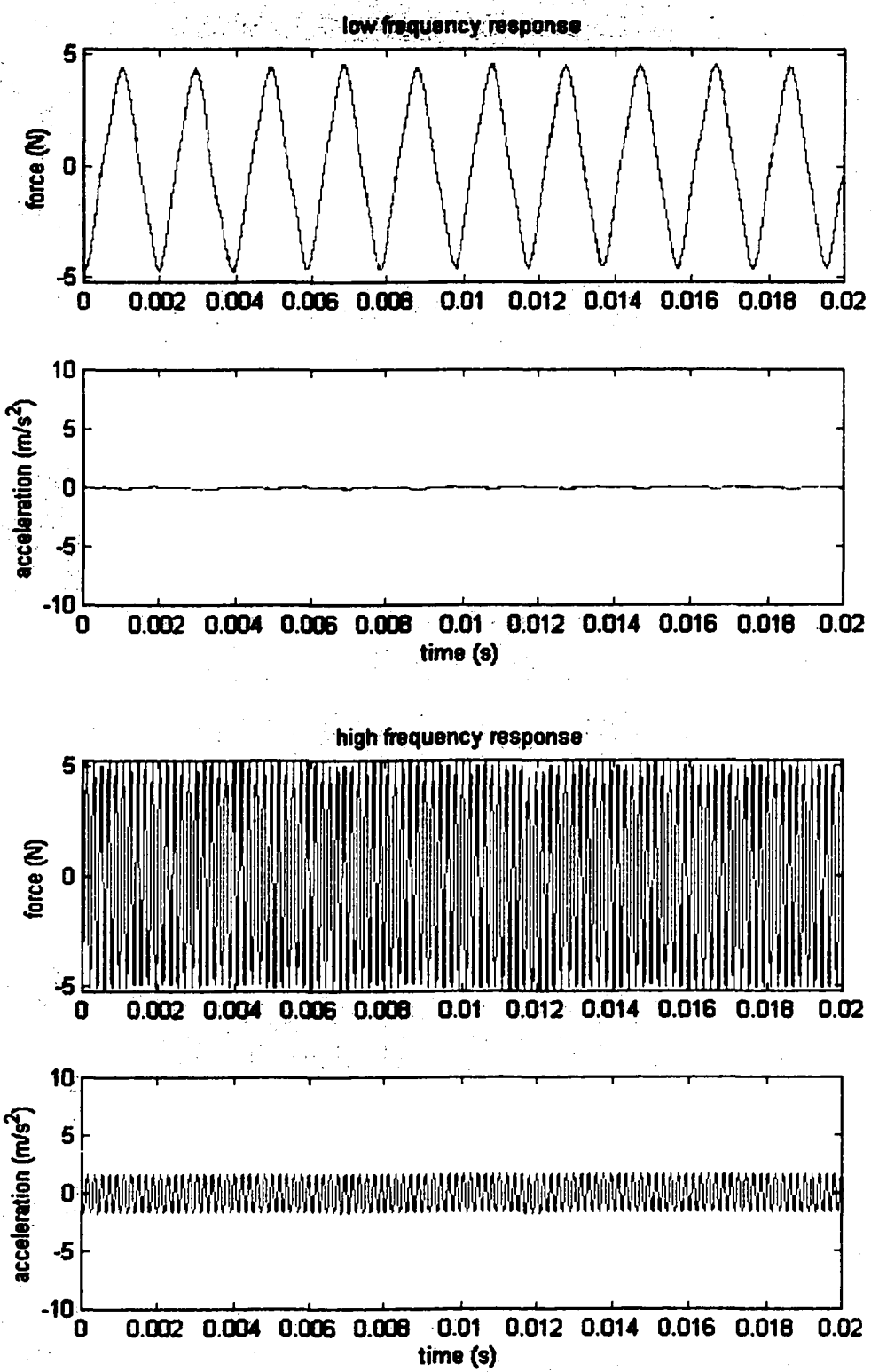


Fig.3.10 Measured Low Frequency and High Frequency Responses

### 3.4 Vibration Prediction Model

The transfer function of the stator vibrations and the normal forces acting on the stator is composed of a sum of second order high-pass filters. It can be written as (transfer function from stator-rotor normal force to stator acceleration):

$$H(s) = \frac{a(s)}{F(s)} \cong \sum_i A_i \frac{s^2}{s^2 + 2\zeta_i \omega_{ni} s + \omega_{ni}^2} \quad (3-22)$$

Where  $\omega_{ni}$  is the resonant natural frequency of mode  $i$ ,  $\zeta_i$  is the damping ratio of mode  $i$ ,  $A_i$  is the gain relative to mode  $i$ , and  $s$  is the Laplace variable.

Fig.3.11 shows the simulation block of the transient vibration in the SRM. The normal force is calculated from the look-up table shown in Fig.2.6, using phase current results from the simulation described in the previous chapter.

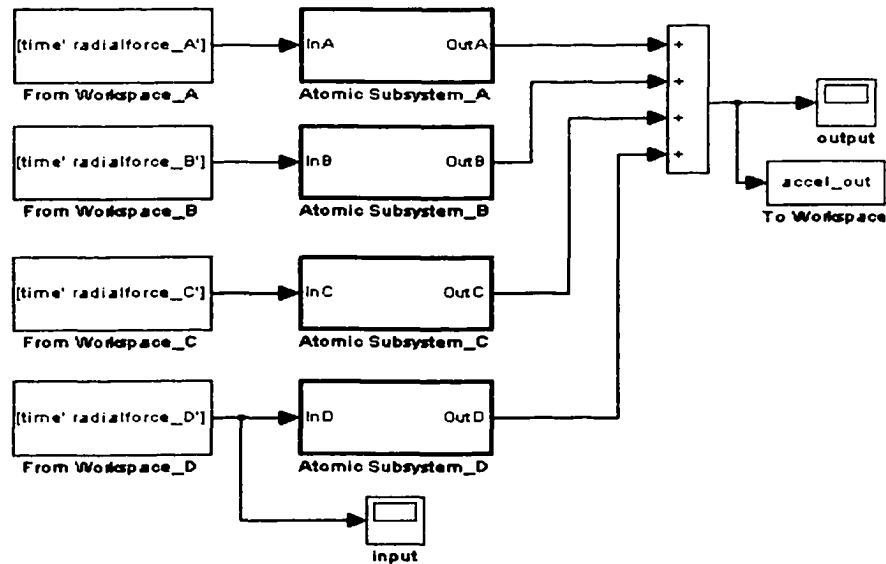


Fig.3.11 Transient Vibration Simulation from Normal Force to Stator Acceleration

The input of the model shown in Fig.3.11 is from the previous chapter, the normal force calculated from measured phase current or simulated current, using the normal force look-up table. The output will be the simulated acceleration response. The simulated acceleration response is a maximum in the area of the peak of the mode shape. For accelerations in other areas, a correction factor should be added, which will be a sinusoidal function of the angle deviation from the peak area of the mode shape.

This method of simulation uses the time signal as an input directly to the SIMULINK model. It is time-consuming because the phase current waveform is composed of thousands of data points. The transfer function model based on sinusoidal excitation tests described in the previous section is used in this model. The simulation result will be compared with the measured stator acceleration in the next section.

### **3.5 Vibration Prediction Results**

#### **3.5.1 Running Motor Test Results**

Fig.3.12 shows the test setup for the running SRM acceleration experiment. The SRM is controlled by a TASC Drive, from which the speed is adjustable. The SRM is suspended by four ropes from a solid bench to maintain a free vibration condition. Acceleration responses from two different locations of the machine stator are recorded via the storage oscilloscope, from 500RPM to 1,700RPM in steps of 50RPM. Another storage oscilloscope (not enough channels in one oscilloscope) is used to record the phase current waveform of the SRM. The current waveform can be used in the previously described look-up table for the normal force, and used in the model shown in Fig.3.11 for predicting the stator vibration.

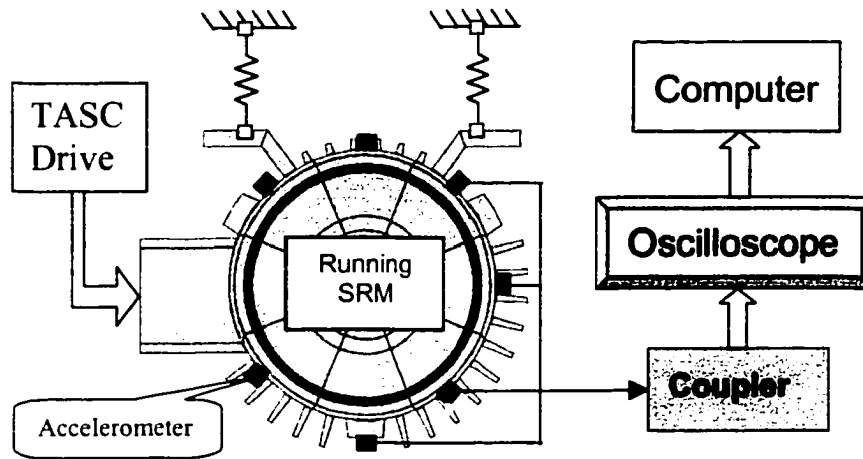


Fig.3.12 Test Setup of Running SRM Acceleration Experiment

Fig.3.13 shows the time and frequency domain acceleration response under one of the selected 25 different speeds (1450RPM). The frequency domain response is more useful and straightforward. As seen in the figure, a peak can be easily observed. The responses under all other speeds are recorded and analyzed in the same way, and are plotted in Fig.3.16, Fig.3.17 and Fig.3.18. This experiment is done under no-load.

Fig.3.14 shows the calculated normal force at 1450rpm, using the measured phase current (steady current at 1450rpm), the FFT of the normal force and simulated stator acceleration, in both the time and frequency domains.

In the time domain, the measured stator acceleration has the same scale as that in the simulated result, although they are not exactly the same. However, as seen in the frequency domain, they have the same magnitude at the resonant frequency.

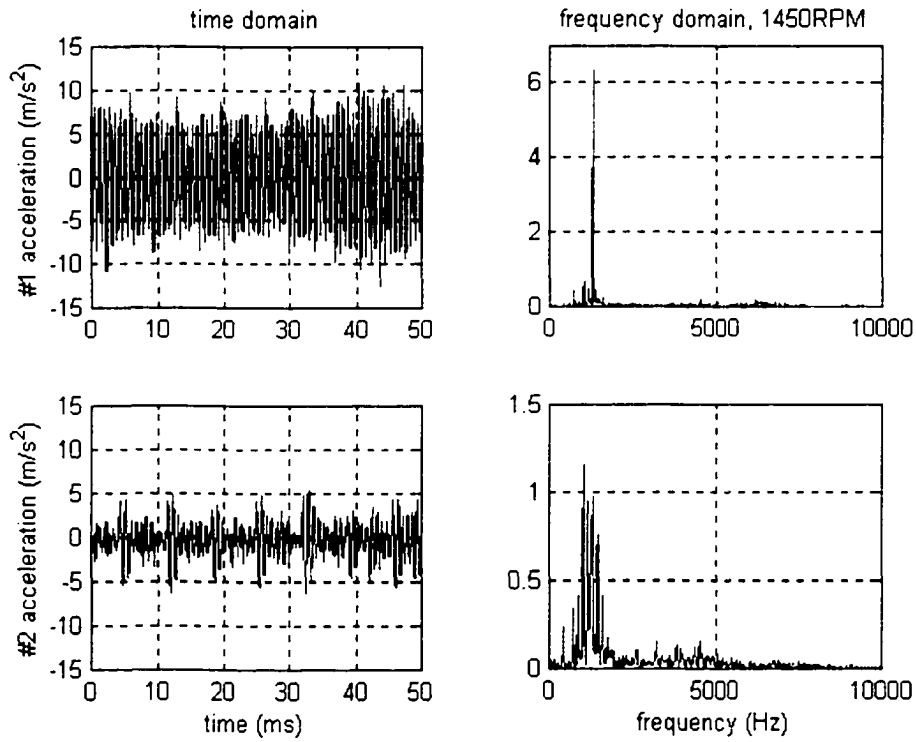


Fig.3.13 Measured Acceleration Response in Time & Frequency Domains at a Speed of 1450RPM

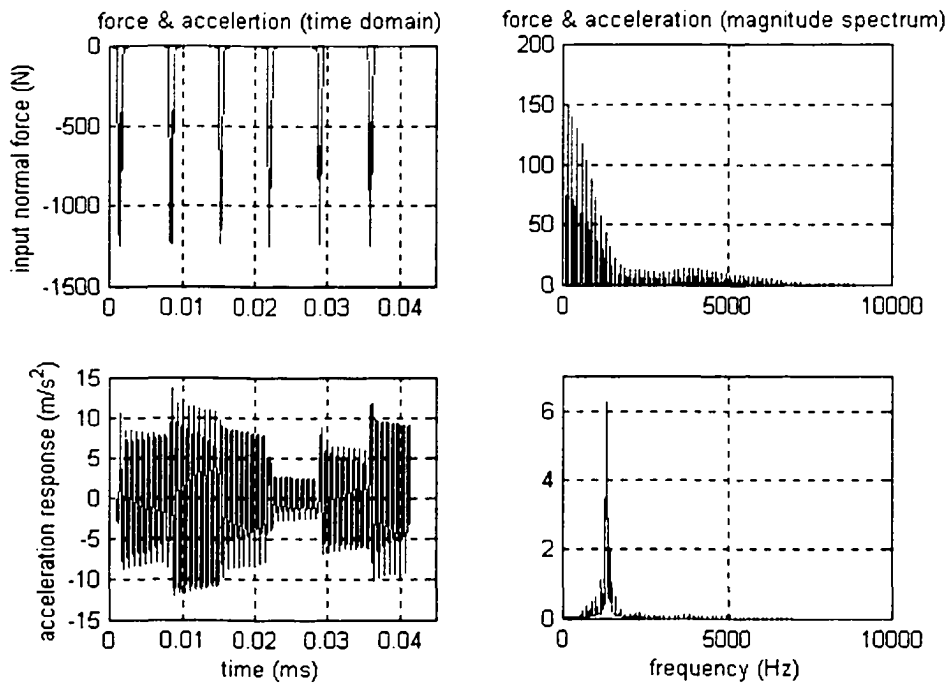


Fig.3.14 Input Normal Force and Predicted Output Acceleration Using the Vibration Prediction Model and Measured Current

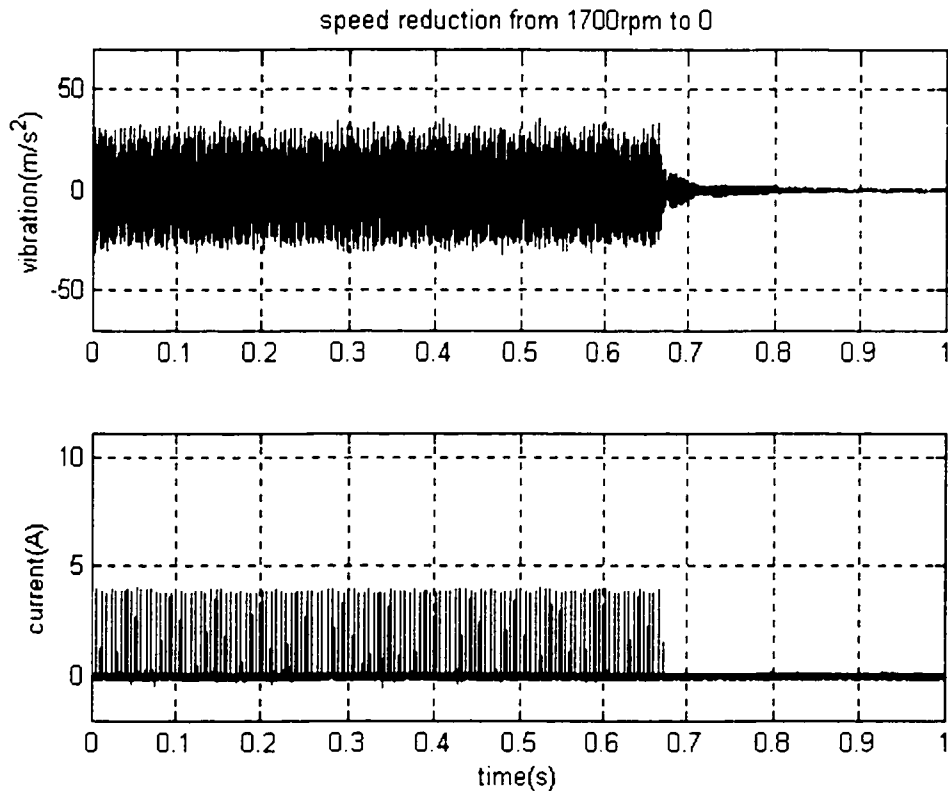


Fig.3.15 Measured Transient Stator Vibration and Phase Current during Power-off

Fig.3.15 shows the stator vibration after the motor is shut down. It is clearly shown that when there is no current in the phase winding, there will not be a normal force between the stator and rotor poles, hence a rapid reduction in the stator vibration.

Fig.3.16 shows the 3-D view of the magnitude spectra of acceleration responses measured at different speeds (500rpm to 1700rpm, in steps of 50rpm) at two locations of the SRM stator. Fig.3.17 shows the Speed-Magnitude view of acceleration responses, and Fig.3.18 shows the Frequency-Magnitude view of acceleration responses.

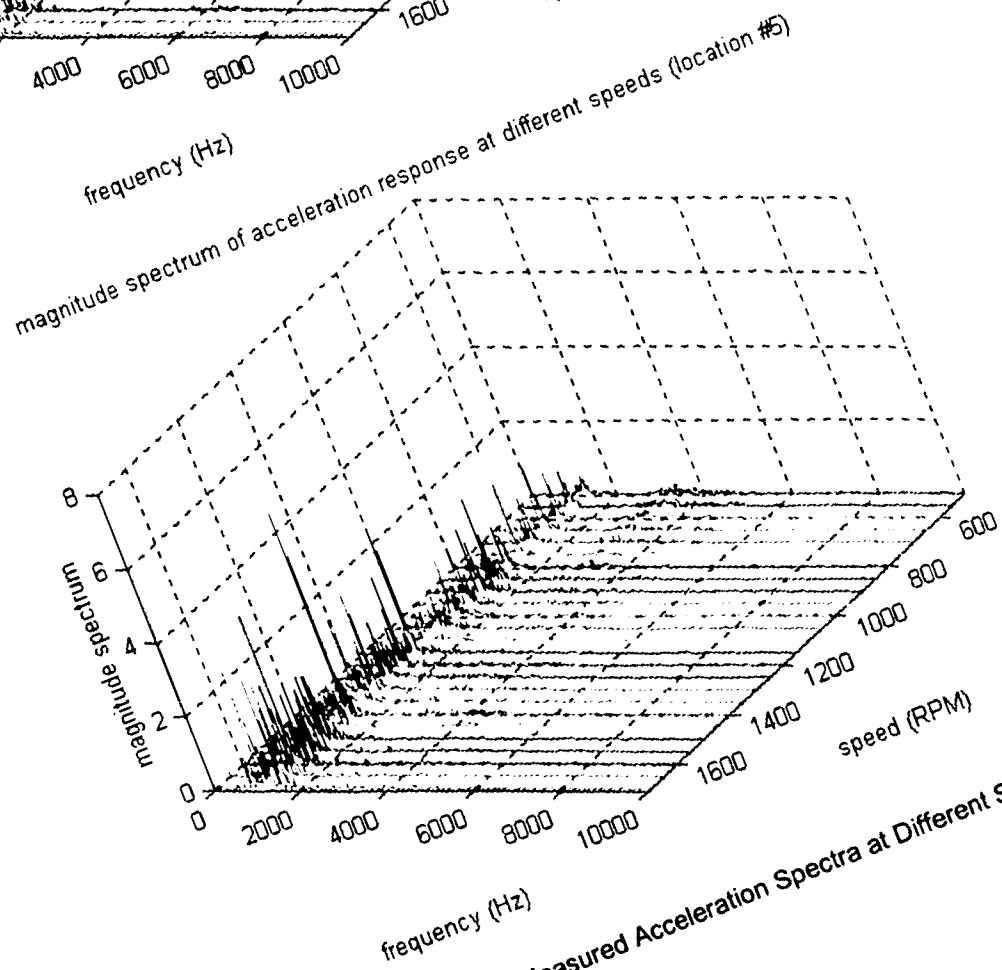
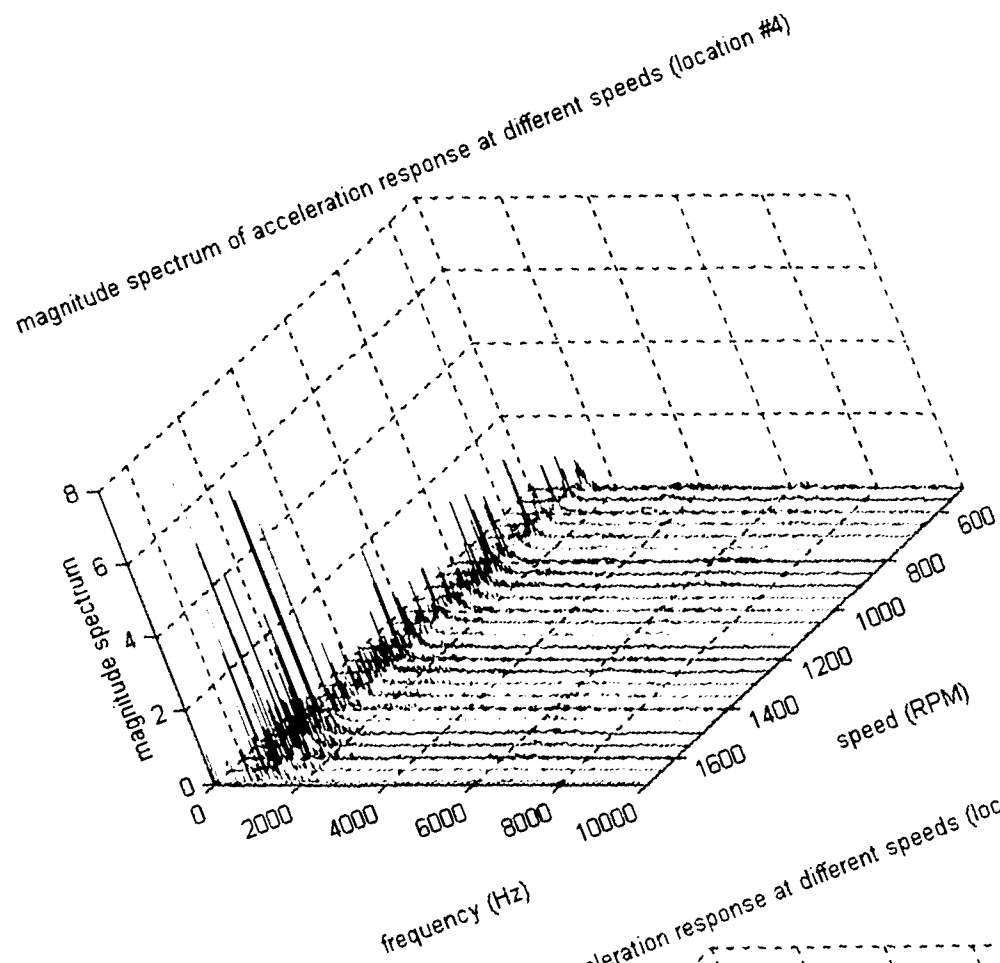


Fig.3.16 3-D View of Measured Acceleration Spectra at Different Speeds

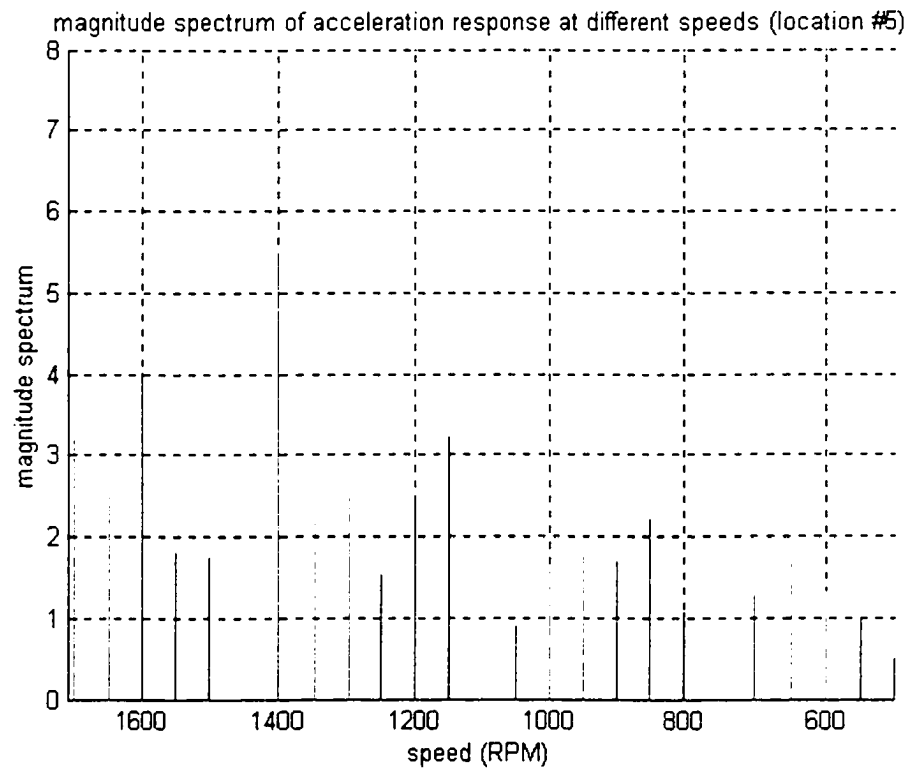
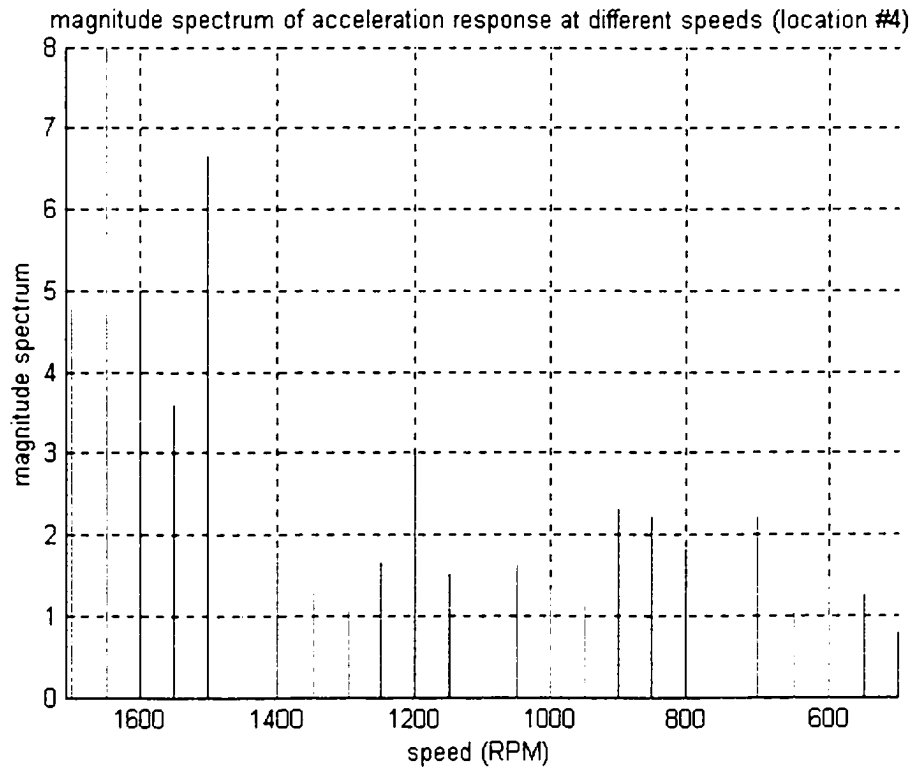


Fig.3.17 Speed-Magnitude View of Measured Acceleration Response



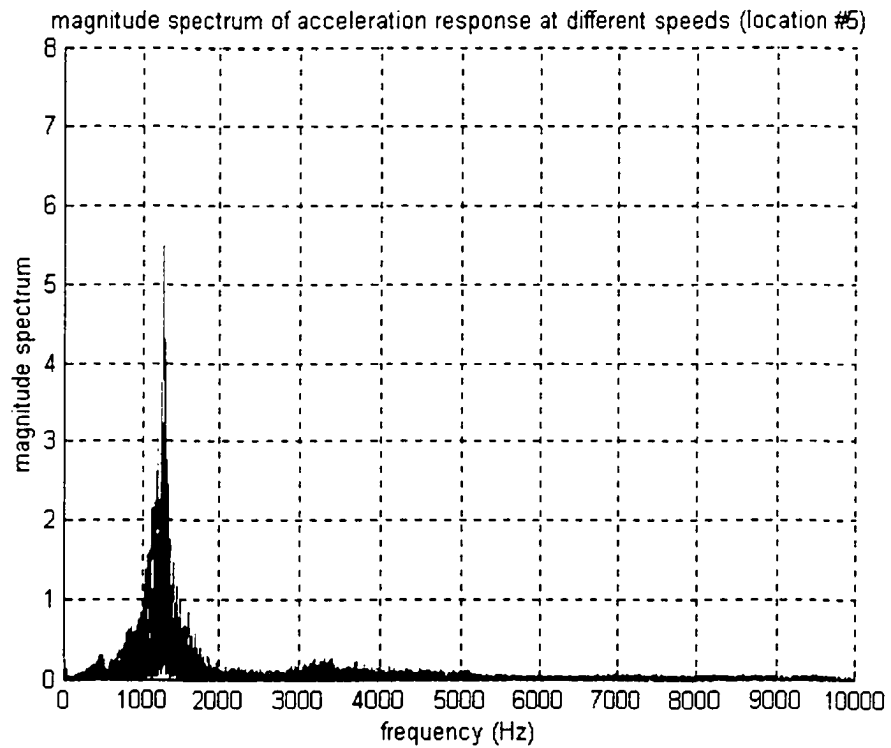
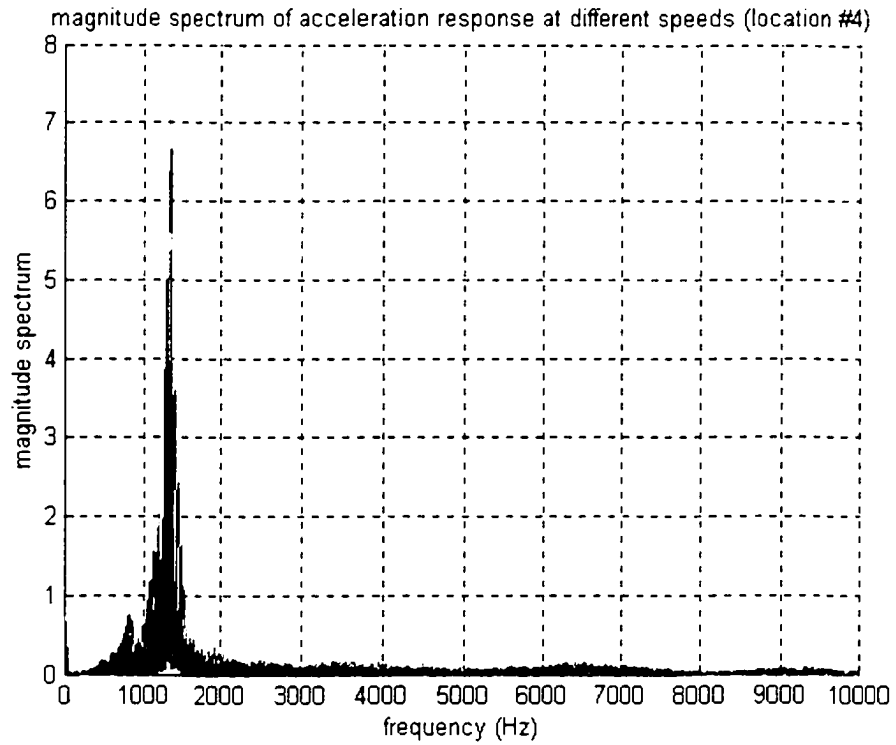


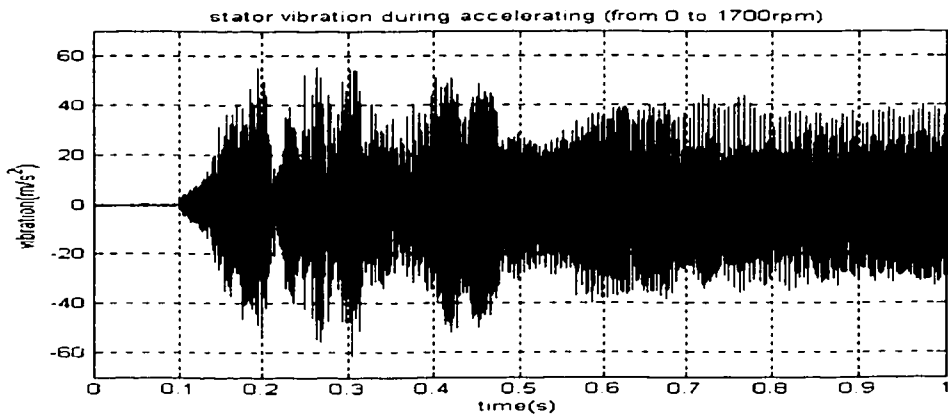
Fig.3.18 Frequency-Magnitude View of Measured Acceleration Response

For the running motor test, there is always a peak in the vibration acceleration response in the frequency domain, which is around 1,345Hz, the 2<sup>nd</sup> mode resonant frequency for the test motor. Secondly, the vibration acceleration is dominant around the 2<sup>nd</sup> resonant frequency when compared to the other frequencies. Thirdly, at any speed, the vibration acceleration is different at different locations on the motor. Finally, the vibration acceleration response of all frequencies except the 2<sup>nd</sup> mode resonant frequency are negligible because of their much lower magnitudes.

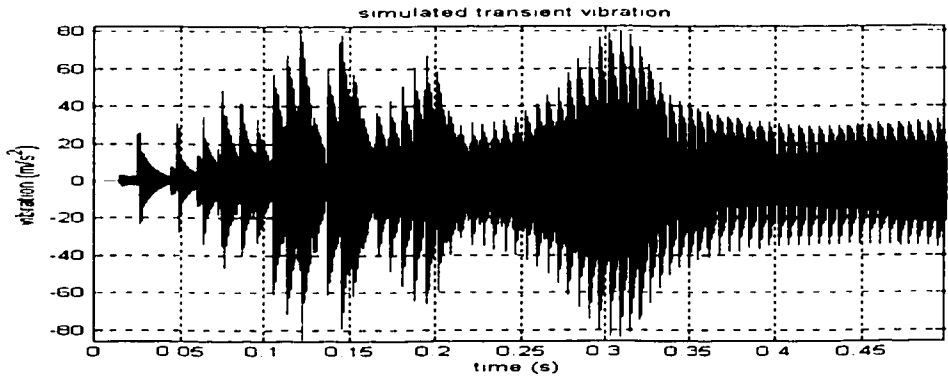
### **3.5.2 Transient Vibration Prediction**

The calculated radial forces described in Chapter 2 are used in the vibration simulation model shown in Fig.3.11. Fig.3.19 shows the comparison between the measured and simulated stator accelerations during start-up of the motor. The results have the same scale although they are not exactly the same. The discrepancy is because the control topology of the driver used for experiment is unknown, which results in slightly different phase currents, especially during the low speed phase of motor acceleration.

Using the normal forces calculated in Chapter 2, Fig.3.20 shows the simulated stator accelerations during motor accelerating, sudden change of load and braking, using the model shown in Fig.3.11. It shows that the stator vibration increases with an increase of rotor speed and then reaches steady state, as the motor speed becomes constant.



(a) Measured Stator Vibration during Accelerating (0 to 1700rpm)



(b) Simulated Stator Vibration during Accelerating (using Measured Current)

Fig.3.19 Comparison of Measured and Simulated Stator Vibration during Accelerating

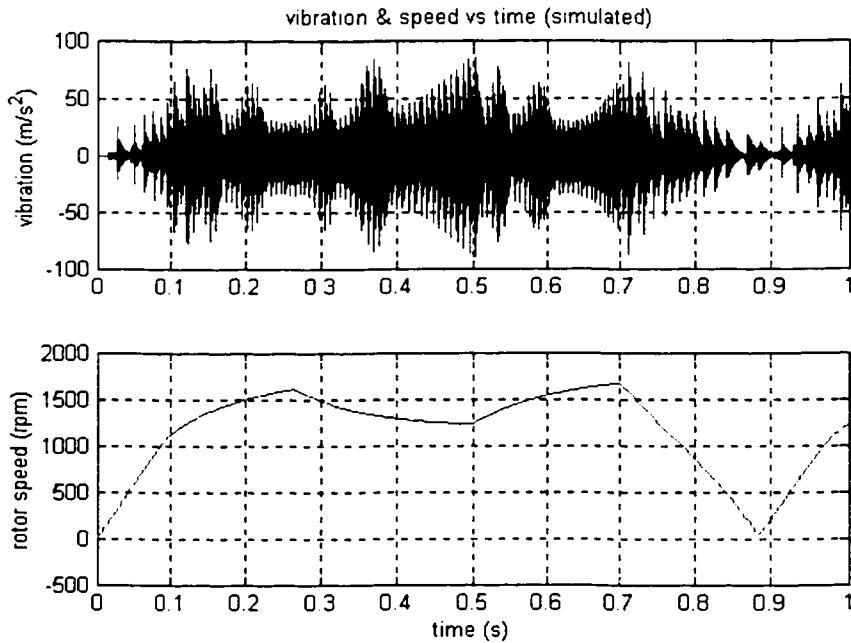


Fig.3.20 Simulated Stator Acceleration vs. Motor Speed

### **3.6 Conclusions**

The transfer function from normal force to vibration (stator acceleration) is constructed in this chapter, using a Sinusoidal Excitation Test. A vibration prediction simulation model is built using Matlab/SIMULINK for the transfer function. High frequency and low frequency responses are simulated using this model.

Using the vibration prediction model and normal force calculated in Chapter 2, the stator vibration of the SRM is predicted here, both in the time and frequency domains. The predicted accelerations are compared with the measured results.

Motor running tests are done in this chapter. Vibrations at different speeds are measured together with the phase current waveform. The results are compared with the predicted vibration described in the previous chapter, with acceptable accuracy.

With the power of vibration prediction, the designers of SRMs can develop optimal designs in order to reduce the vibrations in the SRM, through the control of phase current waveform, turn-on and turn-off angles and speed of the motor. This model will also be useful in simulating the vibration under multiple-phase operation, controller design, etc.

This model is verified here using running motor tests, which shows reasonable accuracy. The tests are done under no-load, where the current level is low. The simulation results (including start-up, sudden change of load and braking operations) will be more practical if tests are under load. A dSPACE-based controller is needed to control the speed, turn-on and turn-off angle, so that the model can be better verified.

## Chapter 4

# Analysis of Mounting Effects on Vibrations of SRMs

### 4.1 Summary

SRMs are attracting considerable interest because of its advantages relating to manufacturing and robustness. In order to solve the acoustic noise and vibration problems, research has been done on the free vibration tests and modeling. However, the effects of mountings on the vibrations in the SRM have been neglected. In many industrial applications, vibrations and acoustic noise of electric machines are sensitive to motor mountings. This chapter examines the effects of the mounting and in particular the deviation from free vibration results.

### 4.2 Introduction

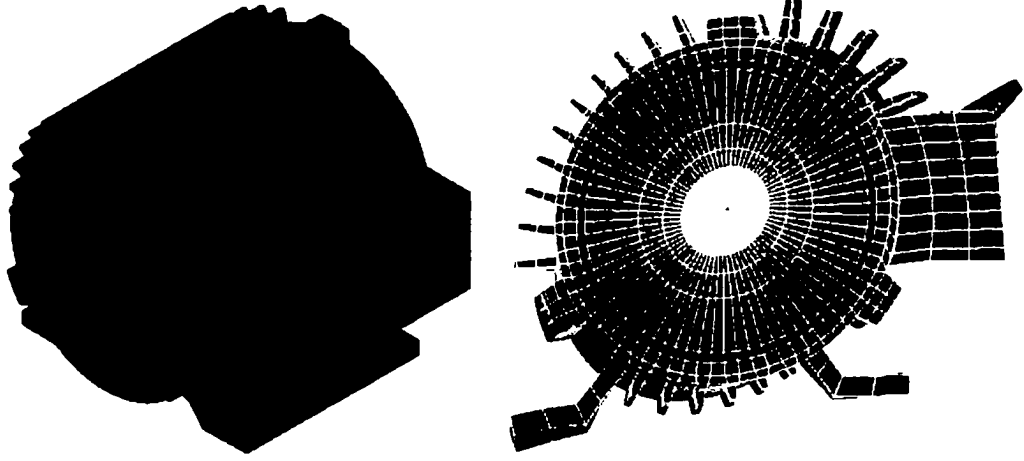
Vibrations in the switched reluctance motor are known to be caused by the ovalizing deformation of the stator lamination stack due to its radial magnetic attraction to the rotor [21]. Thus far, research on the SRM vibrations has concentrated on free vibration tests and calculations [25,30,31,32]. The effects of mountings on the vibrations of the SRM have been neglected. As is well known, in many industrial applications, vibration and acoustic noise of electric machines are very sensitive to the motor mountings. There has been some work done on other machines [48], but the effects on the SRM remains unknown.

This chapter investigates the effects of mountings on the vibrations in the SRM using Finite Element calculations and impact hammer test results. The calculated and test results are compared to verify the validity of the theoretical methods. Firstly, the finite element method is used to calculate the resonant frequencies for free vibrations and different mounting conditions. Secondly, vibration tests are done with different mountings: free hanging, foot-mounted on a plate with rubber cushions and foot-mounted on a plate without rubber cushions. The results are summarized in the form of guidelines for mounting.

### **4.3 Finite Element Calculations**

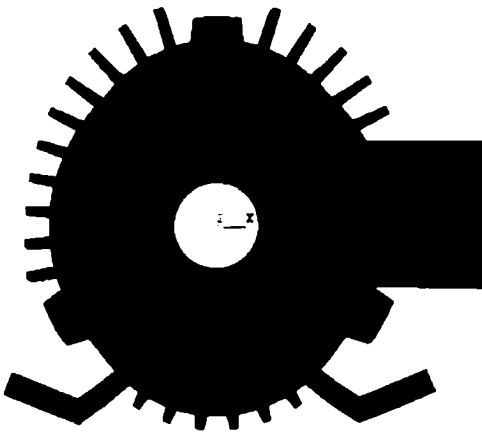
A 4kW 8/6 4-phase SRM is used for research in this chapter. The FE model is constructed according to the actual motor dimensions, with winding effects considered. The complex structure of the motor is carefully defined, with end-bells, cooling fins, mounting feet and terminal box. Fig.4.1(a) shows the mesh for the entire motor (no rotor) using ANSYS. Vibration calculations can be done here with different boundary conditions: free vibration, foot-mounted, or face-mounted.

For free vibration calculations, no constraints have been defined for the model. Fig.4.1(b)~(f) show mode shapes at different orders, with 2<sup>nd</sup> mode resonant frequency at 1259.9Hz and 1325.5Hz. The other resonant frequencies are 2595Hz for the 3<sup>rd</sup> mode, 3639Hz and 5183Hz for the 4<sup>th</sup> mode.

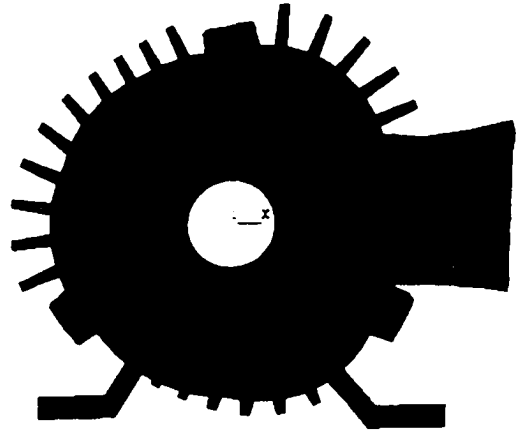


(a) FE Model for free vibration

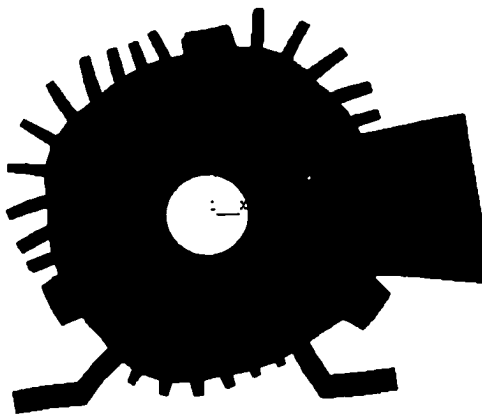
(b) 2<sup>nd</sup> Mode at 1259.9Hz



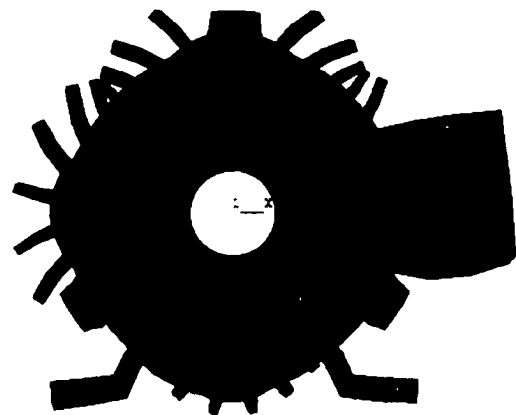
(c) 2<sup>nd</sup> Mode at 1325.5Hz



(d) 3<sup>rd</sup> Mode at 2595Hz



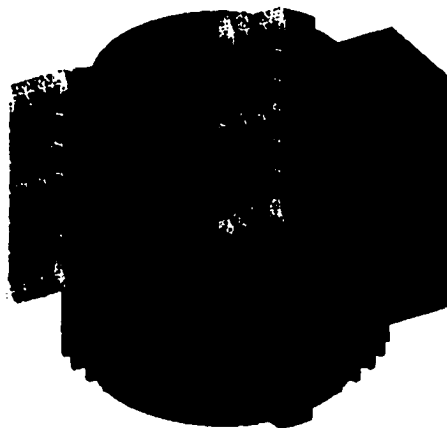
(e) 4<sup>th</sup> Mode at 3639Hz



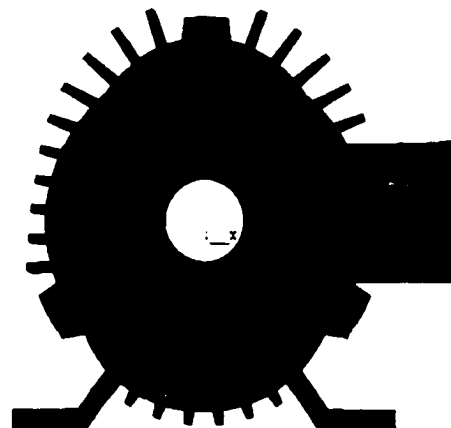
(f) 4<sup>th</sup> Mode at 5183Hz

Fig.4.1 Free Vibration FE Model and Mode Shapes

In the foot-mounted case (including foot-mounted without rubber cushions and with cushions), the mounting feet areas (at the bottom surfaces around the mounting bolts) are defined as no displacement, which is equivalent to mounting the SRM on an infinite base. Fig.4.2(a) shows the FE model for foot-mounted vibration analysis. Fig.4.2(b) and (c) show the 2<sup>nd</sup> mode shapes at resonant frequencies of 1367.4Hz and 1423Hz. Note that one of the 2<sup>nd</sup> mode resonant frequencies is changed to be 1364.7 Hz, very close to the free vibration result (which is 1325.5Hz), a 3.0% difference in the frequency. Three other motions are found in this condition, they are 408.3Hz, 636.5Hz and 909.6Hz respectively, referring to the motor swinging around the mounting feet in three different axes. They are not emphasized here because the electromagnetic forces in the motor would not normally excite these modes. The other higher order mode shapes are shown in Fig.4.2(d)–(f), with the 3<sup>rd</sup> mode resonant frequency at 2791Hz, 4<sup>th</sup> mode resonant frequencies at 3498Hz and 5357Hz. Compared with free vibration results, they have differences of 7.6%, 3.9% and 3.4% respectively. They are less important compared with the 2<sup>nd</sup> mode. The effect of rubber cushions cannot be easily modeled here. It is assumed that rubber cushions work as dampers, and they don't change the resonant frequencies.



(a) FE Model for Foot-mounted



(b) 2<sup>nd</sup> Mode at 1364.7Hz



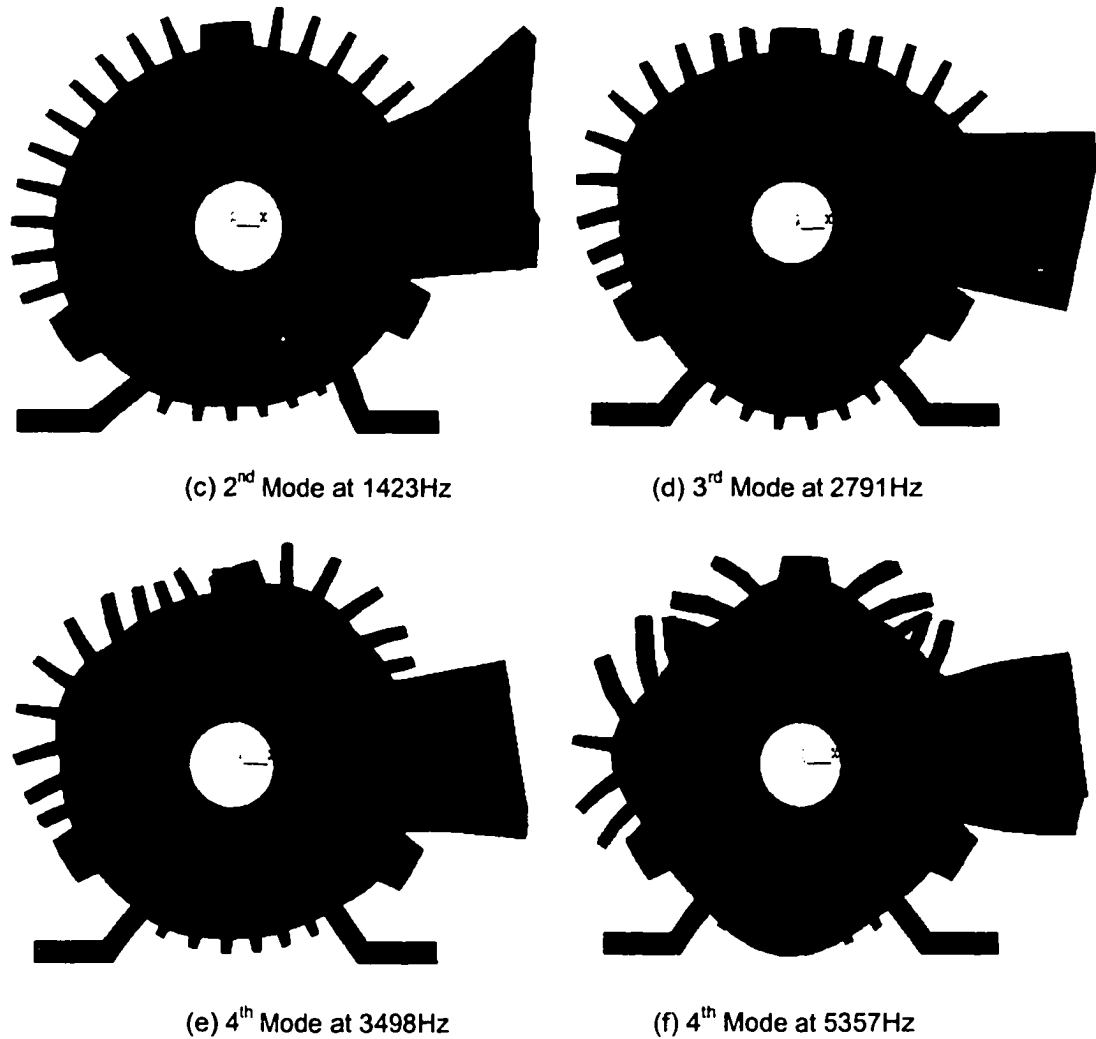
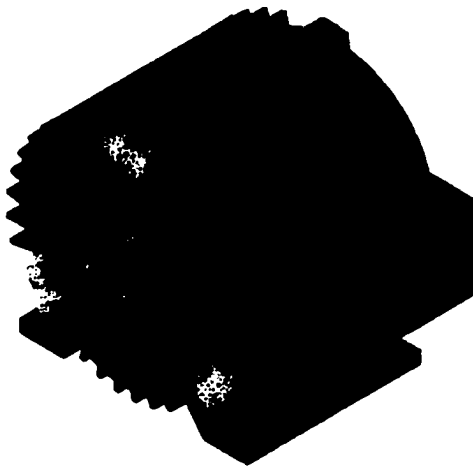


Fig.4.2 Foot-mounted FE Model and Mode Shapes

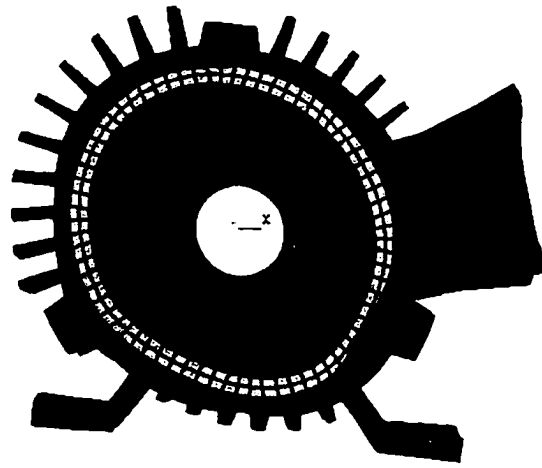
Fig.4.3(a) shows the FE model for the face-mounted (with mounting feet still attached) vibration calculation. One end-bell is removed and three constraints (x, y and z directions) are added on the bolt areas of the stator case. The 2<sup>nd</sup> mode resonant frequencies are found to change to 1506Hz and 1623Hz, compared with 1259.9Hz and 1325.5Hz for the free hanging condition, a change of 20% and 22%. Three new resonant frequencies, namely 880.6Hz, 899.2Hz and 1337.1Hz appear. They are all connected

with out-of-plane mode shapes, which will not be considered here because they will not be excited under normal conditions.

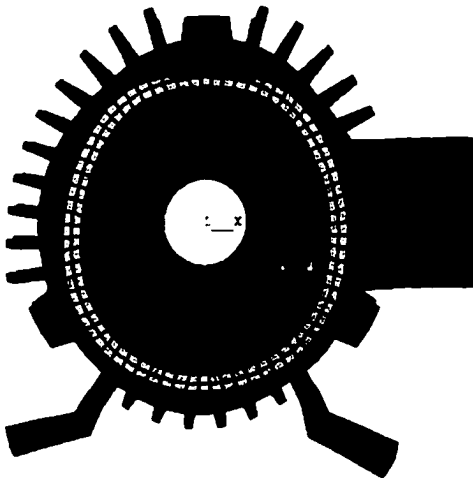
The 3<sup>rd</sup> and 4<sup>th</sup> mode shapes are identified, as shown in Fig.4.3(d), (e) and (f), with resonant frequencies of 2647Hz, 3712Hz and 5280Hz respectively. Compared with free vibration calculation results (2595Hz for the 3<sup>rd</sup> mode, 3639Hz and 5183Hz for the 4<sup>th</sup> mode), the differences are 2.0%, 2.0% and 1.8% respectively.



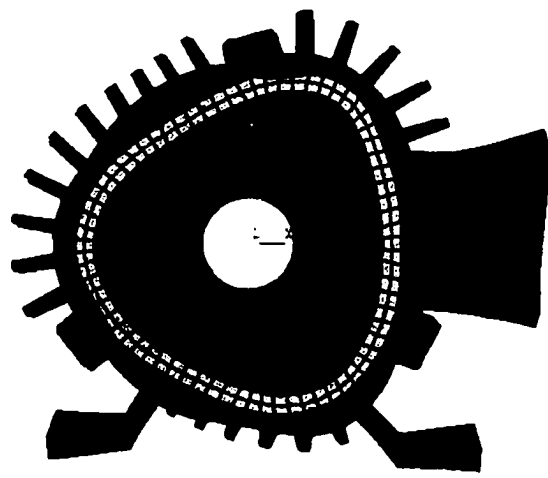
(a) FE Model for Face-mounted (with mounting feet)



(b) 2<sup>nd</sup> Mode of 1506Hz



(c) 2<sup>nd</sup> Mode of 1623Hz



(d) 3<sup>rd</sup> Mode of 2647Hz

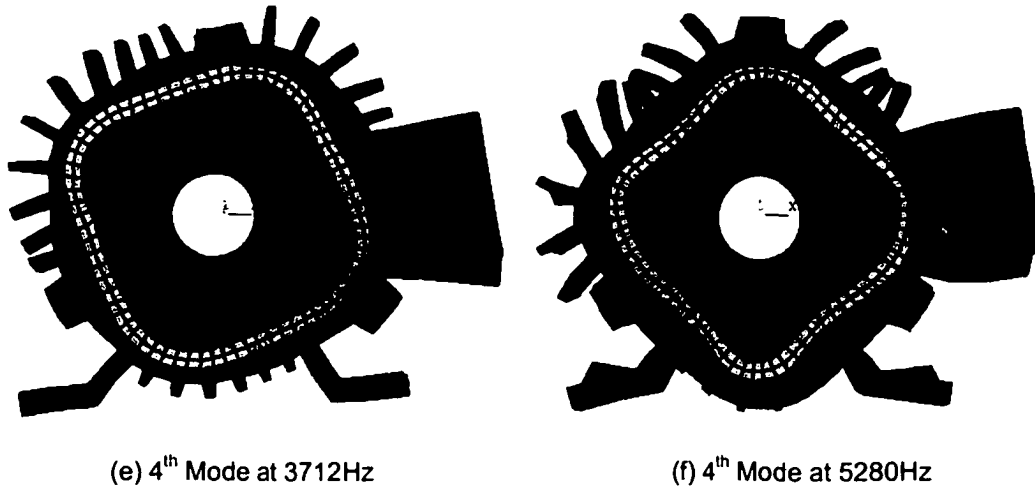
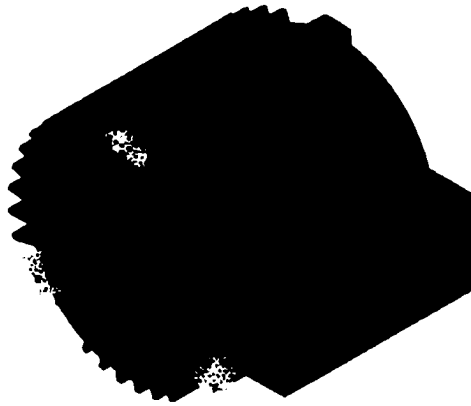


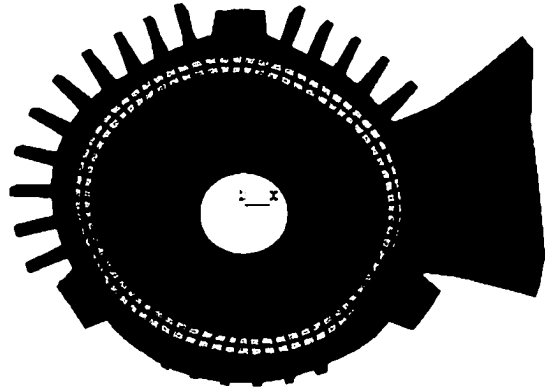
Fig.4.3 Face-mounted FE Model and Mode Shapes (with mounting feet)

Fig.4.4(a) shows the FE model for the face-mounted vibration calculation with mounting feet removed. Constraints (x, y and z directions) are added on three bolt areas of the stator case. The 2<sup>nd</sup> mode resonant frequencies are found to change to 1589.4Hz and 1604.5Hz (close to the frequencies of foot-mounted with mounting feet), compared with 1259.9Hz and 1325.5Hz for the free vibration condition, a change of 26.2% and 21.0%. Three new resonant frequencies, namely 896.5Hz, 932.4Hz and 1567.3Hz appear (both higher than the frequencies in foot-mounted with mounting feet case). They are all connected with out-of-plane mode shapes, which will not be considered here because they will not be excited under normal conditions.

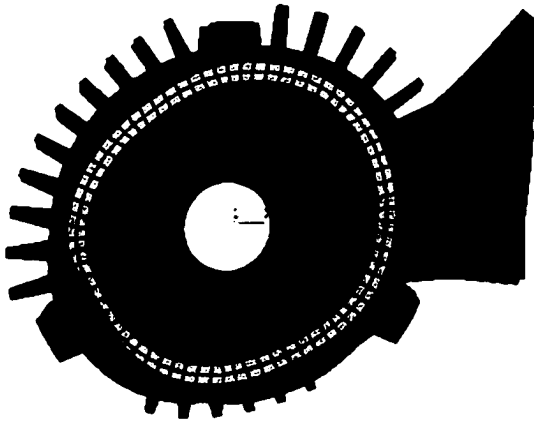
The 3<sup>rd</sup> and 4<sup>th</sup> mode shapes are identified, as shown in Fig.4.4(d), (e) and (f), with resonant frequencies of 2726Hz, 3729Hz and 5314Hz respectively. Compared with free vibration calculation results (2595Hz for the 3<sup>rd</sup> mode, 3639Hz and 5183Hz for the 4<sup>th</sup> mode), the differences are 5%, 2.5% and 2.5% respectively.



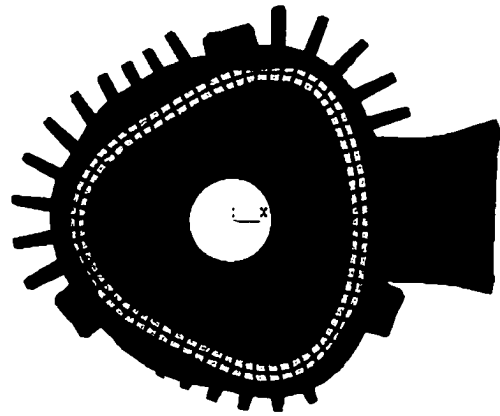
(a) FE Model for Face-mounted (without mounting feet)



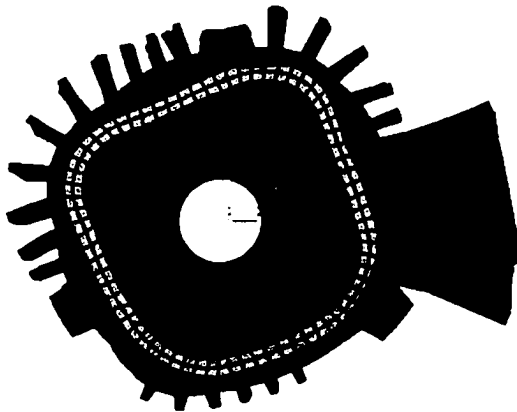
(b) 2<sup>nd</sup> Mode at 1589.4Hz



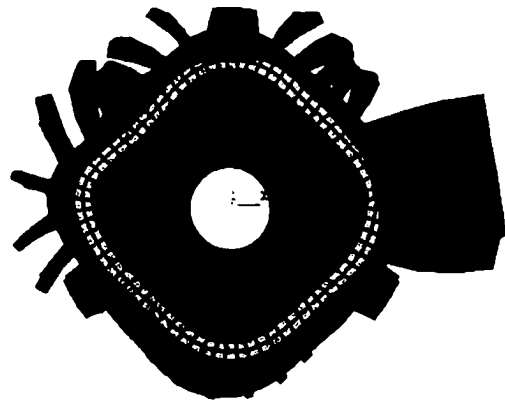
(c) 2<sup>nd</sup> Mode at 1604.5Hz



(d) 3<sup>rd</sup> Mode at 2726Hz



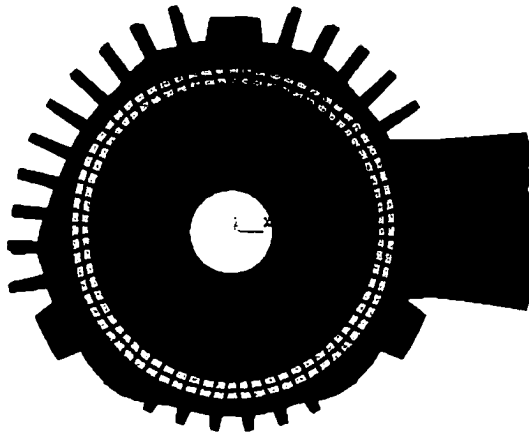
(e) 4<sup>th</sup> Mode at 3729Hz



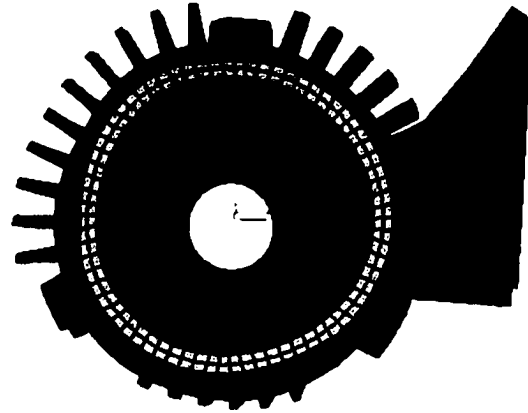
(f) 4<sup>th</sup> Mode at 5314Hz

Fig.4.4 Face-mounted FE Model and Mode Shapes (without mounting feet)

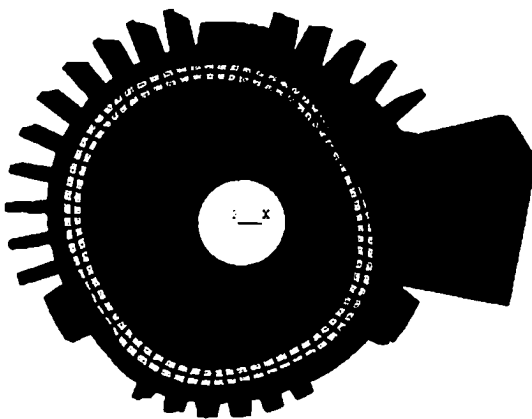
Fig.4.5 shows some other mode shapes that cannot be identified clearly in terms of modes because they are too complicated. Normally they won't be excited by electromagnetic normal forces.



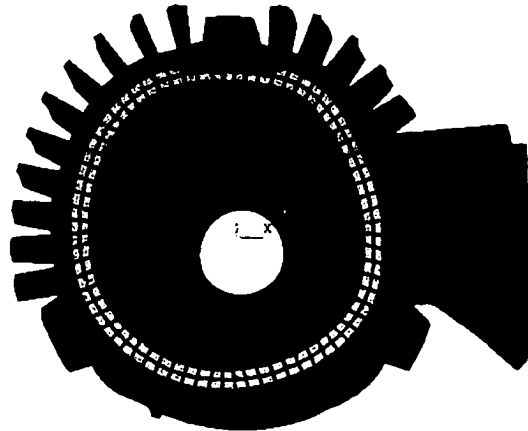
(a) Mode Shape at 1832Hz



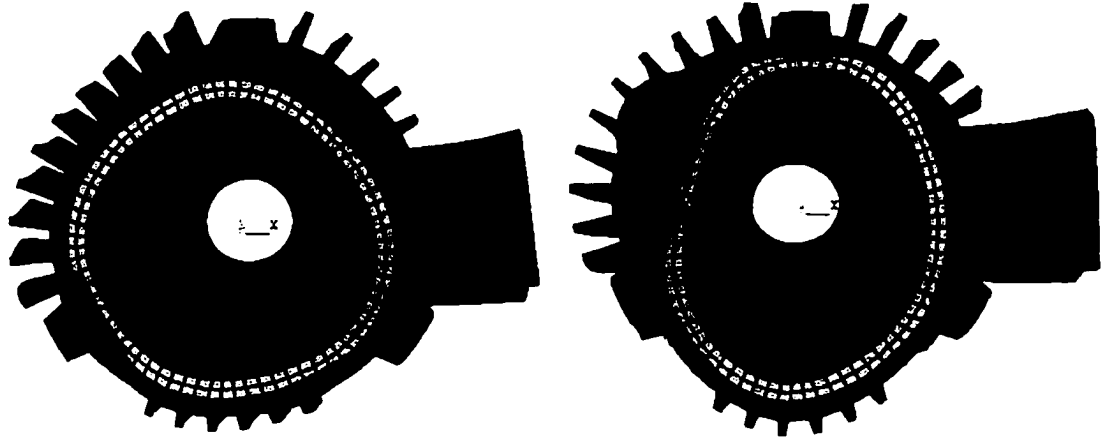
(b) Mode Shape at 1989Hz



(c) Mode Shape at 2156Hz



(d) Mode Shape at 2231Hz



(e) Mode Shape at 2279Hz

(f) Mode Shape at 2580Hz

Fig.4.5 Some Complicated Mode Shapes

Table 4.1 shows the FE results of resonant frequencies of different modes under different mounting conditions, including percentage errors. Compared with the free vibration condition, most of resonant frequencies rise, which can be beneficial since it is less likely to be excited by low frequency excitation. The 2<sup>nd</sup> mode resonant frequencies rise substantially, especially for the face-mounted case. The results show that the mounting effect has to be considered for the research of SRM vibrations.

Table 4.1 Comparisons of FE Results under Different Mounting Conditions

	Free Vibration	Foot-mounted	Face-mounted (with mounting feet)	Face-mounted (without mounting feet)
2 <sup>nd</sup>	1259.9Hz	1423Hz (12.9%)	1506Hz (19.5%)	1589.4Hz (26.2%)
	1325.5Hz	1364.7Hz (3.0%)	1623Hz (22.4%)	1604.5Hz (21.0%)
3 <sup>rd</sup>	2595Hz	2791Hz (7.6%)	2647Hz (2.0%)	2726Hz (5.0%)
4 <sup>th</sup>	3639Hz	3498Hz (-3.9%)	3712Hz (2.0%)	3729Hz (2.5%)
	5183Hz	5357Hz (3.4%)	5280Hz (1.9%)	5314Hz (2.5%)

## 4.4 Vibration Tests under Different Mounting Conditions

### 4.4.1 Test Setup and Procedure

Fig.4.6 is the experimental setup for the impulse hammer excitation for the free vibration test of the SRM. A modal hammer (ENDEVCO 2302-10, 500lb range, frequency range 8kHz, sensitivity 10mV/lb) is used to supply an impulse force signal (broad band force excitation). The setup is the same as that of the shaker excitation experiment, except that the hammer is used to supply the excitation source instead of shaker.

The procedure for the hammer excitation method is much simpler than for the shaker excitation method. The hammer can be moved anywhere for the tester's interests and convenience, which is sometimes impossible for shaker. With one hit, information for all the frequencies within interest can be recorded and ready for analysis.

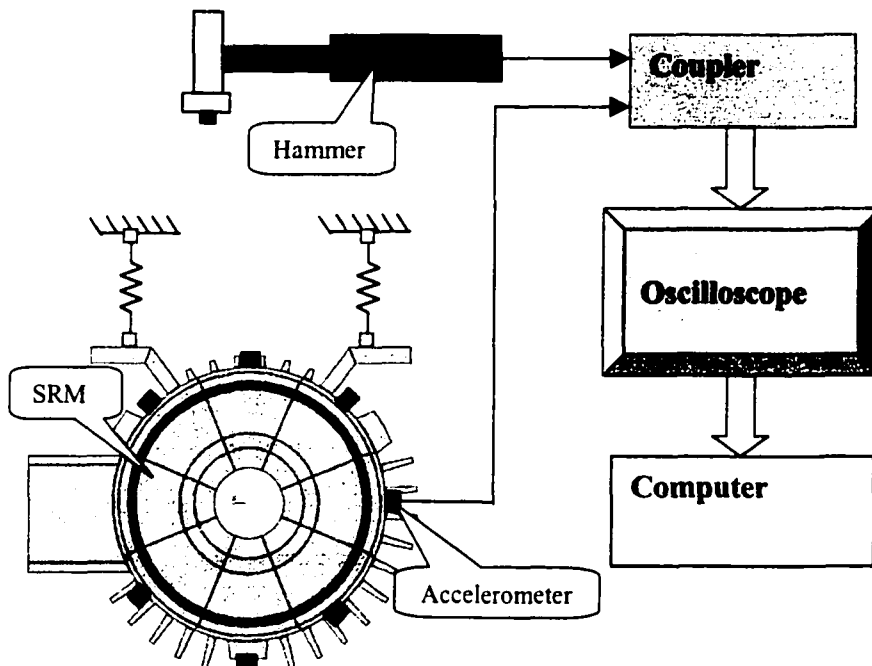


Fig.4.6 Test Setup of Impulse Force Hammer Excitation Experiment

#### 4.4.2 Test Results

Fig.4.7 shows the impulse force and measured acceleration in the frequency domain and the transfer function of the motor in the free vibration condition, where the SRM is suspended from the bench through four ropes. The 2<sup>nd</sup> mode resonant frequency of the motor is 1346.5Hz.

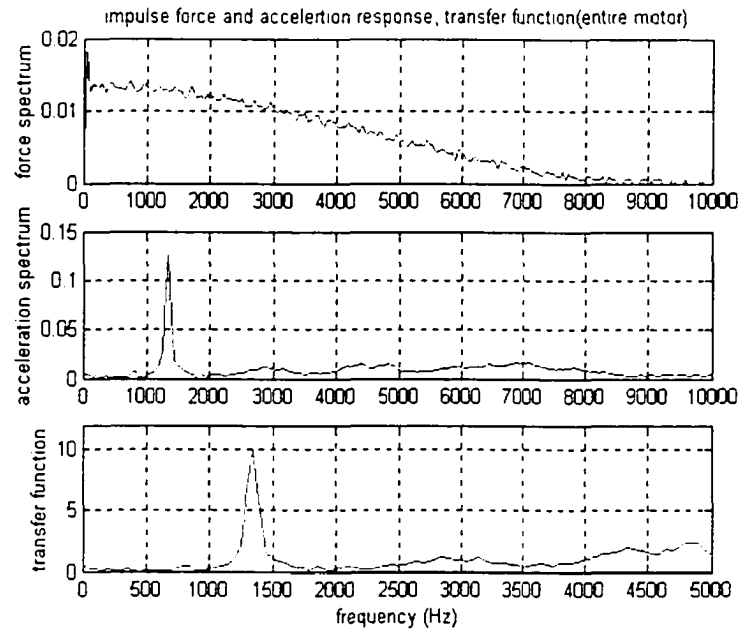


Fig.4.7 Impulse Force and Acceleration Response (free vibration)

Fig.4.8 is the impulse force and acceleration responses (in both time and frequency domains) of the SRM foot-mounted on a base plate (without rubber cushions). The resonant frequency measured is 1377.2Hz, compared to 1346.5Hz for the free vibration, a difference of 2.3% for solid foot mounting. Fig.4.9 is the impulse force and acceleration response of the SRM foot-mounted on a base plate with rubber cushions. The resonant frequency measured is 1357.3Hz, compared to 1346.5Hz for the free vibration, a difference of 0.8% for soft foot mounting. Both results are close enough to the FE result,



which is 1364.7Hz. The FE errors are 0.9% and 0.5% respectively. The difference between foot-mounted with and without rubber cushions is 1.4%.

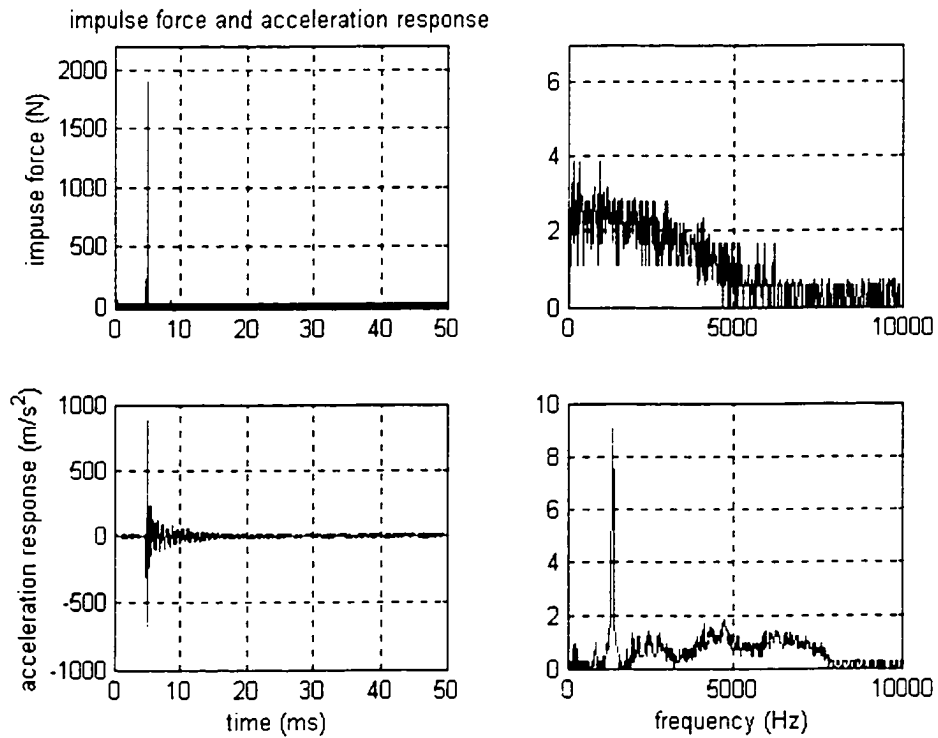


Fig.4.8 Impulse Force and Acceleration Response (foot-mounted without rubber cushions)

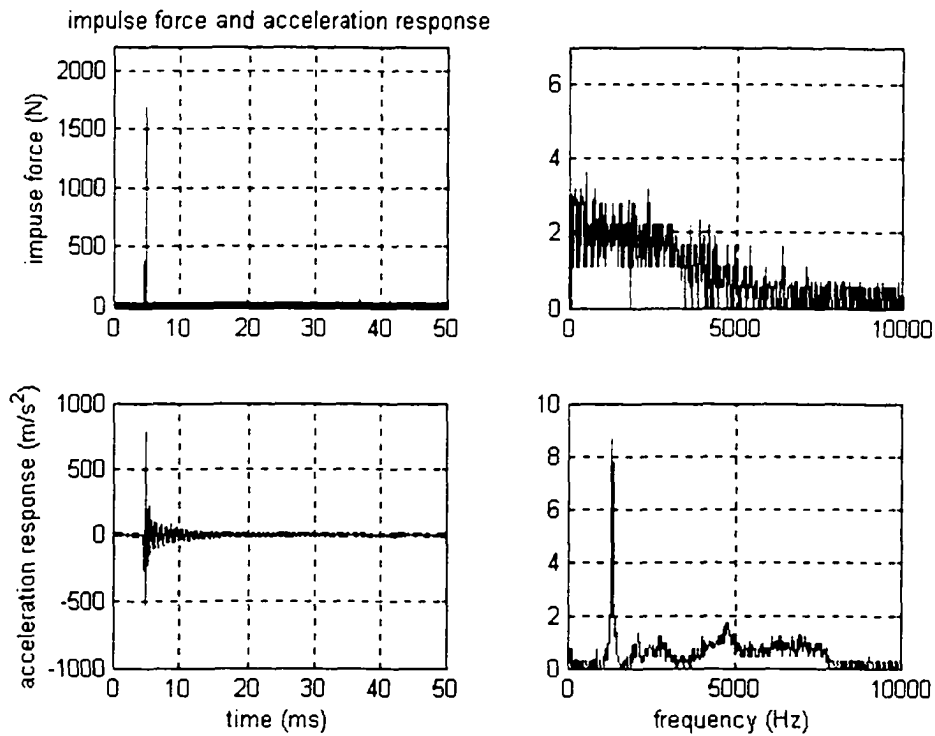


Fig.4.9 Impulse Force and Acceleration Response (foot-mounted with rubber cushions)

#### 4.5 Mounting Effects on Vibrations of SRMs

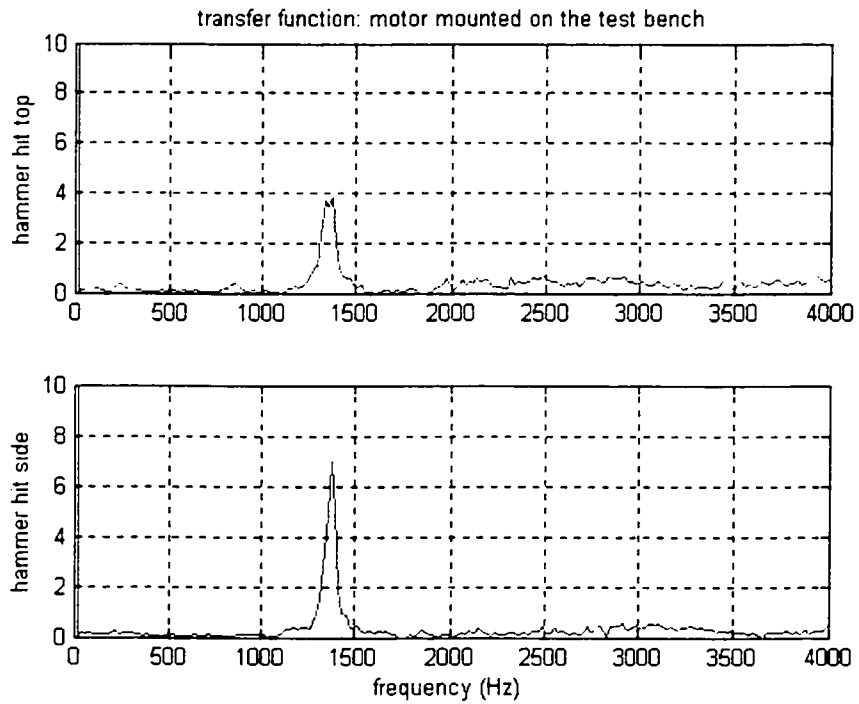
Table 4.2 lists the comparisons of FE results and force hammer test results for different mounting conditions, including the error percentages. It is shown that FE methods used in this chapter are accurate enough for the research of mounting effects on SRM stator vibrations, with all errors less than 2%.

Table 4.2 Comparisons of FE and Experimental Results

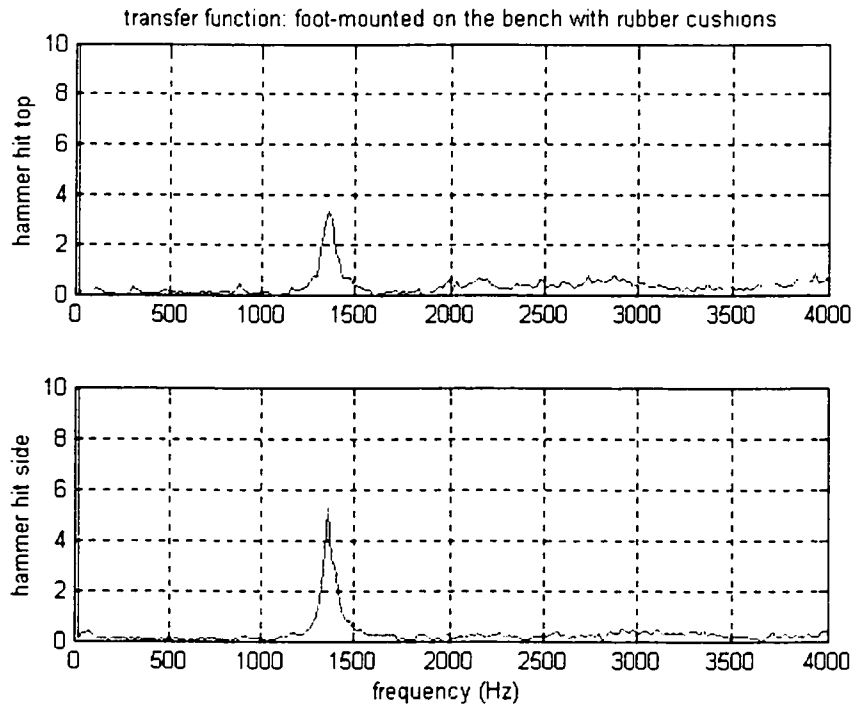
	FE Results (2 <sup>nd</sup> Mode)	Test Results	Error (%)	New Frequencies
Free Hanging	1325.5Hz	1346.5Hz	1.6	N/A
Foot-mounted (without cushions)	1364.7Hz	1377.2Hz	0.9	408.3Hz, 636.5Hz and 909.6Hz
Foot-mounted (with cushions)		1357.3Hz	-0.5	
Face-Mounted (with mounting feet)	1506Hz, 1623Hz	N/A	N/A	880.6Hz, 899.2Hz and 1337.1Hz
Face-Mounted (without mounting feet)	1589.4Hz, 1604.5Hz	N/A	N/A	896.5Hz, 932.4Hz and 1567.3Hz

Three different conditions of mountings were investigated in this chapter, foot-mounted without rubber cushions, foot-mounted with rubber cushions and face-mounted. Compared with free hanging vibration, the resonant frequencies from foot-mounted (without and with rubber cushions) are slightly different, with about a 3% increase. However the face-mounted condition changes the resonant frequency noticeably — not only do the resonant frequencies increase by more than 13%, but it also induces another 2<sup>nd</sup> mode. Both mounted cases make the mode shapes more complicated due to the bolted effects. The impulse force hammer experiment results show that the FE calculations of resonant frequencies are accurate enough for the research of mounting effects on SRM vibrations, with errors less than 2%.

Fig.4.10(a) and (b) compare the effects of rubber cushions on SRM vibrations. Both figures show the transfer functions of stator vibration to force excitation, with the hammer hitting from the top and side of the motor. It is shown that the resonant frequency of the 2<sup>nd</sup> mode doesn't change much, with 1377.2 and 1357.3Hz respectively. However the magnitude of response does change, which means that the cushion is an effective way of reducing the magnitude of the vibration, assuming the resonant frequencies are not changed. The rubber cushions in this case produce an approximate 20% decrease in the amplitude of the stator vibrations.



(a) foot-mounted without rubber cushions



(b) foot-mounted with rubber cushions

Fig.4.10 Effect of Cushions on the Vibration

## 4.6 Conclusions

The effects of mountings on the vibration in the SRM are investigated in this chapter. Finite Element calculations are done here to calculate the modal frequencies of the motor stator for free vibrations and different mounting conditions. Force hammer tests are used to measure the resonant frequencies and the vibration transfer function for free vibrations and for different mounting conditions. The test results are compared with finite element calculations, with good accuracy. The FE method used in this chapter is thus proved to be effective for the research of the mounting effects on SRM vibrations.

While both mounting cases increase the 2<sup>nd</sup> and other mode resonant frequencies, they all induce some new modes of vibration due to the effects of bolts. The mode shapes also become more complicated, adding to the difficulty of dealing with the effects of mountings. The effects of mounting have to be considered for industrial applications. Free vibration analysis results cannot be used directly where there are mountings.

# Chapter 5

## SRM Vibration Measurements

### 5.1 Summary

Some additional experimental methods and results are introduced in this chapter, beyond those presented previously. White noise shaker tests can be used to identify the mode shapes of the motor stator and locate the resonant frequencies. Practical measurements of mode shapes using this method are described for the 2<sup>nd</sup> and 3<sup>rd</sup> mode resonant frequencies and mode shapes for free vibration. Impulse hammer tests are described and the advantages and disadvantages compared with shaker excitation are discussed.

A convenient and nondestructive method for the measurement of Young's modulus of stacked laminations in electric motor stators is introduced. It will be proved in this chapter that the commonly used Young's modulus value is not appropriate for the calculation of stator resonant frequencies. The results are validated by a 3-D FE calculation and force hammer vibration tests. The effects of other materials properties like Poisson's ratio, stacking factor of the stator core laminations and windings are also discussed.

## **5.2 Mode Shapes Identification with White Noise Shaker Tests**

### **5.2.1 Test Setup**

White noise excitation is a broadband excitation method, which is used for random forcing inputs. With this type of excitation, statistical parameters (rather than discrete values) are used. Individual time records in the analyzer contain data with random amplitude and phase at each frequency in this method. On average, the spectrum is flat and continuous, containing energy at approximately the same level for all frequencies. Due to the random characteristic of the signal, the structure is excited over a wide force range at each frequency. This randomizes any non-linear effects, and averaging then gives a best linear approximation.

Fig.5.1 shows the test setup of the white noise shaker excitation experiment. The SRM is suspended by four elastic ropes through its mounting holes to a solid bench, to establish a so-called free-free condition. A White Noise Generator (General Radio 1383, 20Hz~20MHz Random-Noise Generator) supplies white noise signals over a wide frequency range to the Power Amplifier (B&K 2706). A shaker (B&K 4809) is driven by the white noise signal and excites the SRM. A force transducer is stud-mounted onto the body frame (through a threaded hole) and connected to the shaker by the stinger. The shaker is placed directly on the ground where the reaction force will be absorbed. Accelerometers are screwed onto the body frame at several different locations to pick up the acceleration signals. Force and acceleration outputs are recorded in a storage oscilloscope (LeCroy 9304AM, QUAD 200MHz, 100MS/s) through a coupler (Kistler 5134), and then used in a computer program for data processing.

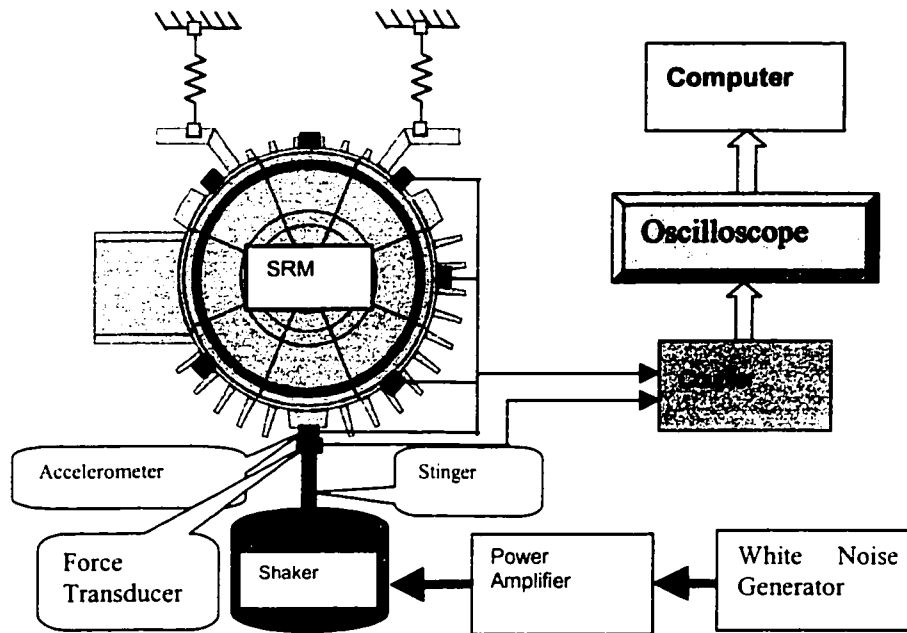


Fig.5.1 White Noise Shaker Excitation Experiment

## 5.2.2 Test Results

Fig.5.2 shows the force spectrum, acceleration spectrum and transfer function obtained under white noise excitation. This is the result from one location of the motor stator. There are 28 test points around the motor stator. For each point force and acceleration information is recorded and analyzed in the same way as shown in Fig.5.2. Two resonant frequencies, namely 1346Hz and 2480Hz, are located in the 0~5000Hz range, which are later proved to be the 2<sup>nd</sup> and 3<sup>rd</sup> mode resonant frequencies of the motor.

Fig.5.3 shows the magnitude responses of the transfer function at different locations of the motor stator at the resonant frequency of 1346Hz, using white noise excitation. It is clear that the magnitude responses shows a sinusoidal pattern, which is a reminder that it should be drawn on a cylindrical axis, as shown in Fig.5.4(b). The accelerometers



around the stator are not located evenly because of the complexity of the stator shapes, cooling fins, etc. The terminal box of the motor on one side of the stator also prevents any accelerometer to be installed. However, the 2<sup>nd</sup> mode shape at the resonant frequency of 1346Hz is still shown clearly from Fig.5.4(b), as compared with the ideal 2<sup>nd</sup> mode shape shown in Fig.5.4(a).

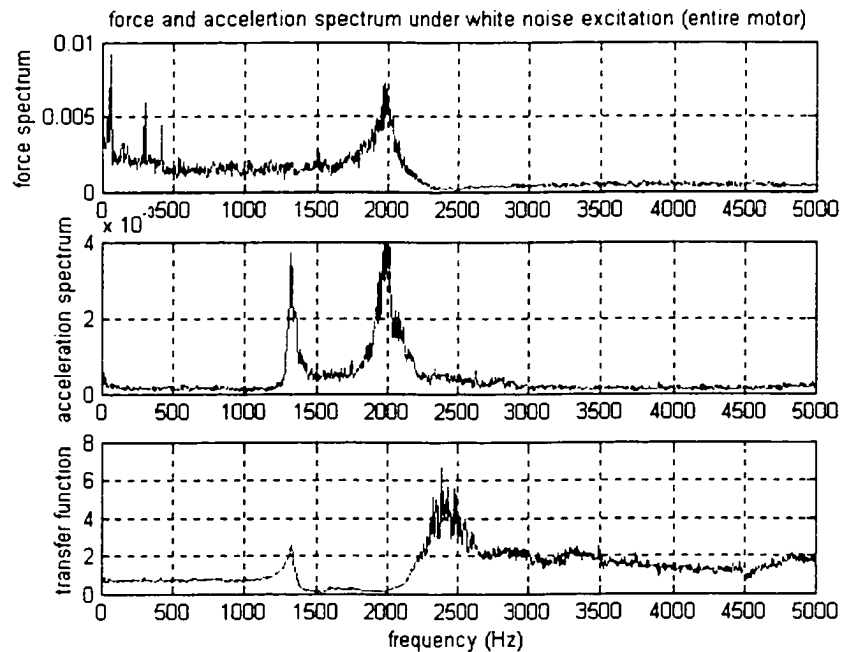


Fig.5.2 Force Spectrum, Acceleration Spectrum and Transfer Function

Similarly, the 3<sup>rd</sup> mode shape at the resonant frequency of 2480Hz is also obtained, which is shown in Fig.5.4(d), compared with the ideal 3<sup>rd</sup> mode shape shown in Fig.5.4(c). It is also very close to the mode shape drawn in Fig.4.2 from FE calculation.

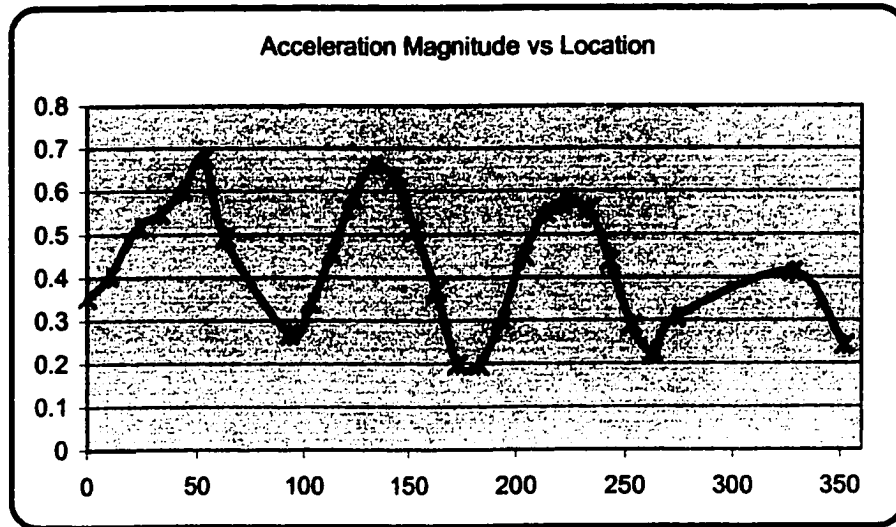
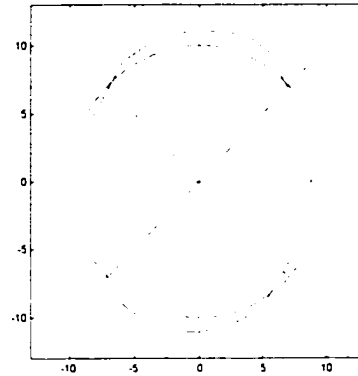


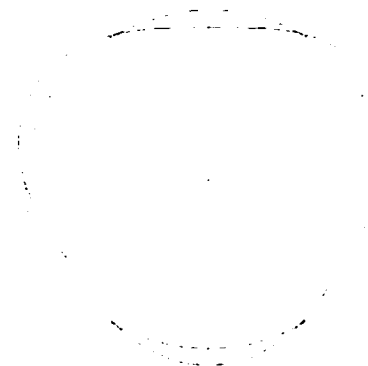
Fig.5.3 Magnitude Responses at Different Points at the Resonant Frequency of 1346Hz



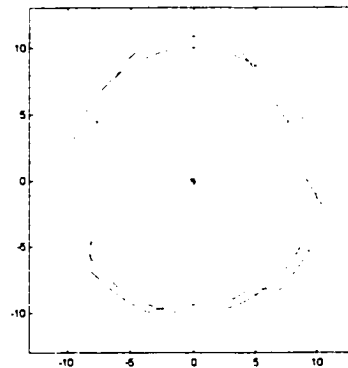
(a) Ideal 2<sup>nd</sup> Mode Shape



(b) Measured 2<sup>nd</sup> Mode Shape



(c) Ideal 3<sup>rd</sup> Mode Shape



(d) Measured 3<sup>rd</sup> Mode Shape

Fig.5.4 Comparison of Ideal and Measured Mode Shapes

Compared with the sinusoidal shaker excitation method, which is used to identify the resonant frequencies and mode shapes, the advantage of white noise excitation is that, more than one mode shape can be identified at one time. As seen in Fig.5.2, the 2<sup>nd</sup> and 3<sup>rd</sup> mode shapes are identified at the same time. With the sinusoidal excitation method, the frequency has to be swept and adjusted very carefully to tune-in with the resonant frequencies. Compared with the impulse hammer excitation method, which is another commonly used method in identifying mode shapes, white noise excitation is more accurate, since the energy from the shaker is much higher than that in a hammer. Moreover, the frequency range in a hammer excitation is very limited, especially when the size of the tested structure increases; while the frequency range with white noise excitation is not a concern — it is relatively easy to select a frequency range with this method.

### **5.3 Wide Band Excitation Experiments — Impulse Hammer Excitation Method**

#### **5.3.1 Introduction**

Mechanical vibration modal tests for electric motors require a precise dynamic force measurement as well as a corresponding acceleration measurement, although there is no theoretical restriction as to the waveform. Precise force measurement can be achieved by electrodynamic or servohydraulic exciters (vibrators) controlled by a signal generator (sinusoidal wave or even white noise signal) via a power amplifier, and a force transducer (load cell) between the exciter and the object to be tested. However, a more

convenient and economical excitation method can be used — a hammer mounted with a high-quality piezoelectric force transducer at its tip. In applications like modal tests for middle size electric motors, where a high crest factor and a limited ability to shape the input force spectrum is of no concern, modal hammer testing is an ideal excitation method. It is also an advantage for impact hammers that they are highly portable for field work and provide no unwanted mass loading to the structure under test.

The Modal Hammer produces an impulse force at one hit, which excites the structure with a constant force over a frequency range of interest. It is also called non-attached broadband excitation. The waveform produced by a modal hammer is an impact — a transient (short duration) energy transfer event. The spectrum is continuous, with maximum amplitude at 0Hz and decaying amplitude with increasing frequency. There are three interchangeable tips provided for the hammer in this test, which determine the width of the input pulse and thus the bandwidth. Typical force impulse and its spectra produced with different tips are shown in Fig.5.5. Different models of hammers together with their tips are compared carefully. The final goal is to excite the structure over the entire frequency range of interest simultaneously.

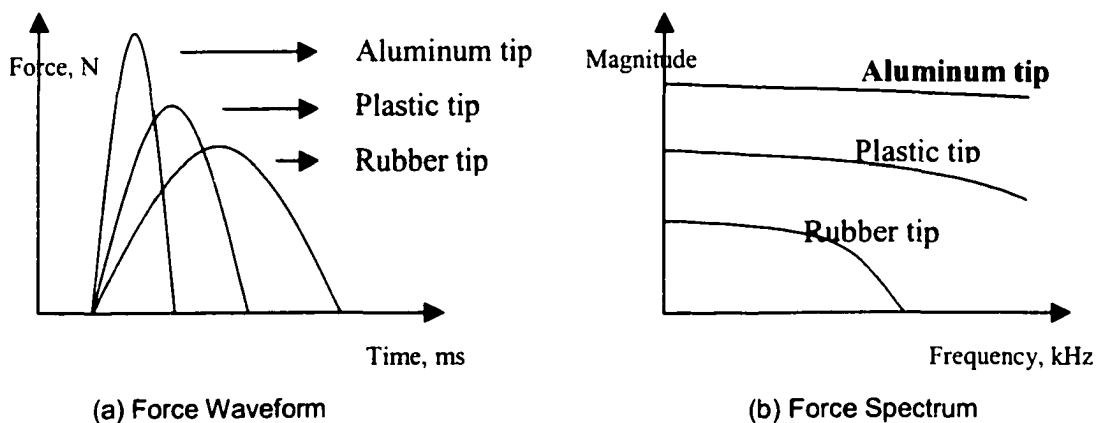


Fig.5.5 Modal Hammer Impact Force Waveform and Spectrum

For relatively larger structures, an optional head extender is generally available to increase the head's mass. For the commercial hammer, its structure is acceleration compensated to avoid glitches in the spectrum due to hammer structure resonance, and the ergonomically designed handle grip helps the users optimize control and reduce the possibility of “double hits”, which has to be avoided during the test.

### **5.3.2 Impulse Hammer Excitation Theory, Setup and Procedure**

#### **5.3.2.1 Hammer Excitation Theory**

The hammer produces an impulse force during the test, which includes a broad band frequency of force signal. If the impulse is “perfect”, the frequency band is from 0Hz to infinity. But of course the “hit” during the test is never “perfect”, so there is a limitation of the usable frequency band according to different models of hammers and different types of tips, as well as the impulse input during the test.

According to vibration theory, the output spectrum can be expressed in terms of the input spectrum weighted by a system descriptor:  $X(\omega) = H(\omega) \bullet F(\omega)$ .

The system descriptor  $H(\omega)$  is called the Frequency Response Function (FRF), and is defined as:  $H(\omega) \equiv \frac{X(\omega)}{F(\omega)}$ .

It represents the complex ratio between output and input, as a function of frequency  $\omega$ . Here “complex” means that the function has a magnitude  $|H(\omega)|$  and a phase  $\angle H(\omega) = \phi(\omega)$ .

The physical interpretation of the FRF is that a sinusoidal input force with a frequency  $\omega$  will produce a sinusoidal output motion or acceleration at the same frequency. The output amplitude will be multiplied by  $|H(\omega)|$ , and the phase, between output and input, will be shifted by  $\angle H(\omega)$ . Here the input refers to the force, output refers to the acceleration.

There is an assumption here that the system being measured is linear, which is quite reasonable in this case. Under this assumption, any input/output spectrum can be considered the sum of sinusoids. Since the FRF describes the dynamic properties of a system independent of the signal type used for the test, it is equally applicable to all kinds of excitations, including sinusoidal, white noise (random noise) and impulse.

The Modal Hammer Excitation Test here is actually measuring a specific function, from force to acceleration, by making measurements sequentially at discrete frequencies or simultaneously at several frequencies. Compared with sinusoidal excitation with shaker, this method gives a dramatic reduction in experimental time where only one frequency can be measured at a time.

### **5.3.2.2 Hammer Excitation Setup**

The experimental system is shown in Fig.5.6. An Oulton 8/6 4kW SRM is suspended over a solid bench by four elastic cords through its four mounting holes, to establish a so-called free-free condition. Accelerometers (Kistler 8730A500, sensitivity 10mV/g, frequency limit 10kHz, 500g range) are screwed into different locations of the stator to pick up the acceleration (vibration) signals during the test. A modal hammer

(ENDEVCO 2302-10, 500lb range, frequency range 8kHz, sensitivity 10mV/lb) is used to supply an impulse force signal (broad band force excitation). A coupler (or called signal conditioner) (ENDEVCO 4416B, or Kistler 5134) is used for force and acceleration signals conditioning. The outputs of the coupler are connected to a storage oscilloscope (Lecroy 9304AM, 200MHz, 100MS/s, 4 channels), where the signals can be stored as a data file on a floppy disk and then used in a MATLAB program for data processing. A MATLAB program is used for data loading, plotting, FFT analysis and transfer function calculation.

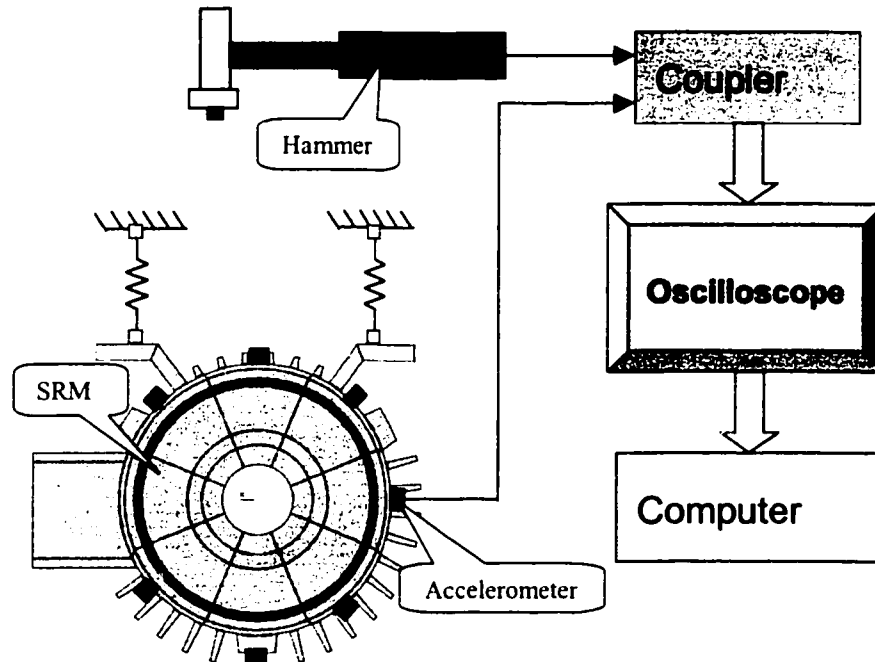


Fig.5.6 Block Diagram of Modal Hammer Excitation Experiment

### 5.3.2.3 Hammer Excitation Procedure

As can be seen in Fig.5.6, the procedure for hammer excitation method is much simpler than sinusoidal shaker excitation method. The hammer can be moved anywhere

for the tester's interests and convenience, which is sometime impossible for shaker. With one hit, information for all the frequencies within interests will be recorded and ready for analysis.

A storage oscilloscope is needed for data recording and transferring to computer, where most of the data processing work will be done with a data processing software like MATLAB.

### **5.3.3 Impulse Hammer Experimental Results**

#### **5.3.3.1 Impulse Force and Acceleration Response in the Time Domain**

Fig.5.7 shows the recorded impulse force and acceleration response in the time domain. As can be seen in the amplified view of the impulse force, it should be as sharp as possible. The sharpness (how close it is to a "perfect" impulse) depends on the hammer model, the tip material, the tested object, and also the experience of the tester.

The acceleration waveform shows a decayed curve of acceleration (vibration). It is clear that there is more than one frequency in it because it shows a "beating" phenomenon (if it is composed of one pure frequency, no "beating" will appear).

#### **5.3.3.2 Impulse Force and Acceleration Response in the Frequency Domain**

Fig.5.8 is the frequency domain representation of the impulse force and acceleration responses. The impulse force has information from 0Hz up to 8kHz, but the usable frequency range is from 0Hz to 5kHz. For the frequency range 5kHz to 8kHz, the energy is really low, so it is hard to excite any resonant mode frequency in this range.



It can also be seen from Fig.5.8 that the peak response of acceleration is 1345Hz, which is the 2<sup>nd</sup> mode resonant frequency for the entire motor (motor with end-bells and rotor). This result is the same as for sinusoidal excitation, white noise excitation and FEM results. The 2<sup>nd</sup> mode vibration dominates in the acceleration spectrum.

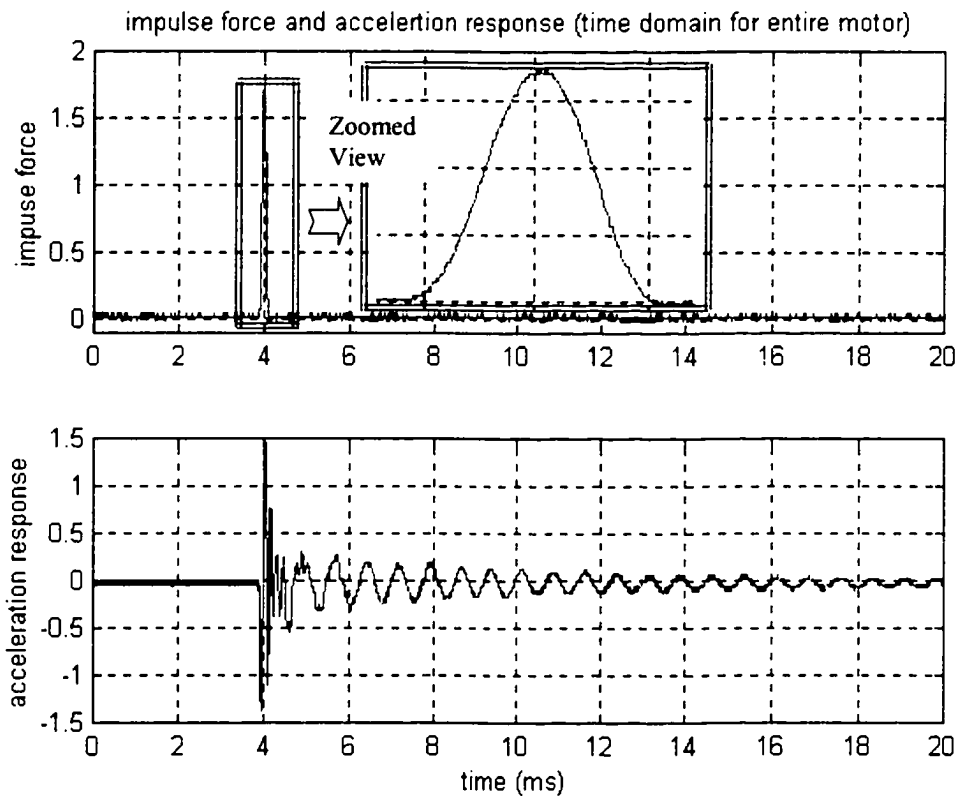


Fig.5.7 Measured Time Domain Waveforms of Force and Acceleration

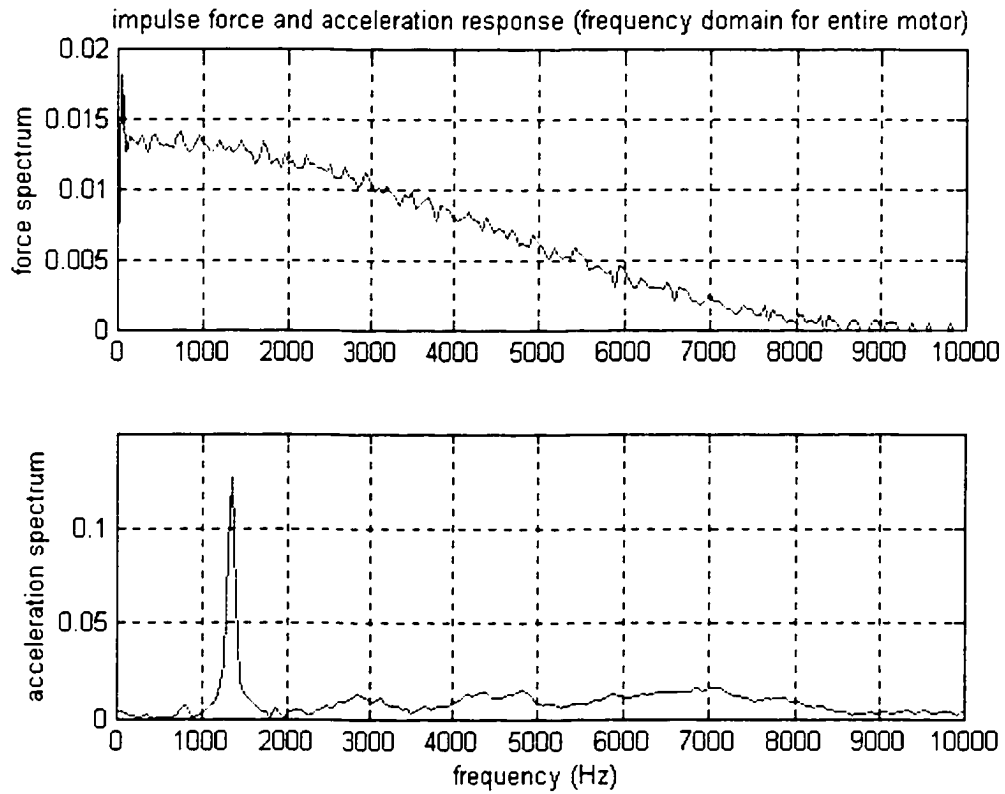


Fig.5.8 Frequency Domain Analysis of Measured Force and Acceleration

### 5.3.3.3 Transfer Function Calculation

Fig.5.9 shows the calculated Transfer Function of SRM vibration. A dominant peak is shown in 1345Hz, which is the 2<sup>nd</sup> mode resonant frequency. The other resonant frequencies are not shown clearly in this function, because on one hand they are very low comparing with the 2<sup>nd</sup> mode, and on the other hand the energy used in the hammer excitation test is too low to excite them.

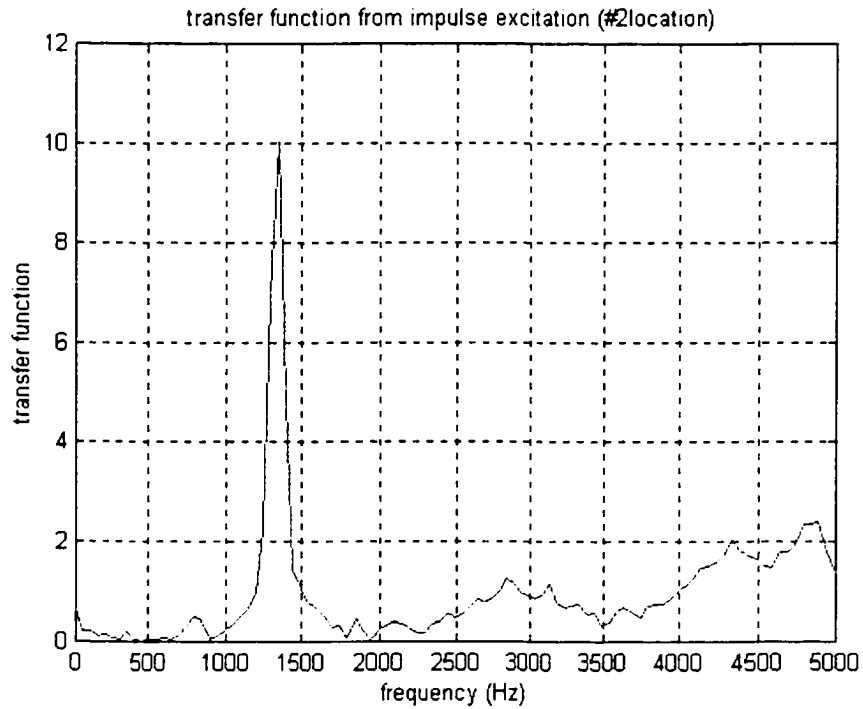


Fig.5.9 Transfer Function Calculation of Force to Acceleration

### 5.3.4 Comparisons between Different Test Methods and FE Calculations

Table 5.1 lists the comparisons between different test methods used in this dissertation, including the sinusoidal shaker excitation, white noise shaker excitation, impulse force hammer excitation, together with FE results. These results are referred to as free vibration calculations and measurements.

Table 5.1 Comparisons of Different Test Methods

	FE Results	Sinusoidal Shaker	White Noise Shaker	Impulse Hmmer
2 <sup>nd</sup> Mode	1325.5Hz	1316.5Hz (0.7%)	1346Hz (1.5%)	1346.5Hz (1.6%)
3 <sup>rd</sup> Mode	2595.5Hz	2480.2 (4.4%)	2480Hz (4.4%)	N/A

## 5.4 Measurement of Young's Modulus for the Switched Reluctance Motor

Techniques for noise reduction require knowledge of the modal frequencies, which depend on mechanical shapes and dimensions as well as material properties, for example, Young's modulus, Poisson's ratio, mass density, etc. This section introduces a simple and nondestructive method for the measurement of Young's modulus; it is then used in a finite element program to determine the resonant frequencies of SRM stator vibration. The effects of mass density and Poisson's ratios are also discussed. The FE results are validated by impulse force hammer tests, which show good accuracy.

### 5.4.1 Introduction

Vibration and acoustic noise in the switched reluctance motor is caused by the ovalizing deformation of the stator lamination stack due to its radial magnetic attraction to the rotor [21]. This is a big disadvantage for industrial applications. There are several ways of determining resonant frequencies and mode shapes of the SRM: analytical calculations, numerical computation (usually by the finite element method), and/or experimental measurements [49]. There is considerable advantage and interest in using numerical methods for the computation of resonant frequencies and mode shapes during motor design. The material properties, like density and Young's modulus are key factors besides stator dimensions and shapes. In the approximate formula for stator natural frequency, the stator resonant frequency has the relation [23]

$$f_r \propto \sqrt{\frac{E}{\rho}} \quad (5-1)$$

Where  $f_r$  is the stator natural frequency,  $E$  and  $\rho$  are the Young's modulus and mass density of the stator material respectively.

The density of the lamination core can be easily determined, however Young's modulus deserves some consideration. The Young's modulus value of stainless steel ( $E = 2.07 \times 10^{11} \text{ N/m}^2$ ) has been widely used by researchers in the area of electric machine vibrations. However, in order to allow theoretical predictions to converge to experimental results, some researchers even varied the value until the predicted natural frequencies converged to the measured values [43]. The fact is that the stator lamination steel of an electric machine is different from stainless steel, in addition, the material properties may change during core lamination or motor manufacturing. Because of the important role it plays in the determination of stator natural frequencies and its complexity, the value of Young's modulus has to be considered seriously.

#### **5.4.2 Development of the Method**

Many useful mechanical properties of materials, like Young's modulus, are obtained from tension tests and/or compression tests [50]. However, these tests are not trivial for an electric machine stator. Firstly, the force load may change the electromagnetic properties of the stator laminations. Secondly, the test may damage the stator lamination and/or windings. Finally, the odd shape of an electric machine stator makes it difficult for mounting.

A method widely used by mechanical and material researchers is an ultrasonic method, which is nondestructive. This is especially good for an electric machine. It will be discussed in detail in this chapter.

The ultrasonic technique is a method for measuring the elastic properties of a material. The sample to be measured is placed between an ultrasonic transmitter (pulser) and receiver, and the time for an ultrasonic pulse to traverse the media between the transducers is measured. The block diagram is shown in Fig.5.10.

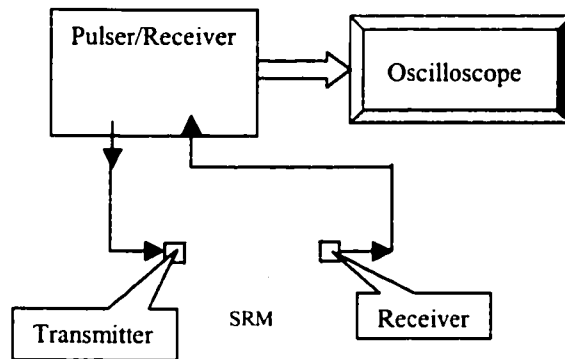


Fig.5.10 Block Diagram of Ultrasonic Method

Stress waves from 20Hz to 20kHz are perceived as sound. Waves above 20kHz are referred to as ultrasonic; ultrasonic frequencies between 1MHz and 10MHz are commonly used in the nondestructive evaluation of engineering materials, for materials characterization.

The ultrasonic wave speed,  $c$ , depends on the stiffness and on the density,  $\rho$ , of the materials under study [51,52]. For longitudinal waves

$$c = \sqrt{\frac{E}{\rho}} \quad (5-2)$$

$E$  is the Young's modulus. This is valid for a long homogeneous rod of length much longer than the wavelength, and width much less than the wavelength. If the width is much larger than the wavelength, then wave speed is governed by the tensorial modulus

$$c = \sqrt{\frac{1-\nu}{(1+\nu)(1-2\nu)} \frac{E}{\rho}} \quad (5-3)$$

Where  $\nu$  is the Poisson's ratio. The test motor stator used in this section belongs to this category. So the Young's modulus of the motor stator can be described as:

$$E = \frac{(1+\nu)(1-2\nu)}{(1-\nu)} \rho c^2 \quad (5-4)$$

Velocity (wave speed  $c$ ) can be measured by determining the time delay for the wave to pass through a sample of material. The velocity is the distance (thickness) divided by the time delay. In this method, one transducer sends the waves and another one receives them.

### 5.4.3 Test Setup

The prototype SRM used in this section is shown in Fig.5.11 (the stator part with windings). Fig.5.12 shows the above-described ultrasonic method that is used to measure the Young's modulus of this 12/8 3-phase SRM stator core lamination. A 200MHz Computer Controlled Pulser/Receiver together with two transducers (KB-Aerotech, GAMA 2.25MHz/.50) are used. The test data is then recorded in a digital oscilloscope and analyzed in a computer program to obtain the wave speed and Young's modulus.

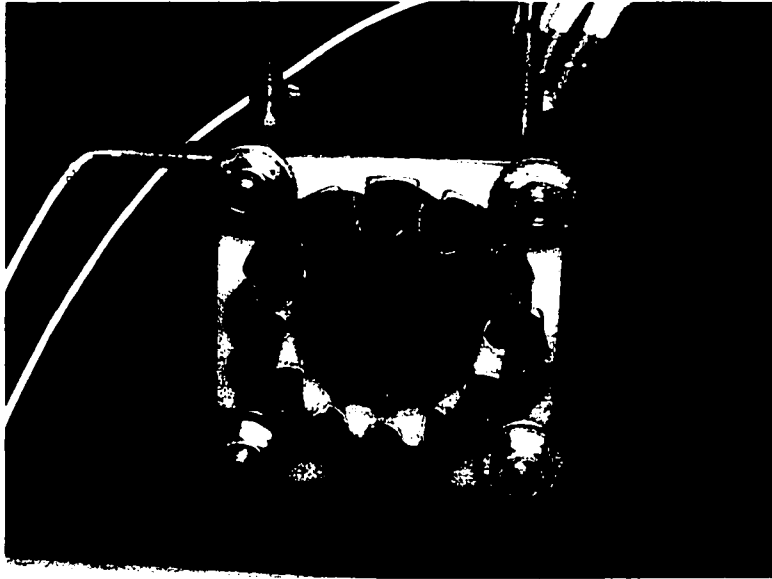


Fig.5.11 Stator of the Prototype SRM

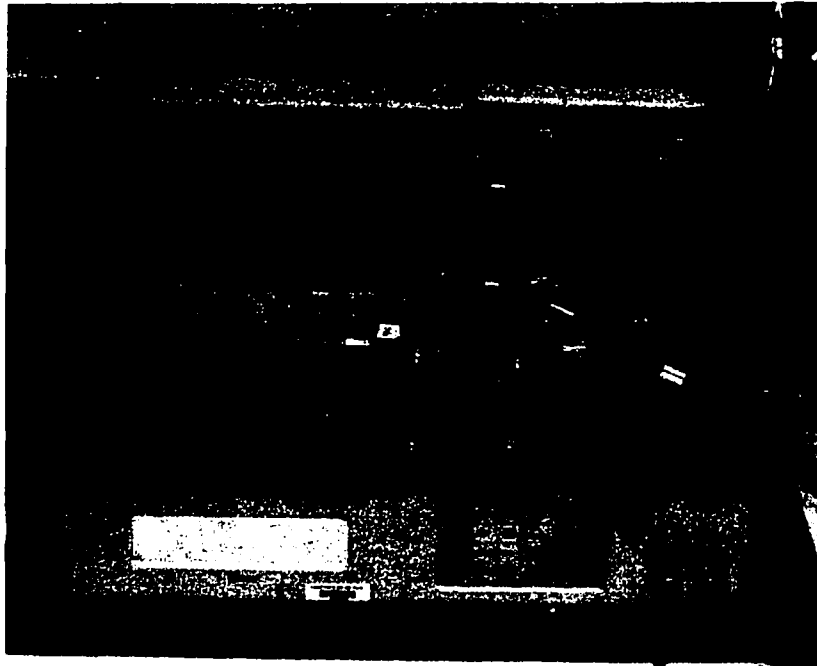


Fig.5.12 Young's Modulus Measurement

Compared with the traditional tension /compression method, the ultrasonic method has several advantages. Firstly, it is fast, convenient, simple and no special hydraulic equipment is needed. Secondly, no special mounting is needed, the transducers are



attached to the test object where needed. Then no damage is done to the stator or to the windings. Finally, it is easy to change the test location, for example, in horizontal direction or vertical direction, or from the inner side of stator pole.

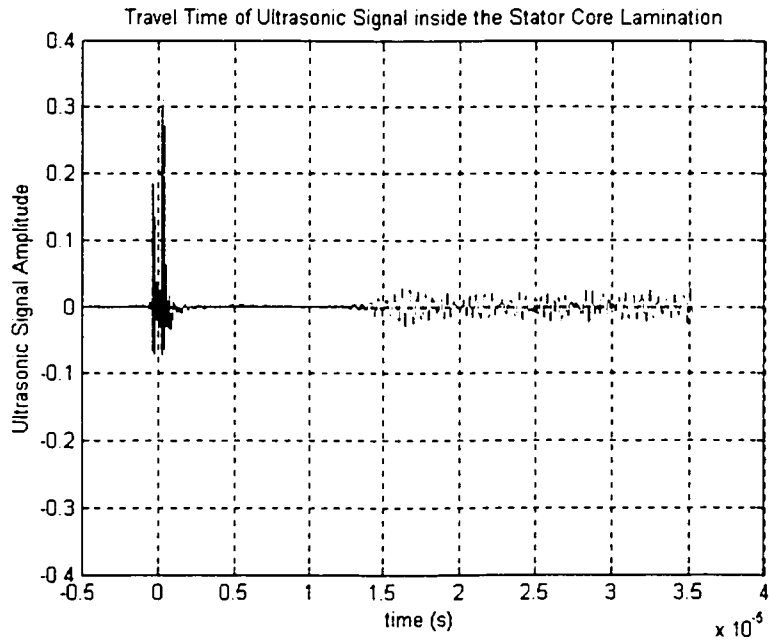
#### 5.4.4 Test Results

Fig.5.13 records the travel time of the ultrasonic signal inside the stator core lamination. The wave speed  $c$  can then be calculated, knowing the length of the test object (SRM stator). Using equation (5-4), Young's modulus  $E$  of the stator lamination is obtained in both the vertical and lateral directions (as viewed in Fig.5.11). Where, Poisson's ratio  $\nu = 0.3$  [48,50,51], mass density  $\rho = 0.935 \times 7.8 \times 10^3 \text{ kg/m}^3$ , 0.935 is the stacking factor (generally it is 0.92~0.95) of the stator core lamination. The measured value is  $1.521 \times 10^{11} \text{ N/m}^2$ , and is the same in both directions, quite different from  $2.07 \times 10^{11} \text{ N/m}^2$  used by most researchers, an error of 26.5%.

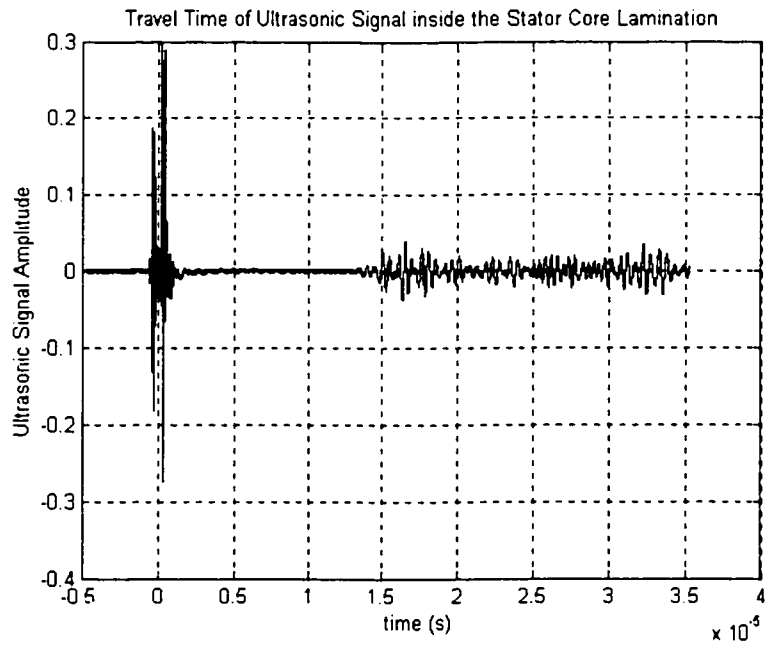
The impact of different Poisson's ratio values is also studied. They are used to calculate the Young's modulus, which are listed in Table 5.2. They will also be used later in a FE program for determination of resonant frequency for comparison purposes.

Table 5.2 Measured Young's Modulus

Poisson's Ratio $\nu$	0.3 (Commonly Used)	0.27	0.34	0 (One-dimensional)
Young's Modulus $E$ ( $\times 10^{11} \text{ N/m}^2$ )	1.521	1.638	1.371	2.047



(a) Vertical Direction



(b) Lateral Direction

Fig.5.13 Travel Time of Ultrasonic Signal inside the Stator Core Lamination

## 5.4.5 Correlation with FE Results and Vibration Tests

### 5.4.5.1 Equivalent Mass Density Determination

The effect of the phase windings on the vibration of electric machines has been discussed in many studies [26,41,47]. Generally it is believed that the windings have effects of both additional mass and vibration damping on the vibrational behavior of electric machines. In this dissertation, the mass of phase windings is treated as an increase of the mass density of the pole to which the winding is attached. According to [47], the concentrated windings of the SRM are installed on the stator poles. There is insulation between a pole and winding. For conventional motors, the contact between pole and winding assembly is tight enough to allow the windings to move with the pole, but cannot add an extra stiffness due to the existence of the insulation. Although the windings may contribute to stiffness if the slot fill factor is high, the increase in the stiffness is low when compared to the mass added by the windings to the stator assembly. Therefore, the effect of windings is equated to an increase of the pole mass. As a result, the geometrical model for finite element computation is the same as the model without considering the winding effect, but the poles are treated as a different material with a different specific mass density. The equivalent mass density of the pole with winding effect will be explained explicitly as follows.

The equivalent mass density  $\rho_e$  can be expressed as  $\rho_e = \frac{m_{pole} + m_{coil}}{V_{pole}}$ , where  $m_{pole}$

is the mass of one pole,  $m_{coil}$  is the mass of the coil attached to one pole,  $V_{pole}$  is the volume of the pole.

The volume of the pole  $V_{pole} = L_{stack} \times H_{pole} \times W_{pole}$ , where  $L_{stack}$  is the length of the pole (which is the same as stator stack length),  $H_{pole}$  is the height of the pole and  $W_{pole}$  is the width of the pole.

The mass of one pole is  $m_{pole} = \rho_{Fe} \times f_{stack} \times V_{pole}$ , where  $\rho_{Fe}$  is the mass density of the steel,  $f_{stack}$  is the stacking factor of the stator lamination, generally it is 0.92~0.95.

The mass of the coil can be calculated as  $m_{coil} = N_{turn} \times m_{turn}$ , where  $N_{turn}$  is the turns of winding per pole and  $m_{turn}$  is the mass of each turn. The mass of each turn of the coil  $m_{turn} = \rho_{cu} \times L_{turn} \times A_{turn}$ , where  $\rho_{cu}$  is the mass density of copper,  $L_{turn}$  is the length of each turn and  $A_{turn}$  is the intersection area of copper wire. Fig.5.14 shows the shape of one turn of the coil, from which the length of each turn can be calculated,  $L_{turn} = 2\pi R_{oh} + 2L_{copper}$ , where  $R_{oh}$  is the radius of the winding overhang,  $L_{copper}$  is the length of the straight line shown in Fig.5.14, which is longer than the stator stack length.

The intersection area of copper wire can be calculated as  $A_{turn} = \pi \left( \frac{D_{barewire}}{2} \right)^2$ , where

$D_{barewire}$  is the diameter of the bare copper wire with corresponding A.W.G.

Finally, the equation for equivalent mass density of the pole is:

$$\rho_e = \frac{\rho_{Fe} \times f_{stack} \times (L_{stack} \times H_{pole} \times W_{pole}) + N_{turn} \times \left\{ \rho_{cu} \times (2\pi R_{oh} + 2L_{stack}) \times \left[ \pi \left( \frac{D_{barewire}}{2} \right)^2 \right] \right\}}{(L_{stack} \times H_{pole} \times W_{pole})} \quad (5-5)$$

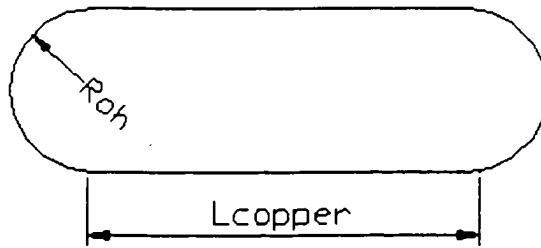
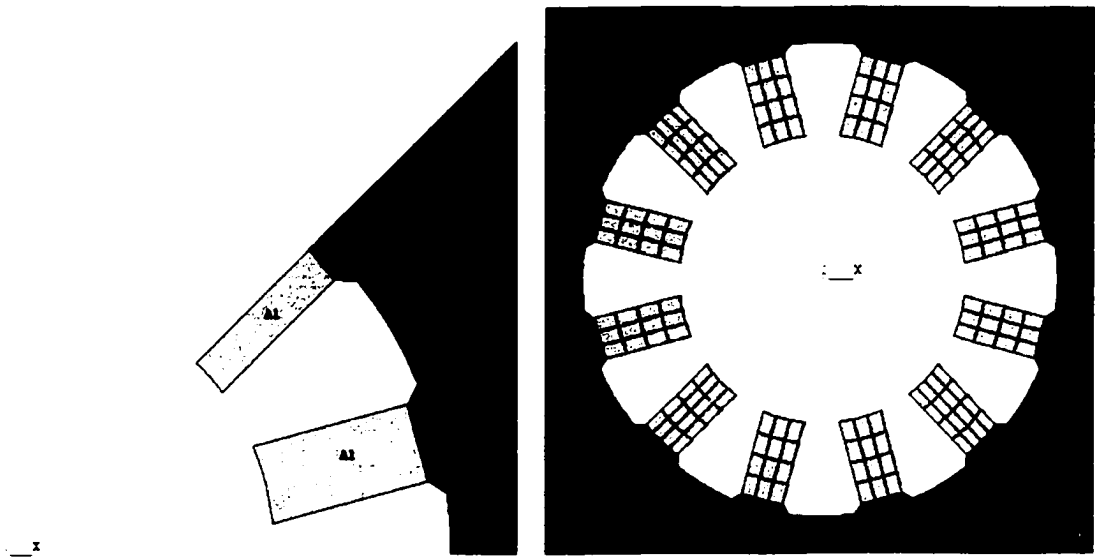


Fig.5.14 One Turn of the Coil

A Matlab file is written for the calculation of equation (5-5), and is listed in Appendix F, including key parameters of this motor. The equivalent density of the pole is  $20.29 \times 10^3 \text{ kg/m}^3$ .

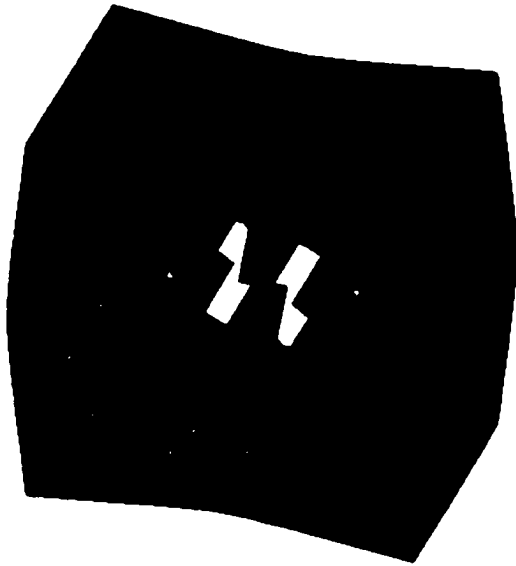
#### 5.4.5.2 FE Calculation Results

A 3-D FE model is constructed for this motor, as shown in Fig.5.15. The measured Young's modulus  $E$  is used with the ANSYS 3-D model to determine the natural frequencies, with the 2<sup>nd</sup> modes being at 1563.8Hz and 2578.1Hz. The source ANSYS code is listed in Appendix G.

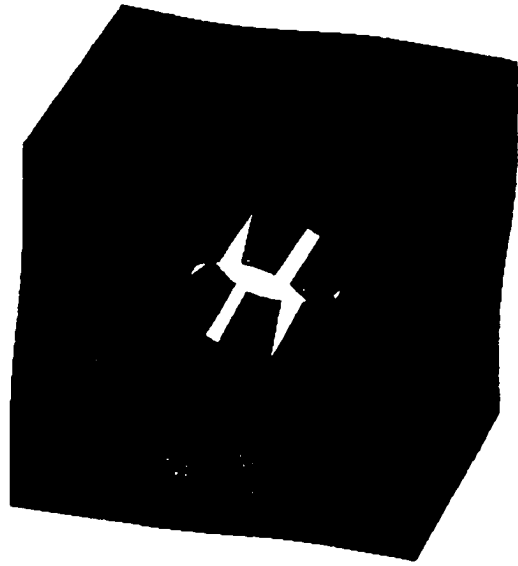


(a) Basic Area

(b) Basic Elements



(c) 2<sup>nd</sup> Mode Shape at 1563.8Hz



(d) 2<sup>nd</sup> Mode Shape at 2578.1Hz

Fig.5.15 FE Basic Area, Mesh and 2<sup>nd</sup> Mode Shapes (with measured Young's modulus)

The commonly used Young's modulus ( $2.07 \times 10^{11} \text{ N/m}^2$ ) is also used in the FE program to re-evaluate the resonant frequencies. Both are given in Table 5.3. To evaluate the effect of Poisson's ratio on the resonant frequencies, different Poisson's ratio

values,  $\nu = 0.34$  and  $0.27$  [48,51], are used in the FE program, with all the other material properties kept the same. No effect has been observed by changing this value. Some detailed explanations for Table 5.3 are done after the experimental measurements of stator resonant frequencies.

Table 5.3 Effect of Young's Modulus on the Resonant Frequencies of the 2<sup>nd</sup> Mode Shapes

	E	$\rho_1$	$\rho_2$	$\nu$	$f_2$	$f_2$ (error %)	$f_2'$	$f_2'$ (error %)
1)	1.521	20.29	7.8×0.935	0.3	1563.8	4.5	2578.1	-2.9
2)	2.07	20.29	7.8×0.935	0.3	1824.3	21.9	3007.7	13.3
3)	1.521	20.29	7.8×0.935	0.27	1562.9	4.4	2577.4	-2.9
4)	1.521	20.29	7.8×0.935	0.34	1565.1	4.6	2579.2	-2.9
5)	1.521	20.29	7.8×0.935	0	1558.6	4.1	2573.2	-3.1
6)	1.638	20.29	7.8×0.935	0.27	1621.9	8.3	2674.7	0.7
7)	1.371	20.29	7.8×0.935	0.34	1485.9	-0.7	2448.7	-7.8
8)	2.047	20.29	7.8×0.935	0	1808.1	20.8	2985.7	12.5
9)	1.627	20.80	7.8	0.3	1586.4	6.0	2608.6	-1.7
10)	2.07	7.8	7.8	0.3	2344.9	56.6	3621.3	36.4
11)	2.07	7.8×0.935	7.8×0.935	0.3	2425.1	62.0	3745.0	41.1
12)	1.521	7.8×0.935	7.8×0.935	0.3	2078.8	38.9	3210.2	20.9
13)	1.521	28.59	7.8×0.935	0.3	1383.5	-7.6	2326.7	-12.4

Note: The measured 2<sup>nd</sup> resonant frequencies are 1497Hz and 2655Hz respectively (see also the next section), which are used as basis for calculating percentage errors.

E = Young's modulus ( $\times 10^{11}$  N/m<sup>2</sup>)

$\rho_1$  = mass density of stator pole ( $\times 10^3$  kg/m<sup>3</sup>)

$\rho_2$  = mass density of stator core lamination ( $\times 10^3$  kg/m<sup>3</sup>)

$\nu$  = Poisson's ratio

$f_2, f_2'$  = 2<sup>nd</sup> mode resonant frequencies

0.935 is the stator core lamination stacking factor (generally it is 0.92~0.95)

### 5.4.5.3 Experimental Validation

In order to validate the FE calculations of resonant frequencies, a force hammer test is carried out for the SRM (the test procedure and setup can be found in the previous section). Fig.5.16 shows the time domain hammer impulse force, damped transient stator acceleration and frequency domain acceleration. It can be clearly seen that the 2<sup>nd</sup> mode resonant frequencies, which are 1497Hz and 2655Hz respectively, are very close to the

calculated ones with the measured Young's modulus (the peak of 2095Hz appearing in this figure is the resonant frequency of the test setup). The errors between the calculated and measured resonant frequencies are less than 4.5% for both resonant frequencies, as shown in Table 5.3, row 1). The errors of the calculated resonant frequencies using commonly used Young's modulus are 21.9% and 13.3% respectively, as listed in Table 5.3, row 2).

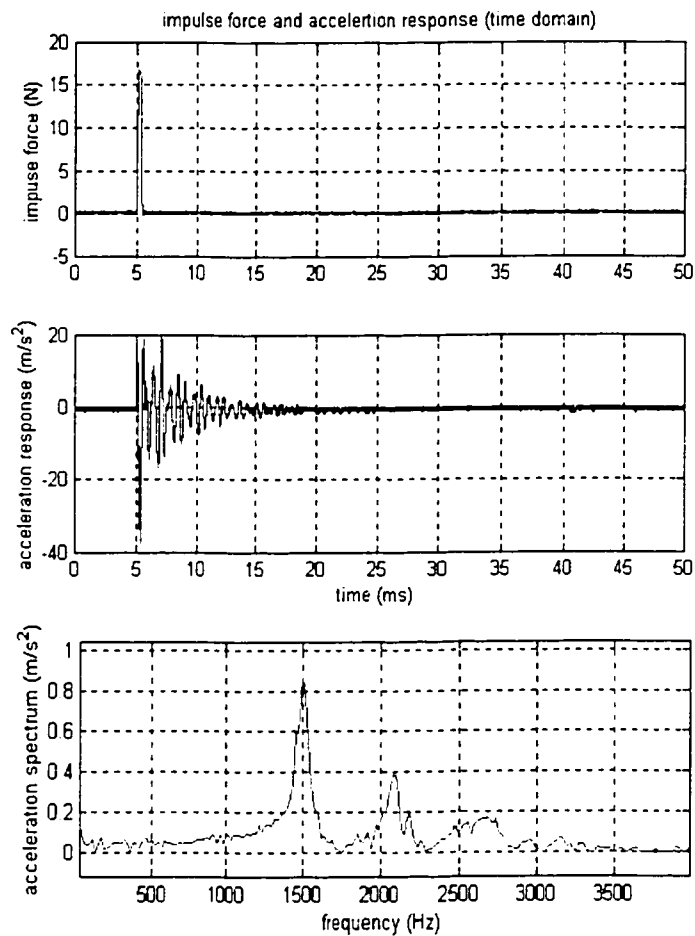


Fig.5.16 Force Hammer Test Result: Force Impulse and Stator Acceleration



### 5.4.6 Comparisons

The effects of Young's modulus, equivalent mass Poisson's ratio and stator core lamination stacking factor on the resonant frequencies are studied. These results are compared with impulse hammer test results, as shown in Table 5.3.

Row 1) shows the calculated resonant frequencies with measured Young's modulus, commonly used Poisson's ratio, consideration of winding effect and stacking factor. Both errors are less than 4.5% compared with the impulse force hammer tests.

Row 2) shows the calculated results with commonly used Young's modulus ( $2.07 \times 10^{11} \text{ N/m}^2$ ), the calculation error are not acceptable, at 21.9% and 13.3% respectively, although the winding effect and stacking factor are considered.

Rows 3), 4), 5) show the effect of Poisson's ratio on the resonant frequencies, no major effect has been found. The Poisson's ratio  $\nu = 0$  here refers to the so-called "one-dimensional" material.

Rows 6), 7), 8) show the role of Poisson's ratio on the accurate determination of Young's modulus during ultrasonic measurements, which is based on equation (5-4). Compared with row 1), the commonly used Poisson's ratio  $\nu = 0.3$  has the best result, while  $\nu = 0.27$  and  $0.34$  have acceptable results, both errors are around 8%.  $\nu = 0$ , which refers to homogeneous one-dimensional structure, leads to a 20% error. The Young's modulus determination of electric machine stators can't be treated as homogeneous structure.

Rows 9) reveals the effect of stator core lamination stacking factor on the resonant frequency. The properties of stacked lamination are definitely different from that of iron

or steel, as can be seen from the Young's modulus measurements. The existence of stacking factor will change the mass of the object, hence the resonant frequencies.

Rows 10) and 11) are the calculated results with commonly used Young's modulus without considering winding effects [54]. This is a commonly used method during the electric machine design stage because of the lack of winding parameters. The results reveal the fact that winding effects cannot be neglected, otherwise unacceptable errors will occur. In row 10) errors of 56.6% and 36.4% occur when neglecting the stacking factor, and in row 11) errors are 62.0% and 41.1% when considering the stacking factor. The calculation results are still unacceptable if winding effects are not considered, even though a correct Young's Modulus is used, as seen in row 12), where errors are 38.9% and 20.9% for the two 2<sup>nd</sup> mode frequencies.

Row 13) describes an easily made mistake when determining the equivalent mass density of the stator pole — using the total wire diameter instead of the bare wire diameter (notice that there is an insulation layer for winding copper wires), hence increasing the equivalent mass and lowering the resonant frequencies, in this case errors of 7.6% and 12.4% occur.

The measured Young's modulus ( $1.521 \times 10^{11}$  N/m<sup>2</sup>) is used for stator lamination core in the FE model developed in Chapter 4 for the 8/6 Oulton SRM. The calculated 2<sup>nd</sup> mode resonant frequency becomes 1277.4Hz, a 3.6% difference compared with 1325.5Hz using the commonly used Young's modulus of  $2.07 \times 10^{11}$  N/m<sup>2</sup>. The difference is much smaller when compared with the square motor case used in this section. This means that the Young's modulus is less important for the determination of resonant frequencies in the SRM with a cast iron case.

## 5.5 Conclusions

Practical measurements of mode shapes are introduced here using white noise shaker excitation. The 2<sup>nd</sup> and 3<sup>rd</sup> mode resonant frequencies and mode shapes for free vibration are measured and compared with FE results, with good correlation.

A more convenient and economical excitation method, the modal hammer excitation method, is used for SRM vibration modal tests in this chapter. The transfer function from normal force to acceleration is derived, especially for the 2<sup>nd</sup> mode resonant frequency. The measured resonant frequency is consistent with the other test results.

This chapter also introduces a convenient and nondestructive method for the measurement of Young's modulus of stacked lamination in electric motor stators. It shows the importance of Young's modulus in the calculation of stator resonant frequencies. It is proved here that commonly used Young's modulus values are not appropriate for the calculation of resonant frequencies. The results are validated by a 3-D FE calculation together with force hammer vibration tests.

Poisson's ratio is important for determining the Young's modulus using ultrasonic tests, however it has a small effect on the resonant frequencies. It is necessary to include the stator core lamination stacking factor, the winding effect, together with appropriate Young's modulus value for resonant frequencies determination during the design phase of SRMs.

# Chapter 6

## Conclusions and Future Work

### 6.1 Conclusions

About 13 years ago, Cameron, Lang and Umans [21] presented their milestone experimental study on the vibration and acoustic noise of SRMs. A series of carefully designed experiments were done to eliminate all but one source, which was found to be dominant: the radial deformation of the stator due to its radial magnetic attraction to the rotor. This dissertation adds to the understanding of that work and providing guidelines for motor designers to design quieter SRMs.

Some conclusions can be drawn as follows.

A detailed look-up table of normal force vs. rotor position vs. phase current is constructed using finite element calculations based on rotor position from 0~30° (aligned to unaligned, in steps of 1°) and phase current from 0~25A (in steps of 1A). The normal force acting on the stator-rotor pole can be calculated with this look-up table for an arbitrary phase current waveform.

Using sinusoidal shaker experiments, the essential parameters of the transfer function, namely the resonant frequency, magnitude response and damping ratio, can be calculated. The transfer function from normal force to acceleration of the 2<sup>nd</sup> and 3<sup>rd</sup>

mode resonant frequencies is constructed. Other wide-band excitation methods, such as the impulse hammer excitation, can also be used to obtain the transfer function.

The vibration prediction model is based on the transfer function constructed from sinusoidal shaker tests and the normal force calculated from a look-up table. With this model, the vibration of an SRM at any speed can be predicted once the phase current waveform, turn-on and turn-off angles are known.

The simulation models for SRM transient operations are presented in this dissertation, with results of phase current, transient speed, flux linkage, total torque and transient vibration. The start-up, sudden change of torque and braking operations of the SRM are described, together with the stator vibration associated with each operating condition. An 8/6 4kW SRM is used for experimental validation, with acceptable results.

For the running motor test, there is always a peak in the vibration acceleration response in the frequency domain, which is around 1,345Hz, the 2<sup>nd</sup> mode resonant frequency for the test motor. Secondly, the vibration acceleration is dominant around the 2<sup>nd</sup> resonant frequency when compared to the other frequencies. Thirdly, at any speed, the vibration acceleration is different at different locations on the motor. Finally, the vibration acceleration response of all frequencies except the 2<sup>nd</sup> mode resonant frequency are negligible because of their much lower magnitudes.

The effects of mountings on the vibration in the SRM are investigated. Finite Element calculations are done here to calculate the modal frequencies of the motor stator for the free vibration and different mounting conditions. Force hammer tests and running motor vibration tests are used here to measure the resonant frequencies and vibration

transfer function for the free-free state and different mounting conditions. The results are compared with the finite element calculation, with acceptable results.

The white noise excitation method is introduced, the test setup and procedure are described and the 2<sup>nd</sup> and 3<sup>rd</sup> mode shapes together with resonant frequencies of SRM are identified and measured. These results are consistent with the results from other sources.

A convenient and nondestructive method for the measurement of Young's modulus of stacked laminations in electric motor stators is introduced. It shows the importance of Young's modulus in the calculation of stator resonant frequencies. It is proved here that the commonly used Young's modulus value is not appropriate for the calculation of resonant frequencies. The results are validated by a 3-D FE calculation together with force hammer vibration tests.

## **6.2 Future Work**

The problem of the vibration and acoustic noise on SRMs is far from being solved. The successful commercialization of this attractive new motor depends on the cooperative work of researchers from different fields: electrical machines and drives, power electronics, control, mechanical engineering and material science, etc.

### **6.2.1 Acoustic Noise Prediction and Measurement**

The correlation between stator acceleration and acoustic noise needs to be established. The flow chart of SRM acoustic noise analysis can be described as shown in Fig.6.1.

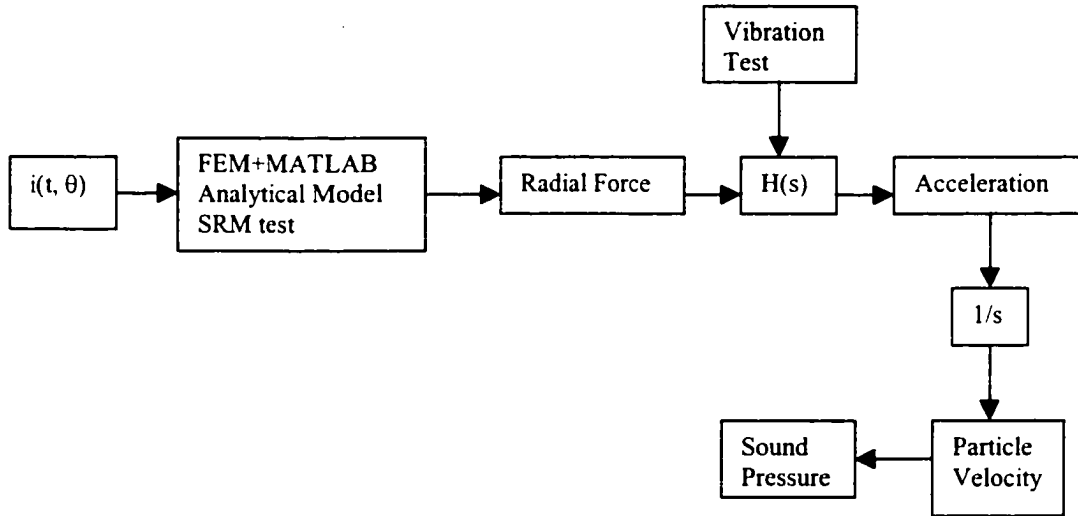


Fig.6.1 Flow Chart of SRM Acoustic Noise Analysis

Where:

$$\text{Transfer function } H(s) \cong \sum_{i=1}^N A_i \frac{\frac{s^2}{\omega_i^2}}{1 + 2c_i \frac{s}{\omega_i} + \frac{s^2}{\omega_i^2}} \quad (6-1)$$

It can be measured from sinusoidal vibration test, as been described in the dissertation.

From acceleration to noise:

$$P(M) = \int_{S_{tr}} \left( P(M_0) \frac{\partial G(M, M_0)}{\partial n} + j\rho\omega V_n(M_0) G(M, M_0) \right) dS(M_0) \quad (6-2)$$

In the case of geometric near field:

$$P(M) = 2j\rho\omega \sum_{j=1}^M V_n(M_j) G(M, M_j) \Delta S(M_j) \quad (6-3)$$

In the case of geometric far field low frequencies:

$$P(M) = j\rho\omega \sum_{i=1}^N V_n(M_i) G(M, M_i) \Delta S(M_i) \quad (6-4)$$

In the case of geometric far field high frequencies:

$$P(M) = j\rho\omega \sum_{i=1}^N (1 + \cos(\theta_i)) V_n(M_i) G(M, M_i) \Delta S(M_i) \quad (6-5)$$

These equations will be used to determine the link between acoustic noise and mechanical vibration.

### 6.2.2 Vibration Reduction Approaches in SRM and Design Sensitivities

Work needs to be done on SRM designs to reduce vibration and acoustic noise. A SRM design software PC-SRD and Finite Element package (ANSYS) can be used for motor design, where the phase current waveform, turn-on and turn-off angles and other motor parameters can be obtained. The vibration and acoustic noise prediction model described in this dissertation can be used to calculate the vibration of motor. Some design constrains, such as the stator-rotor pole number combination, pole shapes, yoke thickness, power-density and/or flux density vs. output torque should be taken into account. The goal is to provide a practical way for SRM designers to have satisfactory motor capability together with acceptable vibration and noise.

The vibration of the SRM is not only related to the motor itself, but also to the drive. This dissertation provides a practical method to predict vibrations once phase



current, turn-on and turn-off angles are known. The simulation model developed in this dissertation can have better results if more information of the drive is known. A classical controller (asymmetric half-bridge) can be built, controlled by dSPACE, so that each phase can be controlled independently, as well as the turn-on, turn-off angles can be adjusted. The phase current, speed of the motor can also be monitored at the same time, so that the analysis and calculation of vibrations can be done. The research of the effects of turn-on and turn-off angles on SRM vibration can be obtained in this way. Attempts to reduce torque ripple in SRMs can also be done in the same way.

The effects of mountings on SRM vibrations are discussed in this dissertation. Because of the limitation of available SRMs, vibration tests on face-mounted SRMs are not done here. In order to obtain a better view of mounting effects, more than one SRM needs to be tested. The higher order mode shapes and frequencies are too complicated to be identified when the cooling fins, terminal box and mounting feet are included in FE models. To find an effective method of modeling these structures in finite element is necessary.

The Young's modulus of stator core laminations is found to be important for the determination of resonant frequencies, especially for motors without a cast iron case. The Young's modulus measurement needs to be done on different motor stators, to further verify its importance.

Sinusoidal shaker excitation tests are done for the vibration transfer function identification in this dissertation. From theory, the white noise shaker excitation and impulse hammer tests can produce the same result. In this dissertation, these results are not compared, because of limitations of the experimental equipment. For example, the

motor used in this dissertation can only be excited from one location, the impulse hammer excitation is found not have enough energy to excite more resonant frequencies other than the 2<sup>nd</sup> mode, etc. Work needs to be done on a range of SRMs to repeat these experiments, if a more comprehensive method of obtaining the vibration transfer function is necessary.

The assumption made in the vibration prediction transfer function is that the line of action of the normal force between stator and rotor poles is in the middle of the stator pole. Actually, when the rotor is moving, the line of action of the force will move as well, thus affecting the transfer function. A “dynamic” (not only the force magnitude changes, but also the line of action) function of the normal force look-up table may be needed for more accurate better vibration prediction.

## References

- [1] B. D. Bedford, U.S. Patents 3678352 and 3679953, 1972.
- [2] P.J. Lawrenson, J.M. Stephenson, P.T. Blenkinson, J. Corda and N.N. Fulton, "Variable-speed switched reluctance motors", IEE Proc., vol. 127, pt. B, no. 4, pp. 253-265, July 1980.
- [3] T.J.E. Miller, "Switched Reluctance Motors and Their Control", Magna Physics Publishing and Clarendon Press, Oxford, 1993, ISBN: 1-881855-02-3.
- [4] T. Miller, "Brushless reluctance-motor drives", Power Engineering Journal, pp. 325-331, November 1988.
- [5] R. Krishnan, R. Arumugam and J.F. Lindsay, "Design procedure for switched reluctance motors", IEEE Trans. Ind. Appl., vol. 24, no. 3, pp. 456-461, May/June 1988.
- [6] W.F. Ray, R.M. Davis and R.J. Blake, "Inverter drive for switched reluctance motor circuits and component ratings", IEE Proc., vol. 128, pt. B, no. 2, pp. 126-136, March 1981.
- [7] W.F. Ray and R.M. Davis, "Inverter drive for doubly salient reluctance motor: its fundamental behavior, linear analysis and cost implications", Electric Power Applications, vol. 2, no. 6, pp. 185-193, December 1979.
- [8] T.J.E. Miller, "Converter volt-ampere requirements of the switched reluctance motor drive", in Conf. Rec. of IEEE Ind. Appl. Soc. Annual Meeting, 1984, pp. 813-819.

- [9] W.F. Ray, P.J. Lawrenson, R.M. Davis, J.M. Stephenson, N.N. Fulton and R.J. Blake, "High performance switched reluctance brushless drives", in Conf. Rec. of IEEE Ind. Appl. Soc. Annual Meeting, 1985, pp. 1769-1776.
- [10] R.J. Blake, P.D. Webster and D.M. Sugden, "The application of G.T.O.s to switched reluctance drives", Conf. Proc. of IEE Power Electronics and Variable Speed Drives, pp. 24-28, November 1986.
- [11] J.V. Byrne and M.F. McMullin, "Design of a reluctance motor as a 10 kW spindle drive", in Proc. of Motorcon '82, Geneva, Switzerland, pp. 10-24, September 1982.
- [12] D.M. Sugden, R.J. Blake, S.P. Randall and J.M. Stephenson, "Switched reluctance drives using mosfets", in 2nd European Power Electronics Conf. Grenoble, pp. 935-940, September 1987.
- [13] J.T. Bass, M. Ehsani, T.J.E. Miller, R.L. Steigerwald, "Development of a unipolar converter for variable reluctance motor drives", in Conf. Rec. of IEEE Ind. Appl. Soc. Annual Meeting, 1985, pp. 1062-1068.
- [14] M. Barnes, C. Pollock and A.M. Michaelides, "The design and performance of a self starting 2-phase switched reluctance drive", in Conf. Proc. of IEE International Conference on Power Electronics and Variable Speed Drives, Nottingham, September 1996, pp. 419 - 423.
- [15] M. Barnes and C. Pollock, "Two phase switched reluctance drive with new power electronic converter for low cost applications", Conf. Proc. of the 6th European Conference on Power Electronics and Applications, Seville, Spain, September 1995, pp. 1.427 - 1.430.

- [16] M. Barnes and C. Pollock, "New Class of Dual Voltage Converters for Switched Reluctance Drives", Accepted for publication in IEE Proceedings in Electric Power Applications.
- [17] R.M. Davies and W.F. Ray, Battery chargers in variable reluctance electric motor systems, U.K. Patent No. GB 1604066, 26 May 1978.
- [18] B.C. Mecrow, "New Winding Configurations for Doubly Salient Reluctance Machines", IEEE Industrial Applications Conference, Houston, October 1992.
- [19] Bolton, H.R and Shakweh, Y, "Performance Prediction of Laws's Relay Actuator", IEE Proc. Vol.137, Pt B, No 1, January 1990.
- [20] J.D. Wale and C. Pollock, "Novel Converter topologies for a two phase switched reluctance motor with fully pitched windings", Conf. Rec. of IEEE Power Electronics Specialist Conference, Baveno, Italy, June 24-27 1996, pp. 1798 - 1803.
- [21] D.E. Cameron, J.H. Lang, S.D.Umans, "The origin and reduction of acoustic noise in doubly salient variable-reluctance motors", IEEE Trans. on Industry Applications, Vol.28, No.6, November/December, 1992, pp.1250~1255.
- [22] C.Y.Wu, C. Pollock, "Time domain analysis of vibration and acoustic noise in the switched reluctance drive", IEE Sixth International Conference on Electrical Machines and Drives, London, UK, 1993, pp.558~563.
- [23] R.S.Colby, F.Mottier, T.J.E.Miller, "Vibration modes and acoustic noise in a 4-phase switched reluctance motor", IEEE Trans. on Industry Applications, vol.32, n6, pp.1357-1364, November / December 1996.
- [24] Yifan Tang, "Characterization, numerical analysis and design switched reluctance

motor for improved material productivity and reduced noise”, Conference Record of the 1996 IEEE Industry Application Society, 31st IAS Annual Meeting, Vol.1, San Diego, USA, Oct. 6-10, 1996, pp.715~722.

- [25] C.Y.Wu, C.Pollock, “Analysis and reduction of acoustic noise and vibration in the switched reluctance drive”, IEEE Trans. on Industry Applications, Vol.31, No.1, January/February, 1995, pp.91~98.
- [26] S.P.Verma, R.S.Girgis, “Method for accurate determination resonant frequencies and vibration behavior of stators of electrical machines”, Proceedings of IEE, Part B, Vol.128, No.1, January 1981, pp.1-11.
- [27] R.S.Girgis, S.P.Verma, “Experimental verification of resonant frequencies and vibration behaviour of stators of electrical machines, part I-models, experimental procedure an apparatus”, Proceedings of IEE, Part B, Vol.128, No.1, January 1981, pp.12~21.
- [28] S.P.Verma, R.S.Girgis, “Experimental verification of resonant frequencies and vibration behaviour of stators of electrical machines, part II-experimental investigations and results”, Proceedings of IEE, Part B, Vol.128, No.1, January 1981, pp.22~32.
- [29] S.P.Verma, K. Williams, R.K. Singal, “Vibrations of long, short laminated stators of electrical machines, part I: Theory, experimental models, procedure and set-up,” Journal of Sound and Vibration, No.129, 1989, pp.1~13.
- [30] C. Pollock, C.Y.Wu, “Acoustic noise cancellation techniques for switched reluctance drives,” Conference Record of the 1995 IEEE Industrial Application Society, 30th IAS Annual Metting, Vol.1, Orlando, USA, Oct. 8-12, 1995,

pp.448-455.

- [31] P.Pillay, W. Cai, "Investigation into vibration in switched reluctance motor", IEEE Transactions on Industry Applications, v 35, n 3, 1999, p 589-596.
- [32] W. Cai, P.Pillay, "Resonant frequencies and mode shapes of switched reluctance motors", IEEE Transactions on Energy Conversion, v 16, n 1, March 2001, 2001, p 43-48.
- [33] Singiresu S. Rao, Mechanical Vibrations, Addison-Wesley Longman, Incorporated, 03/01/1995, ISBN: 0201526867.
- [34] W.Cai, P.Pillay and A.Omekanda, "An analytical model to predict the modal frequencies of switched reluctance motors", IEEE IEMDC, Boston, MA, June 2001, pp. 203-207.
- [35] W.Cai, P.Pillay, Z.Tang, A.Omekanda, "Vibration Measurements in the Switched Reluctance Motor", 2001 Industry Application Society Annual Meeting, Sept.30~Oct.4, 2001, Chicago, Illinois, USA.
- [36] R.C. Stroud, "Excitation, measurement, and analysis methods for modal testing," Sound and Vibration, August 1987, pp12~27.
- [37] Giovanni Franceschini, Stefano Pirani, Mario Rinaldi, Carla Tassoni, "Spice-Assisted Simulation of Controlled Electric Drives: An Application to Switched Reluctance Drives", IEEE Trans. on Industry Applications, Vol.27, No.6, Nov./Dec. 1991, pp.1103~1110.
- [38] F.Soaes, P.J.Costa Branco, "Simulation of a 6/4 Switched Reluctance Motor Based on Matlab/Simulink Environment", IEEE Trans. on Aerospace and Electronic Systems, Vol.37, No.3, July 2001, pp.989~1009.

- [39] H.H. Wang, "Variable-Speed Control Technology of Switched Reluctance Motors"(in Chinese), Machinery Industry Press, Beijing, P.R.China, 1998, ISBN: 7-111-04623-4 / TM 575(G).
- [40] Khwaja M. Rahman, Steven E. Schulz, "High Performance Fully Digital Switched Reluctance Motor Controller for Vehicle Propulsion", 2001 Industry Application Society Annual Meeting, Sept.30~Oct.4, 2001, Chicago, Illinois, USA.
- [41] C. Yongxiao, W. Jiahua, H. Jun, "Analytical Calculation of Natural Frequencies of Stator of Switched Reluctance Motor", IEE EMD97, Sept.1~3, 1997, pp.81~85.
- [42] A.M.Michaelides, C.Pollock, "Modeling and Design of Switched Reluctance Motors with Two Phases Simultaneously Excited", IEE Proc.-Electr. Power Appl., Vol.143, No.5, Sept.1996, pp.361~370.
- [43] S.A.Long, Z.Q.Zhu, D.Howe, "Vibration Behavior of Stators of Switched Reluctance Motors", IEE Proceedings: Electric Power Applications, Vol.148, No.3, May 2001, pp.257~264.
- [44] M.Besbes, C.Picod, F.Camus, M.Gabsi, "Influence of Stator Geometry upon Vibratory Behavior and Electromagnetic Performances of Switched Reluctance Motors", IEE Proceedings: Electric Power Applications, Vol.145, No.5, Sept.1998, pp.462~467.
- [45] M.N.Anwar, Iqbal Husain, "Radial Force Calculation and Acoustic Noise Prediction in Switched Reluctance Machines", IEEE Transactions on Industry Applications, v36, n6, Nov.2000, pp.1589~1597.



- [46] W.Cai, P.Pillay and K.Reichert, "Accurate Computation of Electromagnetic Forces in Switched Reluctance Motors", Proceedings of the 5<sup>th</sup> International Conference on Electrical Machines & Systems, Aug 18-20, 2001, Shenyang, China.
- [47] W.Cai, P.Pillay, Z.Tang, "Impact of Stator Windings and End Bells on Resonant Frequencies and Mode Shapes of Switched Reluctance Motors", IEEE Transactions on Industry Applications, Vol.38, No.4, July/August 2002, pp.1027~1036.
- [48] Z.Q.Zhu, L.Xu, D.Howe, "Influence of Mounting and Coupling on the Natural Frequencies and Acoustic Noise Radiated by a PWM Controlled Induction Machine", IEE Conference Publication, n468, 1999, Proceedings of the 1999 9th International Conference on Electrical Machines and Drives (EMD99), Sep 1-Sep 3 1999, Canterbury, UK, pp.164~168.
- [49] Praveen Vijayraghavan, R. Krishnan, "Noise in electric machines: A review", IEEE Trans. on Industry Applications, vol.35, n5, Sep.1999, pp.1007-1013.
- [50] Roy R. Craig, JR., "Mechanics of Materials", ISBN 0-471-50284-7, John Wiley & Sons, 1996.
- [51] W. Michael Lai, David Rubin, Erhard Krempl, "Introduction to Continuum Mechanics", ISBN 0-7506-2894-4, Butterworth-Heinemann, 1993.
- [52] Karl F. Graff, "Wave Motion in Elastic Solids", ISBN 0-486-66745-6, Dover Publications, 1975.
- [53] C. Cetinkaya, "Localization of Longitudinal Waves in Bi-periodic Elastic Structures with Disorder", Journal of Sound and Vibration, 1999, 221(1),

pp.49~66.

- [54] W.Cai, P.Pillay and A.Omekanda, "Low Vibration Design of SRMs for Automotive Applications Using Modal Analysis", IEEE IEMDC, Boston, MA, June 2001, pp.261~266.
- [55] W.Cai, "Vibrations in Switched Reluctance Motors", Ph.D. thesis, Clarkson University, 2000.

# Appendices

## Appendix A Dimensions and Material Properties for the 8/6 4kW SRM

The geometrical and material properties of the Oulton 8/6 4kW 4-phases SRM are listed as follows.

### Stator side

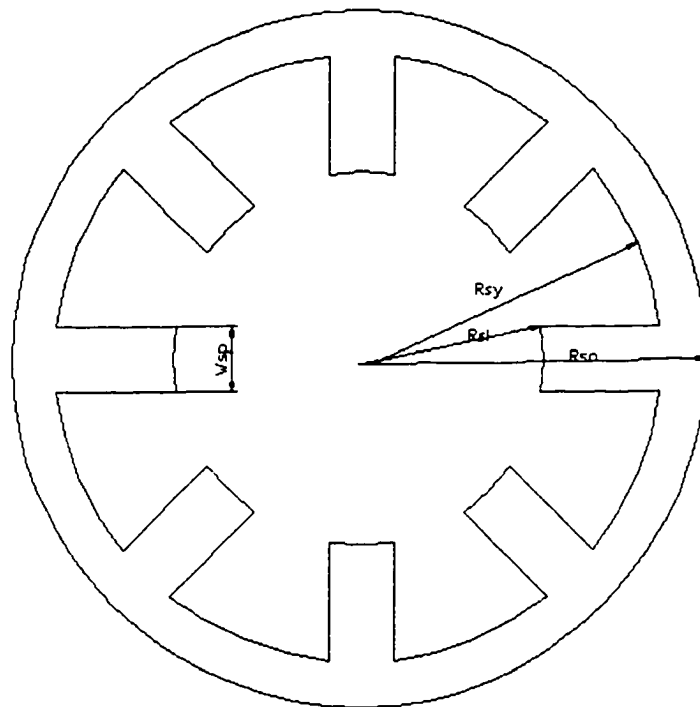


Fig.A.1 Stator Dimensions of a 4kW SRM with 8/6 Poles and 4 Phases

Lamination outer radius	$R_{so}=8.98 \times 10^{-2} \text{ (m)}$
Yoke inner radius	$R_{sy}=7.84 \times 10^{-2} \text{ (m)}$
Pole inner radius	$R_{si}=4.818 \times 10^{-2} \text{ (m)}$

The pole arc of stator	$\beta_s=20.2^\circ$
Width of stator pole	$W_{sp}=1.69\times 10^{-2}(\text{m})$
Winding area	$2.4\times 0.7\times 10^{-4}(\text{m}^2)$
Stator stack length	$L_{sy}=15.1\times 10^{-2}(\text{m})$
Stator pole number	$N_s=8$
Turns per phase	$N=176$ (turns, measured result)
Wire gauge of windings	AWG #14

### Rotor Side

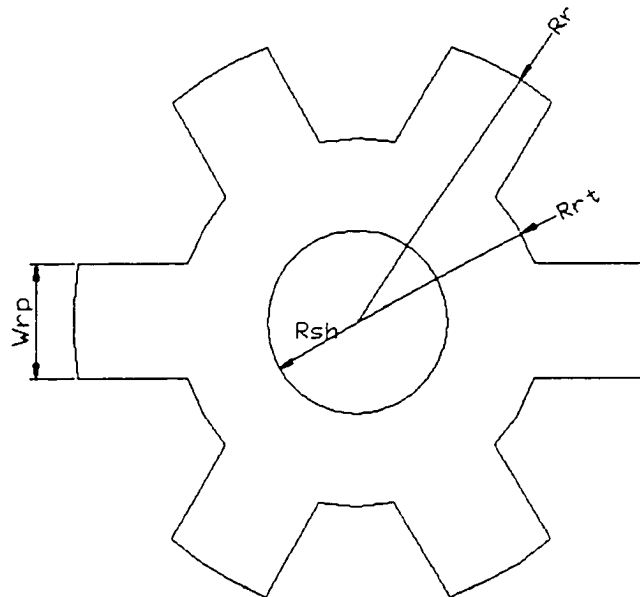


Fig.A.2 Rotor Dimensions of a 4kW SRM with 8/6 Poles and 4 Phases

Lamination outer radius	$R_r=4.782\times 10^{-2}(\text{m})$
Yoke outer radius	$R_{rt}=3.03\times 10^{-2}(\text{m})$

Shaft radius	$R_{sh}=1.5 \times 10^{-2}(\text{m})$
Shaft length	$L_{sh}=0.365(\text{m})$
Width of rotor pole	$W_{rp}=1.866 \times 10^{-2}(\text{m})$
Pole arc of rotor	$\beta_r=22.5^\circ$
Rotor stack length	$L_{st}=0.15024(\text{m})$
Rotor pole number	$N_r=6$

### **Lamination stack**

Mass density	$\rho_{Fe}=7800(\text{kg}/\text{m}^3)$
Young's elasticity modulus	$E=2.07 \times 10^{11} \text{ N}/\text{m}^2$
Poisson's ratio	$\nu=0.3$
Specific mass of windings (copper)	$\rho_c=8.9 \times 10^3(\text{kg}/\text{m}^3)$

### **Casting frame**

Mass density	$\rho_{Fe}=7800(\text{kg}/\text{m}^3)$
Young's elasticity modulus	$E=1.60 \times 10^{11}(\text{N}/\text{m}^2)$
Poisson's ratio	$\nu=0.275$

## Appendix B ANSYS Code for Electromagnetic Analysis for the SRM

```

/BATCH
!/COM,ANSYS RELEASE
5.5 UP19981001.1
12:58:48 10/23/2000
/input,menust,tmp
,,,,,,,,,1
!*
/NOPR
/PMETH,OFF
KEYW,PR_SET,1
KEYW,PR_STRUC,0
KEYW,PR_THERM,0
KEYW,PR_FLUID,0
KEYW,PR_ELMAG,1
KEYW,MAGNOD,1
KEYW,MAGEDG,0
KEYW,MAGHFE,0
KEYW,MAGELC,0
KEYW,PR_MULTI,0
KEYW,PR_CFD,0
/GO
!*
!/COM,
!/COM,Preferences for GUI
filtering have been set to
display:
!/COM, Magnetic-Nodal
!*
/PREP7
!*
ET,1,PLANE53
!*
/UI,MESH,OFF
MOPT,AMESH,MAIN
MOPT,QMESH,DEFA
MOPT,VMESH,DEFA
MOPT,TIMP,1
MOPT,PYRA,ON
MOPT,SPLIT,1
MSHKEY,1
MSHMID,0
MSHPATTERN,0
KEYW,ACCEPT,0
!*
MSHA,1,2D
MSHA,0,3D
!*
! SAVE, Oulton_EM,db,
K,1,0,0,0,
K,2,-0.0069282,0.004,0,
K,3,-0.0069282,-0.004,0,
K,4,-0.0129904,0.0075,0,
K,5,-0.0129904,-0.0075,0,
K,6,-0.0181865,0.0105,0,
K,7,-0.0181865,-0.0105,0,
K,8,-0.0225167,0.013,0,
K,9,-0.0225167,-0.013,0,
K,10,-0.0262406,0.01515,0,
K,11,-0.0262406,-0.01515,0,
K,12,-0.0288280,0.093292,0,
K,12,-0.028828,0.0093292,0,
K,13,-0.028828,-
0.0093292,0,
!/REPLOT
! SAVE, Oulton_EM,db,
LSTR, 1, 2
LSTR, 1, 3
LSTR, 2, 4
LSTR, 3, 5
LSTR, 4, 6
LSTR, 5, 7
LSTR, 6, 8
LSTR, 7, 9
LSTR, 8, 10
LSTR, 9, 11
LARC, 1, 2, 3
!*
LARC,2,3,1,0.008,
!*
LARC,4,5,1,0.015,
!*
LARC,6,7,1,0.021,
!*
LARC,8,9,1,0.026,
!*
LARC,10,12,1,0.0303,
!*
LARC,12,13,1,0.0303,
!*
LARC,13,11,1,0.0303,
! SAVE, file,db,
FLST,2,3,4
FITEM,2,1
FITEM,2,2
FITEM,2,11
AL,P51X
FLST,2,4,4
FITEM,2,12
FITEM,2,5
FITEM,2,13
FITEM,2,6
AL,P51X
FLST,2,4,4
FITEM,2,8
FITEM,2,14
FITEM,2,7
FITEM,2,13
AL,P51X
FLST,2,6,4
FITEM,2,16
FITEM,2,15
FITEM,2,14
FITEM,2,9
FITEM,2,10
FITEM,2,17
AL,P51X
! ERASE
GPLOT
! LPLOT
FLST,5,11,4,ORDE,2
FITEM,5,1
FITEM,5,-11
CM,_Y,LINE
LSEL,,,P51X
!*
CM,_Y1,LINE
CMSEL,,_Y
LESIZE,_Y1,,1,1,
CMDEL,_Y
CMDEL,_Y1
!*
FLST,5,3,4,ORDE,3
FITEM,5,11
FITEM,5,15
FITEM,5,17
CM,_Y,LINE
LSEL,,,P51X
!*
CM,_Y1,LINE
CMSEL,,_Y
LESIZE,_Y1,,2,1,
CMDEL,_Y
CMDEL,_Y1
!*
FLST,5,1,4,ORDE,1
FITEM,5,12

```

CM,_Y,LINE	K,29,-0.0319665,-	LSTR, 35, 37
LSEL,,,P51X	0.009392,0,	LSTR, 37, 39
!* CM,_Y1,LINE	K,30,-0.0350807,0.009392,0,	!* LARC,14,28,1,0.0333,
CMSEL,,_Y	K,31,-0.0350807,-	!* LARC,28,29,1,0.0333,
LESIZE,_Y1,,4,1,	0.009392,0,	!* LARC,29,15,1,0.0333,
CMDEL,_Y	K,32,-0.0381766,0.009392,0,	!* LARC,17,31,1,0.0363,
CMDEL,_Y1	K,33,-0.0381766,-	!* LARC,31,30,1,0.0363,
!* FLST,5,2,4,ORDE,2	0.009392,0,	!* LARC,30,16,1,0.0363,
FITEM,5,13	K,34,-0.0412584,0.009392,0,	!* LARC,18,32,1,0.0393,
FITEM,5,16	K,34,-0.0412584,-	!* LARC,32,33,1,0.0393,
CM,_Y,LINE	0.009392,0,	!* LARC,33,19,1,0.0393,
LSEL,,,P51X	K,34,-0.0412584,0.009392,0,	!* LARC,21,35,1,0.0423,
!* CM,_Y1,LINE	K,35,-0.0412584,-	!* LARC,35,34,1,0.0423,
CMSEL,,_Y	0.009392,0,	!* LARC,34,20,1,0.0423,
LESIZE,_Y1,,6,1,	K,36,-0.0443289,0.009392,0,	!* LARC,22,36,1,0.0453,
CMDEL,_Y	K,37,-0.0443289,-	!* LARC,36,37,1,0.0453,
CMDEL,_Y1	0.009392,0,	!* LARC,37,23,1,0.0453,
!* FLST,5,1,4,ORDE,1	GLOT	! /ZOOM,1,SCRN,-
FITEM,5,14	! SAVE, Oulton_EM,db,	0.760797,0.951087,-
CM,_Y,LINE	LSTR, 10, 14	0.566727,0.757065
LSEL,,,P51X	LSTR, 14, 16	LSTR, 22, 24
!* CM,_Y1,LINE	LSTR, 16, 18	LSTR, 24, 26
CMSEL,,_Y	LSTR, 18, 20	! /AUTO, 1
LESIZE,_Y1,,8,1,	LSTR, 20, 22	! /REP
CMDEL,_Y	! /ZOOM,1,SCRN,-	LSTR, 11, 15
CMDEL,_Y1	0.760797,0.951087,-	LSTR, 15, 17
!* ! SAVE, Oulton_EM,db,	0.566727,0.757065	LSTR, 17, 19
! /COM,ANSYS RELEASE	LSTR, 22, 24	LSTR, 19, 21
5.5 UP19981001.1	LSTR, 24, 26	LSTR, 21, 23
22:26:20 10/23/2000	! /ZOOM,1,SCRN,-	! /ZOOM,1,SCRN,-
! ERASE	0.810266,-0.833152,-	0.779824,0.939674,-
GLOT	0.509647,-1.030978	0.620001,0.833152
/PREP7	LSTR, 23, 25	! /AUTO, 1
! klist,all	LSTR, 25, 27	! /REP
K,14,-0.0288386,0.01665,0,	! /ZOOM,1,SCRN,-	!* LARC,24,38,1,0.04782,
K,15,-0.0288386,-0.01665,0,	0.810266,-0.833152,-	!* LARC,38,39,1,0.04782,
K,16,-0.0314367,0.01815,0,	0.509647,-1.030978	! /ZOOM,1,SCRN,-
K,17,-0.0314367,-0.01815,0,	LSTR, 23, 25	0.726550,-0.886413,-
K,18,-0.0340348,0.01965,0,	LSTR, 25, 27	0.631417,-0.962500
K,19,-0.0340348,-0.01965,0,	! /AUTO, 1	! /AUTO, 1
K,20,-0.0366329,0.02115,0,	! /REP	! /REP
K,21,-0.0366329,-0.02115,0,	LSTR, 12, 28	!* LARC,39,25,1,0.04782,
K,22,-0.0392310,0.02265,0,	LSTR, 28, 30	! /ZOOM,1,SCRN,-
K,23,-0.039231,-0.02265,0,	LSTR, 30, 32	0.753187,-0.867391,-
K,24,-0.0414133,0.02391,0,	LSTR, 32, 34	0.616196,-0.928261
K,25,-0.0414133,-0.02391,0,	LSTR, 34, 36	! /AUTO, 1
K,26,-0.0415173,0.02397,0,	LSTR, 36, 38	! /REP
K,27,-0.0415173,-0.02397,0,	LSTR, 13, 29	! /ZOOM,1,SCRN,-
K,28,-0.0319665,0.009392,0,	LSTR, 29, 31	0.737965,0.935870,-
	LSTR, 31, 33	0.612391,0.886413
	LSTR, 33, 35	

```

!/AUTO, 1
!/REP
!*
LARC,27,26,1,0.04794,

FLST,2,4,4
FITEM,2,18
FITEM,2,15
FITEM,2,32
FITEM,2,44
AL,P51X
FLST,2,4,4
FITEM,2,32
FITEM,2,16
FITEM,2,38
FITEM,2,45
AL,P51X
FLST,2,4,4
FITEM,2,38
FITEM,2,17
FITEM,2,25
FITEM,2,46
AL,P51X
FLST,2,4,4
FITEM,2,26
FITEM,2,47
FITEM,2,39
FITEM,2,46
AL,P51X
FLST,2,4,4
FITEM,2,39
FITEM,2,45
FITEM,2,48
FITEM,2,33
AL,P51X
FLST,2,4,4
FITEM,2,33
FITEM,2,44
FITEM,2,19
FITEM,2,49
AL,P51X
FLST,2,4,4
FITEM,2,49
FITEM,2,20
FITEM,2,50
FITEM,2,34
AL,P51X
FLST,2,4,4
FITEM,2,34
FITEM,2,51
FITEM,2,48
FITEM,2,40
AL,P51X
FLST,2,4,4
FITEM,2,40
FITEM,2,47

```

```

FITEM,2,52
FITEM,2,27
AL,P51X
FLST,2,4,4
FITEM,2,28
FITEM,2,53
FITEM,2,52
FITEM,2,41
AL,P51X
FLST,2,4,4
FITEM,2,41
FITEM,2,51
FITEM,2,54
FITEM,2,35
AL,P51X
FLST,2,4,4
FITEM,2,50
FITEM,2,55
FITEM,2,21
FITEM,2,35
AL,P51X
FLST,2,4,4
FITEM,2,22
FITEM,2,56
FITEM,2,55
FITEM,2,36
AL,P51X
FLST,2,4,4
FITEM,2,36
FITEM,2,54
FITEM,2,57
FITEM,2,42
AL,P51X
FLST,2,4,4
FITEM,2,42
FITEM,2,53
FITEM,2,29
FITEM,2,58
AL,P51X
FLST,2,4,4
FITEM,2,43
FITEM,2,58
FITEM,2,30
FITEM,2,61
AL,P51X
FLST,2,4,4
FITEM,2,43
FITEM,2,60
FITEM,2,57
FITEM,2,37
AL,P51X
FLST,2,4,4
FITEM,2,59
FITEM,2,56
FITEM,2,23
FITEM,2,37

```

```

AL,P51X
FLST,2,6,4
FITEM,2,24
FITEM,2,62
FITEM,2,59
FITEM,2,60
FITEM,2,61
FITEM,2,31
AL,P51X
GPLOT
!/ZOOM,1,SCRN,-
0.718939,0.920652,-
0.661859,0.859783
! LPLOT
!/FOC, 1 ,,-0.300000,,1
!/REP,FAST
!/FOC, 1 ,,-0.300000,,1
!/REP,FAST
!/FOC, 1 ,,-0.300000,,1
!/REP,FAST
!/FOC, 1 ,,-0.300000,,1
!/REP,FAST
!/FOC, 1 ,,-0.300000,,1
!/REP,FAST
!/FOC, 1 ,,-0.300000,,1
!/REP,FAST
!/FOC, 1 ,,-0.300000,,1
!/REP,FAST
!/FOC, 1 ,,-0.300000,,1
!/REP,FAST
!/FOC, 1 ,,-0.300000,,1
!/REP,FAST
!/FOC, 1 ,,-0.300000,,1
!/REP,FAST
!/FOC, 1 ,,-0.300000,,1
!/REP,FAST
!/AUTO, 1
!/REP

FLST,5,22,4,ORDE,8
FITEM,5,18
FITEM,5,-22
FITEM,5,24
FITEM,5,-29
FITEM,5,31
FITEM,5,-36
FITEM,5,38
FITEM,5,-42
CM,_Y,LINE
LSEL, , , ,P51X
!*
CM,_Y1,LINE
CMSEL, , ,_Y
LESIZE, , ,_Y1, , , ,1,1,
CMDEL, , ,_Y
CMDEL, , ,_Y1

```



```

!*
FLST,5,5,4,ORDE,5
FITEM,5,45
FITEM,5,48
FITEM,5,51
FITEM,5,54
FITEM,5,57
CM,_Y,LINE
LSEL,, , ,P51X
!*
CM,_Y1,LINE
CMSEL,,_Y
LESIZE,_Y1, , ,6,1,
CMDEL,_Y
CMDEL,_Y1
!*
FLST,5,2,4,ORDE,2
FITEM,5,44
FITEM,5,46
CM,_Y,LINE
LSEL,, , ,P51X
!*
CM,_Y1,LINE
CMSEL,,_Y
LESIZE,_Y1, , ,3,1,
CMDEL,_Y
CMDEL,_Y1
!*
FLST,5,2,4,ORDE,2
FITEM,5,47
FITEM,5,49
CM,_Y,LINE
LSEL,, , ,P51X
!*
CM,_Y1,LINE
CMSEL,,_Y
LESIZE,_Y1, , ,4,1,
CMDEL,_Y
CMDEL,_Y1
!*
FLST,5,2,4,ORDE,2
FITEM,5,50
FITEM,5,52
CM,_Y,LINE
LSEL,, , ,P51X
!*
CM,_Y1,LINE
CMSEL,,_Y
LESIZE,_Y1, , ,5,1,
CMDEL,_Y
CMDEL,_Y1
!*
FLST,5,2,4,ORDE,2
FITEM,5,53
FITEM,5,55
CM,_Y,LINE
LSEL,, , ,P51X
!*
CM,_Y1,LINE
CMSEL,,_Y
LESIZE,_Y1, , ,6,1,
CMDEL,_Y
CMDEL,_Y1
!*
FLST,5,2,4,ORDE,2
FITEM,5,56
FITEM,5,58
CM,_Y,LINE
LSEL,, , ,P51X
!*
CM,_Y1,LINE
CMSEL,,_Y
LESIZE,_Y1, , ,7,1,
CMDEL,_Y
CMDEL,_Y1
!*
FLST,5,2,4,ORDE,2
FITEM,5,59
FITEM,5,61
CM,_Y,LINE
LSEL,, , ,P51X
!*
CM,_Y1,LINE
CMSEL,,_Y
LESIZE,_Y1, , ,19,1,
CMDEL,_Y
CMDEL,_Y1
!*
FLST,5,1,4,ORDE,1
FITEM,5,60
CM,_Y,LINE
LSEL,, , ,P51X
!*
CM,_Y1,LINE
CMSEL,,_Y
LESIZE,_Y1, , ,22,1,
CMDEL,_Y
CMDEL,_Y1
!*
FLST,5,1,4,ORDE,1
FITEM,5,62
CM,_Y,LINE
LSEL,, , ,P51X
!*
CM,_Y1,LINE
CMSEL,,_Y
LESIZE,_Y1, , ,60,1,
CMDEL,_Y
CMDEL,_Y1
!*
MSHKEY,0

CM,_Y,AREA
ASEL,, , , 24
CM,_Y1,AREA
CHKMSH,'AREA'
CMSEL,S,_Y
!*
AMESH,_Y1
!*
CMDEL,_Y
CMDEL,_Y1
CMDEL,_Y2
!*
!
/ZOOM,1,SCRN,0.232386,0.
346196,0.289465,0.247283
!
/ZOOM,1,SCRN,0.312297,-
0.779891,0.491146,-
0.475543
! /AUTO, 1
! /REP
!
/ZOOM,1,SCRN,0.201943,0.
079891,0.350350,-0.171196
! /DIST, 1 ,0.729000,1
! /REP,FAST
! /DIST, 1 ,0.729000,1
! /REP,FAST
! /DIST, 1 ,0.729000,1
! /REP,FAST
! /DIST, 1 ,0.729000,1
! /REP,FAST
! /AUTO, 1
! /REP
!
/ZOOM,1,SCRN,0.209554,-
0.007609,0.281855,-
0.125543
! /AUTO, 1
! /REP
! APLOT
MSHKEY,0
FLST,5,15,5,ORDE,2
FITEM,5,6
FITEM,5,-20
CM,_Y,AREA
ASEL,, , ,P51X
CM,_Y1,AREA
CHKMSH,'AREA'
CMSEL,S,_Y
!*
AMESH,_Y1
!*
CMDEL,_Y
CMDEL,_Y1
CMDEL,_Y2

```

```

!*
MSHKEY,0
FLST,5,5,5,ORDE,2
FITEM,5,1
FITEM,5,-5
CM,_Y,AREA
ASEL, , , P51X
CM,_Y1,AREA
CHKMSH,'AREA'
CMSEL,S,_Y
!*
AMESH,_Y1
!*
CMDEL,_Y
CMDEL,_Y1
CMDEL,_Y2
!*
! SAVE, Oulton_EM,db,
! /COM,ANSYS RELEASE
5.5 UP19981001.1
09:49:47 10/24/2000
! ERASE
GPLOT
/PREP7
FLST,5,4,4,ORDE,4
FITEM,5,23
FITEM,5,30
FITEM,5,37
FITEM,5,43
CM,_Y,LINE
LSEL, , , P51X
!*
CM,_Y1,LINE
CMSEL,,_Y
LESIZE,_Y1, , ,2,0.5,
CMDEL,_Y
CMDEL,_Y1
!*
MSHKEY,0
FLST,5,3,3,5,ORDE,2
FITEM,5,21
FITEM,5,-23
CM,_Y,AREA
ASEL, , , P51X
CM,_Y1,AREA
CHKMSH,'AREA'
CMSEL,S,_Y
!*
AMESH,_Y1
!*
CMDEL,_Y
CMDEL,_Y1
CMDEL,_Y2
!*
! SAVE, Oulton_EM,db,
! LPLOT

! EPLOTT
! /RGB,INDEX,100,100,100,
0
! /RGB,INDEX, 80, 80,
80,13
! /RGB,INDEX, 60, 60,
60,14
! /RGB,INDEX, 0, 0, 0,15
! /REPLOT
! /REPLOT,RESIZE
! MPLIST
MPDELE,ALL,1,1,1,
FLST,5,13,5,ORDE,13
FITEM,5,6
FITEM,5,8
FITEM,5,-9
FITEM,5,11
FITEM,5,-12
FITEM,5,14
FITEM,5,-15
FITEM,5,17
FITEM,5,-18
FITEM,5,20
FITEM,5,-21
FITEM,5,23
FITEM,5,-24
CM,_Y,AREA
ASEL, , , P51X
CM,_Y1,AREA
CMSEL,S,_Y
!*
CMSEL,S,_Y1
AATT, , , 1, 0
CMSEL,S,_Y
CMDELE,_Y
CMDELE,_Y1
!*
/UI,MESH,OFF
FLST,5,13,5,ORDE,13
FITEM,5,6
FITEM,5,8
FITEM,5,-9
FITEM,5,11
FITEM,5,-12
FITEM,5,14
FITEM,5,-15
FITEM,5,17
FITEM,5,-18
FITEM,5,20
FITEM,5,-21
FITEM,5,23
FITEM,5,-24

CM,_Y,AREA
ASEL, , , P51X
CM,_Y1,AREA
CMSEL,S,_Y
!*
UIMP,1,ENTH, , , ,
UIMP,1,HF, , , ,
UIMP,1,QRATE, , , ,
UIMP,1,VISC, , , ,
UIMP,1,SONC, , , ,
UIMP,1,MURX, , , ,
UIMP,1,MGXX, , , ,
UIMP,1,RSVX, , , ,
UIMP,1,PERX, , , 1,
!*
TB,BH,2, ,38, ,
!*
TBMODIF,1,1,15.92
TBMODIF,1,2,0.04
TBMODIF,2,1,22.28
TBMODIF,2,2,0.08
TBMODIF,3,1,26.66
TBMODIF,3,2,0.12
TBMODIF,4,1,29.84
TBMODIF,4,2,0.16
TBMODIF,5,1,32.63
TBMODIF,5,2,0.2
TBMODIF,6,1,38.197
TBMODIF,6,2,0.28
TBMODIF,7,1,42.574
TBMODIF,7,2,0.36
TBMODIF,8,1,44.96
TBMODIF,8,2,0.4
TBMODIF,9,1,52.521
TBMODIF,9,2,0.52
TBMODIF,10,1,58.88
TBMODIF,10,2,0.6
TBMODIF,11,1,79.577
TBMODIF,11,2,0.8
TBMODIF,12,1,98.675
TBMODIF,12,2,0.92
TBMODIF,13,1,116.18
TBMODIF,13,2,1
TBMODIF,14,1,155.17
TBMODIF,14,2,1.12

```

TBMODIF,15,1,193.37	TBMODIF,3,2,0.2356	! TBPLOT,BH,3,
TBMODIF,15,2,1.2	TBMODIF,4,1,157.6	! APLOT
TBMODIF,16,1,262.6	TBMODIF,4,2,0.31	FLST,5,2,5,ORDE,2
TBMODIF,16,2,1.28	TBMODIF,5,1,197	FITEM,5,1
TBMODIF,17,1,318.31	TBMODIF,5,2,0.3876	FITEM,5,-2
TBMODIF,17,2,1.32	TBMODIF,6,1,236.4	CM,_Y,AREA
TBMODIF,18,1,397.88	TBMODIF,6,2,0.4651	ASEL, , , ,P51X
TBMODIF,18,2,1.36	TBMODIF,7,1,315.2	CM,_Y1,AREA
TBMODIF,19,1,505.3	TBMODIF,7,2,0.5973	CMSEL,S,_Y
TBMODIF,19,2,1.4	TBMODIF,8,1,394	!*
TBMODIF,20,1,684.36	TBMODIF,8,2,0.7131	CMSEL,S,_Y1
TBMODIF,20,2,1.44	TBMODIF,9,1,472.8	AATT, 3, , 1, 0
TBMODIF,21,1,954.92	TBMODIF,9,2,0.8062	CMSEL,S,_Y
TBMODIF,21,2,1.48	TBMODIF,10,1,591	CMDELE,_Y
TBMODIF,22,1,1352.8	TBMODIF,10,2,0.9147	CMDELE,_Y1
TBMODIF,22,2,1.52	TBMODIF,11,1,788	!*
TBMODIF,23,1,1989.4	TBMODIF,11,2,1.0387	FLST,2,24,5,ORDE,2
TBMODIF,23,2,1.58	TBMODIF,12,1,985	FITEM,2,1
TBMODIF,24,1,2785.2	TBMODIF,12,2,1.1364	FITEM,2,-24
TBMODIF,24,2,1.6	TBMODIF,13,1,1182	ACLEAR,P51X
TBMODIF,25,1,3899.3	TBMODIF,13,2,1.2093	! APLOT
TBMODIF,25,2,1.64	TBMODIF,14,1,1576	FLST,5,2,5,ORDE,2
TBMODIF,26,1,5252.1	TBMODIF,14,2,1.3178	FITEM,5,1
TBMODIF,26,2,1.68	TBMODIF,15,1,1970	FITEM,5,-2
TBMODIF,27,1,6047.9	TBMODIF,15,2,1.3798	CM,_Y,AREA
TBMODIF,27,2,1.7	TBMODIF,16,1,2364	ASEL, , , ,P51X
TBMODIF,28,1,7002.8	TBMODIF,16,2,1.4232	CM,_Y1,AREA
TBMODIF,28,2,1.72	TBMODIF,17,1,2358	CMSEL,S,_Y
TBMODIF,29,1,8833	TBMODIF,17,2,1.4573	!*
TBMODIF,29,2,1.76	TBMODIF,18,1,3152	CMSEL,S,_Y1
TBMODIF,30,1,11380	TBMODIF,18,2,1.4852	AATT, 3, , 1, 0
TBMODIF,30,2,1.8	TBMODIF,19,1,3546	CMSEL,S,_Y
TBMODIF,31,1,14006	TBMODIF,19,2,1.5162	CMDELE,_Y
TBMODIF,31,2,1.84	TBMODIF,20,1,3940	CMDELE,_Y1
TBMODIF,32,1,17030	TBMODIF,20,2,1.5441	!*
TBMODIF,32,2,1.88	TBMODIF,21,1,5910	FLST,5,9,5,ORDE,8
TBMODIF,33,1,21088	TBMODIF,21,2,1.6124	FITEM,5,3
TBMODIF,33,2,1.92	TBMODIF,22,1,7880	FITEM,5,-5
TBMODIF,34,1,27056	TBMODIF,22,2,1.6713	FITEM,5,7
TBMODIF,34,2,1.96	TBMODIF,23,1,11820	FITEM,5,10
TBMODIF,35,1,35014	TBMODIF,23,2,1.7612	FITEM,5,13
TBMODIF,35,2,2	TBMODIF,24,1,15760	FITEM,5,16
TBMODIF,36,1,51725	TBMODIF,24,2,1.8139	FITEM,5,19
TBMODIF,36,2,2.04	TBMODIF,25,1,19700	FITEM,5,22
TBMODIF,37,1,65253	TBMODIF,25,2,1.848	CM,_Y,AREA
TBMODIF,37,2,2.06	TBMODIF,26,1,23640	ASEL, , , ,P51X
TBMODIF,38,1,79557	TBMODIF,26,2,1.8666	CM,_Y1,AREA
TBMODIF,38,2,2.08	TBMODIF,27,1,27580	CMSEL,S,_Y
! TBPLOT,BH,2,	TBMODIF,27,2,1.8914	!*
TB,BH,3, ,29, ,	TBMODIF,28,1,31520	CMSEL,S,_Y1
!*	TBMODIF,28,2,1.9222	AATT, 2, , 1, 0
TBMODIF,1,1,78.8	TBMODIF,29,1,41472	CMSEL,S,_Y
TBMODIF,1,2,0.1503	TBMODIF,29,2,2	CMDELE,_Y
TBMODIF,2,1,98.5	! TBPLOT,BH,3,	CMDELE,_Y1
TBMODIF,2,2,0.193	!*	!*
TBMODIF,3,1,118.2	TBMODIF,17,1,2758	

FLST,5,13,5,ORDE,13	/PREP7	LSTR, 65, 64
FITEM,5,6	! klist,all	LSTR, 64, 63
FITEM,5,8	K,40,0.0338987,0.0338987,,	!
FITEM,5,-9	K,41,0.0339836,0.0339836,,	/ZOOM,1,SCRN,0.371953,-
FITEM,5,11	K,42,0.0340684,0.0340684,,	0.257260,0.383389,-
FITEM,5,-12	K,43,0.0355149,0.0355149,,	0.341107
FITEM,5,14	K,43,0.0355149,0.0275660,,	LSTR, 63, 47
FITEM,5,-15	K,44,0.0474334,0.0084492,,	LSTR, 47, 46
FITEM,5,17	K,45,0.04794,0,,	LSTR, 46, 45
FITEM,5,-18	K,46,0.04806,0,,	!/ZOOM,1,SCRN,-
FITEM,5,20	K,47,0.04818,0,,	0.177005,-0.040018,-
FITEM,5,-21	K,48,0.0361588,0.0361588,,	0.096949,-0.120054
FITEM,5,23	K,49,0.0529704,0.0529704,,	!/AUTO, 1
FITEM,5,-24	K,50,0.0554372,0.0554372,,	!/REP
CM,_Y,AREA	K,51,0.059397,0.059397,,	LSTR, 55, 54
ASEL, , , P51X	K,52,0.0634982,0.0634982,,	LSTR, 54, 53
CM,_Y1,AREA	! klist,all	LSTR, 53, 43
CMSEL,S,_Y	K,53,0.0416363,0.0296873,,	LSTR, 57, 56
!*	K,54,0.0586068,0.0466579,,	LSTR, 57, 54
CMSEL,S,_Y1	K,55,0.0610888,0.0491398,,	LSTR, 56, 53
AATT, 1, , 1, 0	K,56,0.0465860,0.0247376,,	LSTR, 58, 59
CMSEL,S,_Y	K,57,0.0635566,0.0417081,,	LSTR, 59, 61
CMDELE,_Y	K,58,0.0504334,0.0154492,,	LSTR, 58, 60
CMDELE,_Y1	K,59,0.0744334,0.0154492,,	LSTR, 60, 44
!*	K,60,0.0504334,0.0084492,,	LSTR, 60, 61
!/PNUM,KP,0	K,61,0.0744334,0.0084492,,	LSTR, 61, 62
!/PNUM,LINE,0	K,62,0.0779434,0.0084492,,	! SAVE, Oulton_EM.db,
!/PNUM,AREA,0	K,63,0.0511363,0,,	!*
!/PNUM,VOLU,0	K,64,0.0749114,0,,	LARC,52,67,1,0.0898,
!/PNUM,NODE,0	K,65,0.0784,0,,	!*
!/PNUM,TABN,0	K,66,0.084,0,,	LARC,51,66,1,0.084,
!/PNUM,SVAL,0	K,67,0.0898,0,,	!*
!/NUM,0	! klist,all	LARC,50,55,1,0.0784,
!*	K,43,0.0395149,0.0275660,,	!*
!/PNUM,MAT,1	!/REPLOTT	LARC,55,62,1,0.0784,
!/REPLOT		!*
!*	LSTR, 52, 51	LARC,62,65,1,0.0784,
	LSTR, 51, 50	!*
FLST,5,24,5,ORDE,2	LSTR, 50, 49	LARC,57,59,1,0.0760198,
FITEM,5,1	LSTR, 49, 48	!*
FITEM,5,-24	!	LARC,49,54,1,0.0749114,
CM,_Y,AREA	/ZOOM,1,SCRN,0.570187,0.	!*
ASEL, , , P51X	287750,0.589248,0.116243	LARC,61,64,1,0.0749114,
CM,_Y1,AREA	GLOT	!*
CHKMSH,'AREA'	LSTR, 48, 42	LARC,56,58,1,0.0527466,
CMSEL,S,_Y	!/ZOOM,1,SCRN,-	!*
!*	0.062639,-	LARC,48,53,1,0.0511363,
AMESH,_Y1	0.203902,0.112723,-	!*
!*	0.470690	LARC,60,63,1,0.0511363,
CMDEL,_Y	LSTR, 42, 41	!
CMDEL,_Y1	LSTR, 41, 40	/ZOOM,1,SCRN,0.177530,0.
CMDEL,_Y2	!/AUTO, 1	203902,0.181342,0.158167
!*	!/REP	!/AUTO, 1
! ERASE	LSTR, 67, 66	!/REP
GLOT	LSTR, 66, 65	!*
		LARC,42,43,1,0.04818,

```

!*
LARC,43,44,1,0.04818,
!
/ZOOM,1,SCRN,0.352892,-
0.253448,0.368140,-
0.287750
!/AUTO, 1
!/REP
!*
LARC,44,47,1,0.04818,
!
/ZOOM,1,SCRN,0.158469,0.
184846,0.169906,0.154356
!/AUTO, 1
!/REP
!
/ZOOM,1,SCRN,0.352892,-
0.253448,0.356704,-
0.276316
!/AUTO, 1
!/REP
!*
LARC,41,46,1,0.04806,
!
/ZOOM,1,SCRN,0.166094,0.
181034,0.173718,0.165789
!/AUTO, 1
!/REP
!
/ZOOM,1,SCRN,0.345267,-
0.257260,0.364328,-
0.272505
!/AUTO, 1
!/REP
!*
LARC,40,45,1,0.04794,
! SAVE, Oulton_EM,db,
!
/ZOOM,1,SCRN,0.169906,0.
184846,0.177530,0.165789
FLST,5,2,4,ORDE,2
FITEM,5,68
FITEM,5,-69
CM,_Y,LINE
LSEL, , , P51X
!*
CM,_Y1,LINE
CMSEL,,_Y
LESIZE,_Y1, , ,1,1,
CMDEL,_Y
CMDEL,_Y1
!*
!/AUTO, 1
!/REP
!
/ZOOM,1,SCRN,0.352892,-
0.261071,0.352892,-
0.280127
FLST,5,2,4,ORDE,2
FITEM,5,75
FITEM,5,-76
CM,_Y,LINE
LSEL, , , P51X
!*
CM,_Y1,LINE
CMSEL,,_Y
LESIZE,_Y1, , ,1,1,
CMDEL,_Y
CMDEL,_Y1
!*
!/AUTO, 1
!/REP
!
/ZOOM,1,SCRN,0.208028,0.
150544,0.219464,0.078131
FLST,5,1,4,ORDE,1
FITEM,5,100
CM,_Y,LINE
LSEL, , , P51X
!*
CM,_Y1,LINE
CMSEL,,_Y
LESIZE,_Y1, , ,10,1,
CMDEL,_Y
CMDEL,_Y1
!*
!/AUTO, 1
!/REP
!
/ZOOM,1,SCRN,0.356704,-
0.207713,0.368140,-
0.283938
FLST,5,1,4,ORDE,1
FITEM,5,102
CM,_Y,LINE
LSEL, , , P51X
!*
CM,_Y1,LINE
CMSEL,,_Y
LESIZE,_Y1, , ,10,1,
CMDEL,_Y
CMDEL,_Y1
!*
!/AUTO, 1
!/REP
FLST,5,1,4,ORDE,1
FITEM,5,101
CM,_Y,LINE
LSEL, , , P51X
!*
CM,_Y1,LINE
CMSEL,,_Y
LESIZE,_Y1, , ,25,1,
CMDEL,_Y
CMDEL,_Y1
!*
!/AUTO, 1
!/REP
FLST,2,4,4
FITEM,2,63
FITEM,2,89
LESIZE,_Y1, , ,25,1,
CMDEL,_Y
CMDEL,_Y1
!*
!/AUTO, 1
!/REP
FLST,2,4,4
FITEM,2,63
FITEM,2,89

```

FITEM,2,70	FITEM,2,81	!/DIST, 1,1.371742,1
FITEM,2,90	FITEM,2,78	!/REP,FAST
AL,P51X	FITEM,2,82	!/DIST, 1,1.371742,1
FLST,2,6,4	AL,P51X	!/REP,FAST
FITEM,2,64	FLST,2,4,4	!/DIST, 1,1.371742,1
FITEM,2,91	FITEM,2,78	!/REP,FAST
FITEM,2,92	FITEM,2,95	!/DIST, 1,1.371742,1
FITEM,2,90	FITEM,2,66	!/REP,FAST
FITEM,2,93	FITEM,2,98	!/DIST, 1,1.371742,1
FITEM,2,71	AL,P51X	!/REP,FAST
AL,P51X	FLST,2,6,4	!/DIST, 1,1.371742,1
FLST,2,4,4	FITEM,2,82	!/REP,FAST
FITEM,2,95	FITEM,2,97	!/ZOOM,1,SCRN,-
FITEM,2,65	FITEM,2,85	0.119822,0.497368,-
FITEM,2,91	FITEM,2,86	0.028329,0.302995
FITEM,2,77	FITEM,2,79	FLST,2,6,4
AL,P51X	FITEM,2,101	FITEM,2,68
FLST,2,7,4	AL,P51X	FITEM,2,100
FITEM,2,81	FLST,2,4,4	FITEM,2,75
FITEM,2,77	FITEM,2,86	FITEM,2,102
FITEM,2,92	FITEM,2,99	FITEM,2,101
FITEM,2,72	FITEM,2,74	FITEM,2,103
FITEM,2,96	FITEM,2,102	AL,P51X
FITEM,2,84	AL,P51X	!/AUTO, 1
FITEM,2,94	FLST,2,4,4	!/REP
AL,P51X	FITEM,2,79	!
FLST,2,8,4	FITEM,2,98	/ZOOM,1,SCRN,0.158469,0.
FITEM,2,81	FITEM,2,67	192468,0.177530,0.154356
FITEM,2,77	FITEM,2,100	!/AUTO, 1
FITEM,2,92	AL,P51X	!/REP
FITEM,2,93	! SAVE, Oulton_EM,db,	!
FITEM,2,72	!	/ZOOM,1,SCRN,0.352892,-
FITEM,2,96	/ZOOM,1,SCRN,0.200403,0.	0.257260,0.368140,-
FITEM,2,84	146733,0.246150,0.066697	0.283938
FITEM,2,94	!/DIST, 1,1.371742,1	!/AUTO, 1
AL,P51X	!/REP,FAST	!/REP
FLST,2,4,4	!/DIST, 1,1.371742,1	!
FITEM,2,87	!/REP,FAST	/ZOOM,1,SCRN,0.291896,-
FITEM,2,96	!/DIST, 1,1.371742,1	0.001906,0.337643,-
FITEM,2,73	!/REP,FAST	0.055263
FITEM,2,99	!/DIST, 1,1.371742,1	FLST,2,4,4
AL,P51X	!/REP,FAST	FITEM,2,69
FLST,2,4,4	!/DIST, 1,1.371742,1	FITEM,2,76
FITEM,2,87	!/REP,FAST	FITEM,2,104
FITEM,2,84	!/DIST, 1,1.371742,1	FITEM,2,103
FITEM,2,83	!/REP,FAST	AL,P51X
FITEM,2,85	!/DIST, 1,1.371742,1	!/AUTO, 1
AL,P51X	!/REP,FAST	!/REP
FLST,2,4,4	!	! A PLOT
FITEM,2,83	/ZOOM,1,SCRN,0.208028,-	NUMCMP,ALL
FITEM,2,94	0.554537,0.223277,-	FLST,5,5,5,ORDE,5
FITEM,2,80	0.611706	FITEM,5,28
FITEM,2,97	!/DIST, 1,1.371742,1	FITEM,5,31
AL,P51X	!/REP,FAST	FITEM,5,34
FLST,2,4,4	!/DIST, 1,1.371742,1	FITEM,5,37
FITEM,2,80	!/REP,FAST	FITEM,5,-38

CM,_Y,AREA	UIMP,4,VISC, , , ,	KEYW,ACCEPT,0
ASEL, , ,P51X	UIMP,4,SONC, , , ,	!*
CM,_Y1,AREA	UIMP,4,MURX, , , ,1,	MSHA,0,2D
CMSEL,S,_Y	UIMP,4,MGXX, , , ,	MSHA,1,3D
!*	UIMP,4,RSVX, , , ,	!*
CMSEL,S,_Y1	UIMP,4,PERX, , , ,	MSHKEY,0
AATT, 1, , 1, 0	!*	FLST,5,2,5,ORDE,2
CMSEL,S,_Y	FLST,5,2,5,ORDE,2	FITEM,5,37
CMDELE,_Y	FITEM,5,30	FITEM,5,-38
CMDELE,_Y1	FITEM,5,32	CM,_Y,AREA
!*	CM,_Y,AREA	ASEL, , ,P51X
LSTR, 61, 62	ASEL, , ,P51X	CM,_Y1,AREA
ADELE, 28	CM,_Y1,AREA	CHKMSH,'AREA'
FLST,2,4,4	CMSEL,S,_Y	CMSEL,S,_Y
FITEM,2,88	!*	!*
FITEM,2,93	CMSEL,S,_Y1	AMESH,_Y1
FITEM,2,72	AATT, 4, , 1, 0	!*
FITEM,2,96	CMSEL,S,_Y	CMDEL,_Y
AL,P51X	CMDELE,_Y	CMDEL,_Y1
FLST,2,6,4	CMDELE,_Y1	CMDEL,_Y2
FITEM,2,88	!*	!*
FITEM,2,92	! A PLOT	! /ZOOM,1,SCRN,-
FITEM,2,94	NUMCMP,ALL	0.243277,-0.045652,-
FITEM,2,81	! SAVE, Oulton_EM.db,	0.224250,-0.102717
FITEM,2,77	! /COM,ANSYS RELEASE	! /FOC, 1 ,,-0.300000,,1
FITEM,2,84	5.5 UP19981001.1	! /REP,FAST
AL,P51X	12:43:04 10/26/2000	! /FOC, 1 ,,-0.300000,,1
FLST,5,8,5,ORDE,5	! ERASE	! /REP,FAST
FITEM,5,25	G PLOT	! /FOC, 1 ,,-0.300000,,1
FITEM,5,-29	! /RGB,INDEX,100,100,100,	! /REP,FAST
FITEM,5,33	0	! /FOC, 1 ,,-0.300000,,1
FITEM,5,35	! /RGB,INDEX, 80, 80,	! /REP,FAST
FITEM,5,-36	80,13	! /AUTO, 1
CM,_Y,AREA	! /RGB,INDEX, 60, 60,	! /REP
ASEL, , ,P51X	60,14	! A PLOT
CM,_Y1,AREA	! /RGB,INDEX, 0, 0, 0,15	MSHKEY,0
CMSEL,S,_Y	! /REPLOT	CM,_Y,AREA
!*	!	ASEL, , , , 24
CMSEL,S,_Y1	/ZOOM,1,RECT,0.045926,0.	CM,_Y1,AREA
AATT, 2, , 1, 0	589674,0.970614,-0.327174	CHKMSH,'AREA'
CMSEL,S,_Y	! /VIEW, 1 ,,1	CMSEL,S,_Y
CMDELE,_Y	! /ANG, 1	!*
CMDELE,_Y1	! /REP,FAST	!*
!*	! /VIEW, 1 ,,,1	ACLEAR,_Y1
FLST,5,2,5,ORDE,2	! /ANG, 1	AMESH,_Y1
FITEM,5,30	! /REP,FAST	!*
FITEM,5,32	/PREP7	CMDEL,_Y
CM,_Y,AREA	MOPT,AMESH,DEFA	CMDEL,_Y1
ASEL, , ,P51X	MOPT,QMESH,MAIN	CMDEL,_Y2
CM,_Y1,AREA	MOPT,VMESH,DEFA	!*
CMSEL,S,_Y	MOPT,TIMP,1	MSHKEY,0
!*	MOPT,PYRA,ON	CM,_Y,AREA
!*	MOPT,SPLIT,1	ASEL, , , , 24
UIMP,4,ENTH, , , ,	MSHKEY,0	CM,_Y1,AREA
UIMP,4,HF, , , ,	MSHMID,0	CHKMSH,'AREA'
UIMP,4,QRATE, , , ,	MSHPATTERN,0	CMSEL,S,_Y

```

!*
AMESH,_Y1
!*
CMDEL,_Y
CMDEL,_Y1
CMDEL,_Y2
!*
MSHKEY,0
CM,_Y,AREA
ASEL, , , 16
CM,_Y1,AREA
CHKMSH,'AREA'
CMSEL,S,_Y
!*
!*
ACLEAR,_Y1
AMESH,_Y1
!*
CMDEL,_Y
CMDEL,_Y1
CMDEL,_Y2
!*
MSHKEY,0
FLST,5,4,5,ORDE,4
FITEM,5,7
FITEM,5,10
FITEM,5,13
FITEM,5,19
CM,_Y,AREA
ASEL, , , P51X
CM,_Y1,AREA
CHKMSH,'AREA'
CMSEL,S,_Y
!*
!*
ACLEAR,_Y1
AMESH,_Y1
!*
CMDEL,_Y
CMDEL,_Y1
CMDEL,_Y2
!*
MSHKEY,0
FLST,5,2,5,ORDE,2
FITEM,5,1
FITEM,5,-2
CM,_Y,AREA
ASEL, , , P51X
CM,_Y1,AREA
CHKMSH,'AREA'
CMSEL,S,_Y
!*
!*
ACLEAR,_Y1
AMESH,_Y1
!*
CMDEL,_Y
CMDEL,_Y1
CMDEL,_Y2
!*
MSHKEY,0
FLST,5,3,5,ORDE,2
FITEM,5,3
FITEM,5,-5
CM,_Y,AREA
ASEL, , , P51X
CM,_Y1,AREA
CHKMSH,'AREA'
CMSEL,S,_Y
!*
!*
ACLEAR,_Y1
AMESH,_Y1
!*
CMDEL,_Y
CMDEL,_Y1
CMDEL,_Y2
!*
MSHKEY,0
CM,_Y,AREA
ASEL, , , 1
CM,_Y1,AREA
CHKMSH,'AREA'
CMSEL,S,_Y
!*
!*
ACLEAR,_Y1
AMESH,_Y1
!*
CMDEL,_Y
CMDEL,_Y1
CMDEL,_Y2
!*
MSHKEY,0
CM,_Y,AREA
ASEL, , , 24
CM,_Y1,AREA
CHKMSH,'AREA'
CMSEL,S,_Y
!*
GLOT
MOPT,AMESH,MAIN
MOPT,QMESH,DEFA
MOPT,VMESH,DEFA
MOPT,TIMP,1
MOPT,PYRA,ON
CMDEL,_Y
CMDEL,_Y1
CMDEL,_Y2
!*
MOPT,SPLIT,1
MSHKEY,0
MSHMID,0
MSHPATTERN,0
KEYW,ACCEPT,0
!*
MSHA,1,2D
MSHA,1,3D
!*
MSHKEY,0
FLST,5,5,5,ORDE,2
FITEM,5,1
FITEM,5,-5
CM,_Y,AREA
ASEL, , , P51X
CM,_Y1,AREA
CHKMSH,'AREA'
CMSEL,S,_Y
!*
!*
ACLEAR,_Y1
AMESH,_Y1
!*
CMDEL,_Y
CMDEL,_Y1
CMDEL,_Y2
!*
! ERASE
GLOT
!/REPLOT,RESIZE
/PREP7
FLST,5,4,4,ORDE,4
FITEM,5,81
FITEM,5,-82
FITEM,5,84
FITEM,5,-85
CM,_Y,LINE
LSEL, , , P51X
!*
CM,_Y1,LINE
CMSEL,,_Y
LESIZE,_Y1, , ,2,1,
CMDEL,_Y
CMDEL,_Y1
!*
FLST,5,4,4,ORDE,4
FITEM,5,78
FITEM,5,80
FITEM,5,83
FITEM,5,87
CM,_Y,LINE
LSEL, , , P51X
!*
CM,_Y1,LINE
CMSEL,,_Y

```



```

LESIZE,_Y1,,6,1,
CMDEL,_Y
CMDEL,_Y1
!*
MSHKEY,0
FLST,5,2,5,ORDE,2
FITEM,5,30
FITEM,5,32
CM,_Y,AREA
ASEL,, ,P51X
CM,_Y1,AREA
CHKMSH,'AREA'
CMSEL,S,_Y
!*
AMESH,_Y1
!*
CMDEL,_Y
CMDEL,_Y1
CMDEL,_Y2
!*
MOPT,AMESH,DEFA
MOPT,QMESH,MAIN
MOPT,VMESH,DEFA
MOPT,TIMP,1
MOPT,PYRA,ON
MOPT,SPLIT,1
MSHKEY,0
MSHMID,0
MSHPATTERN,0
KEYW,ACCEPT,0
!*
MSHA,0,2D
MSHA,1,3D
!*
MSHKEY,0
FLST,5,2,5,ORDE,2
FITEM,5,30
FITEM,5,32
CM,_Y,AREA
ASEL,, ,P51X
CM,_Y1,AREA
CHKMSH,'AREA'
CMSEL,S,_Y
!*
!*
ACLEAR,_Y1
AMESH,_Y1
!*
CMDEL,_Y
CMDEL,_Y1
CMDEL,_Y2
!*
GPLOT
!/ZOOM,1,SCRN,-
0.741771,-0.243478,-
0.661859,-0.388043

!/AUTO,1
!/REP
FLST,5,6,4,ORDE,6
FITEM,5,91
FITEM,5,93
FITEM,5,95
FITEM,5,-96
FITEM,5,98
FITEM,5,-99
CM,_Y,LINE
LSEL,, ,P51X
!*
CM,_Y1,LINE
CMSEL,,_Y
LESIZE,_Y1,,3,1,
CMDEL,_Y
CMDEL,_Y1
!*
FLST,5,8,4,ORDE,6
FITEM,5,63
FITEM,5,-65
FITEM,5,70
FITEM,5,-72
FITEM,5,77
FITEM,5,88
CM,_Y,LINE
LSEL,, ,P51X
!*
CM,_Y1,LINE
CMSEL,,_Y
LESIZE,_Y1,,1,1,
CMDEL,_Y
CMDEL,_Y1
!*
MSHKEY,0
FLST,5,4,5,ORDE,3
FITEM,5,27
FITEM,5,-29
FITEM,5,33
CM,_Y,AREA
ASEL,, ,P51X
CM,_Y1,AREA
CHKMSH,'AREA'
CMSEL,S,_Y
!*
AMESH,_Y1
!*
CMDEL,_Y
CMDEL,_Y1
CMDEL,_Y2
!*
GPLOT
FLST,5,2,4,ORDE,2
FITEM,5,66
FITEM,5,73
CM,_Y,LINE

LSEL,, ,P51X
!*
CM,_Y1,LINE
CMSEL,,_Y
!*
CLRMSHLN
LESIZE,_Y1,,6,1,
CMDEL,_Y
CMDEL,_Y1
!*
MSHKEY,0
FLST,5,2,5,ORDE,2
FITEM,5,29
FITEM,5,33
CM,_Y,AREA
ASEL,, ,P51X
CM,_Y1,AREA
CHKMSH,'AREA'
CMSEL,S,_Y
!*
AMESH,_Y1
!*
CMDEL,_Y
CMDEL,_Y1
CMDEL,_Y2
!*
FLST,5,1,4,ORDE,1
FITEM,5,94
CM,_Y,LINE
LSEL,, ,P51X
!*
CM,_Y1,LINE
CMSEL,,_Y
LESIZE,_Y1,,8,1,
CMDEL,_Y
CMDEL,_Y1
!*
FLST,5,1,4,ORDE,1
FITEM,5,92
CM,_Y,LINE
LSEL,, ,P51X
!*
CM,_Y1,LINE
CMSEL,,_Y
LESIZE,_Y1,,10,1,
CMDEL,_Y
CMDEL,_Y1
!*
FLST,5,2,4,ORDE,2
FITEM,5,89
FITEM,5,-90
CM,_Y,LINE
LSEL,, ,P51X
!*
CM,_Y1,LINE

```

CMSEL,,_Y	!/ZOOM,1,SCRN,-	!*
LESIZE,_Y1,,16,1,	0.886372,-0.311957,-	/UI,MESH,OFF
CMDEL,_Y	0.871151,-0.357609	MOPT,AMESH,MAIN
CMDEL,_Y1	!/AUTO, 1	MOPT,QMESH,DEFA
!*	!/REP	MOPT,VMESH,DEFA
MSHKEY,0	GPLOT	MOPT,TIMP,1
FLST,5,3,5,ORDE,3	!/ZOOM,1,SCRN,-	MOPT,PYRA,ON
FITEM,5,25	0.916814,-0.239674,-	MOPT,SPLIT,1
FITEM,5,-26	0.897788,-0.270109	MSHKEY,0
FITEM,5,39	!/AUTO, 1	MSHMID,0
CM,_Y,AREA	!/REP	MSHPATTERN,0
ASEL, , , ,P51X	! SAVE, Oulton_EM,db,	KEYW,ACCEPT,0
CM,_Y1,AREA	MSHKEY,0	!*
CHKMSH,'AREA'	CM,_Y,AREA	MSHA,1,2D
CMSEL,S,_Y	ASEL, , , , 24	MSHA,1,3D
!*	CM,_Y1,AREA	!*
AMESH,_Y1	CHKMSH,'AREA'	MSHKEY,0
!*	CMSEL,S,_Y	CM,_Y,AREA
CMDEL,_Y	!*	ASEL, , , , 31
CMDEL,_Y1	AMESH,_Y1	CM,_Y1,AREA
CMDEL,_Y2	!*	CHKMSH,'AREA'
!*	CMDEL,_Y	CMSEL,S,_Y
FLST,5,1,4,ORDE,1	CMDEL,_Y1	!*
FITEM,5,94	CMDEL,_Y2	!*
CM,_Y,LINE	!*	ACLEAR,_Y1
LSEL, , , ,P51X	!/ZOOM,1,SCRN,-	AMESH,_Y1
!*	0.874956,-0.167391,-	!*
CM,_Y1,LINE	0.840708,-0.220652	CMDEL,_Y
CMSEL,,_Y	! EPLLOT	CMDEL,_Y1
!*	! APLLOT	CMDEL,_Y2
CLRMSHLN	!/AUTO, 1	!*
LESIZE,_Y1, , ,6,1,	!/REP	CM,_Y,AREA
CMDEL,_Y	! EPLLOT	ASEL, , , , 31
CMDEL,_Y1	FLST,5,1,4,ORDE,1	CM,_Y1,AREA
!*	FITEM,5,97	CHKMSH,'AREA'
MSHKEY,0	CM,_Y,LINE	CMSEL,S,_Y
CM,_Y,AREA	LSEL, , , ,P51X	!*
ASEL, , , , 39	!*	!*
CM,_Y1,AREA	CM,_Y1,LINE	ACLEAR,_Y1
CHKMSH,'AREA'	CMSEL,,_Y	MSHKEY,1
CMSEL,S,_Y	LESIZE,_Y1, , ,3,1,	AMESH,_Y1
!*	CMDEL,_Y	MSHKEY,0
AMESH,_Y1	CMDEL,_Y1	!*
!*	!*	CMDEL,_Y
CMDEL,_Y	MSHKEY,0	CMDEL,_Y1
CMDEL,_Y1	CM,_Y,AREA	CMDEL,_Y2
CMDEL,_Y2	ASEL, , , , 31	!*
!*	CM,_Y1,AREA	MSHKEY,0
!	CHKMSH,'AREA'	CM,_Y,AREA
/ZOOM,1,SCRN,0.586279,0.	CMSEL,S,_Y	ASEL, , , , 31
220652,0.601500,0.190217	!*	CM,_Y1,AREA
!/AUTO, 1	AMESH,_Y1	CHKMSH,'AREA'
!/REP	!*	CMSEL,S,_Y
	CMDEL,_Y	!*
	CMDEL,_Y1	AMESH,_Y1
	CMDEL,_Y2	!*

```

CMDEL,_Y
CMDEL,_Y1
CMDEL,_Y2
!*
FLST,5,4,4,ORDE,4
FITEM,5,67
FITEM,5,74
FITEM,5,79
FITEM,5,86
CM,_Y,LINE
LSEL,, , ,P51X
!*
CM,_Y1,LINE
CMSEL,,_Y
LESIZE,_Y1,, ,3,2,
CMDEL,_Y
CMDEL,_Y1
!*
!
/ZOOM,1,SCRN,0.582473,0.
270109,0.590084,0.216848
! LPLOT
FLST,5,1,4,ORDE,1
FITEM,5,67
CM,_Y,LINE
LSEL,, , ,P51X
!*
CM,_Y1,LINE
CMSEL,,_Y
LESIZE,_Y1,, ,3,0,5,
CMDEL,_Y
CMDEL,_Y1
!*
!/AUTO, 1
!/REP
!
/ZOOM,1,SCRN,0.685217,0.
155978,0.700438,0.095109
FLST,5,1,4,ORDE,1
FITEM,5,79
CM,_Y,LINE
LSEL,, , ,P51X
!*
CM,_Y1,LINE
CMSEL,,_Y
LESIZE,_Y1,, ,3,0,5,
CMDEL,_Y
CMDEL,_Y1
!*
!/AUTO, 1
!/REP
FLST,5,2,4,ORDE,2
FITEM,5,74
FITEM,5,86
CM,_Y,LINE
LSEL,, , ,P51X
!*
CM,_Y1,LINE
CMSEL,,_Y
LESIZE,_Y1,, ,3,0,5,
CMDEL,_Y
CMDEL,_Y1
!*
MSHKEY,0
FLST,5,3,5,ORDE,2
FITEM,5,34
FITEM,5,-36
CM,_Y,ARFA
ASEL,, , ,P51X
CM,_Y1,AREA
CHKMSH,'AREA'
CMSEL,S,_Y
!*
AMESH,_Y1
!*
CMDEL,_Y
CMDEL,_Y1
CMDEL,_Y2
!*
!/FOC, 1 ,,-0.300000,,1
!/REP,FAST
!/AUTO, 1
!/REP
!
/ZOOM,1,SCRN,0.833623,-
0.201630,0.841234,-
0.243478
! EPLOTT
!/REP,FAST
CM,_Y,AREA
ASEL,, , , 36
CM,_Y1,AREA
CHKMSH,'AREA'
CMSEL,S,_Y
!*
ACLEAR,_Y1
MSHKEY,1
AMESH,_Y1
MSHKEY,0
!*
CMDEL,_Y
CMDEL,_Y1
CMDEL,_Y2
!*
!/FOC, 1 ,,-0.300000,,1
!/REP,FAST
FLST,2,3,4,ORDE,3
FITEM,2,67
FITEM,2,79
FITEM,2,98
LCCAT,P51X
CM,_Y,AREA
ASEL,, , , 36
CM,_Y1,AREA
CHKMSH,'AREA'
CMSEL,S,_Y
!*
MSHKEY,1
AMESH,_Y1
MSHKEY,0
!*
CMDEL,_Y
CMDEL,_Y1
CMDEL,_Y2
!*
MSHKEY,0
CM,_Y,AREA
ASEL,, , , 36
CM,_Y1,AREA
CHKMSH,'AREA'
CMSEL,S,_Y
!*
AMESH,_Y1
!*
CMDEL,_Y
CMDEL,_Y1
CMDEL,_Y2
!*
!/FOC, 1 ,0.300000,,,1
!/REP,FAST
!/AUTO, 1
!/REP
!
/ZOOM,1,SCRN,0.814597,-
0.258696,0.822207,-
0.346196
!/AUTO, 1
!/REP
CM,_Y,LINE
*SET,_Z1,LSINQR(0,13)
LSEL,R,LCCA
*SET,_Z2,LSINQR(0,13)
LDEL,ALL
*SET,_Z3,_Z1-_Z2
*IF,_Z3,NE,0,THEN
CMSEL,S,_Y
CMDEL,_Y
*ENDIF
!*
CM,_Y,LINE
*SET,_Z1,LSINQR(0,13)
LSEL,R,LCCA
*SET,_Z2,LSINQR(0,13)
LDEL,ALL
*SET,_Z3,_Z1-_Z2
*IF,_Z3,NE,0,THEN
CMSEL,S,_Y
CMDEL,_Y
*ENDIF
!*

```

```

!/ZOOM,1,SCRN,-
0.844514,-0.182609,-
0.829293,-0.224457
!/AUTO, 1
!/REP
FLST,5,4,4,ORDE,4
FITEM,5,23
FITEM,5,30
FITEM,5,37
FITEM,5,43
CM,_Y,LINE
LSEL, , , ,P51X
!*
CM,_Y1,LINE
CMSEL,,_Y
!*
CLRMSHLN
LESIZE,_Y1, , ,3,0.5,
CMDEL,_Y
CMDEL,_Y1
!*
!/ZOOM,1,SCRN,-
0.760797,0.068478,-
0.718939,0.003804
!LPLOT
!/AUTO, 1
!/REP
!/ZOOM,1,SCRN,-
0.859735,-0.327174,-
0.840708,-0.365217
!/AUTO, 1
!/REP
!/ZOOM,1,SCRN,-
0.840708,-0.502174,-
0.806461,-0.544022
!/AUTO, 1
!/REP
!/ZOOM,1,SCRN,-
0.753187,-0.757065,-
0.726550,-0.795109
!/AUTO, 1
!/REP
MSHKEY,0
FLST,5,3,5,ORDE,2
FITEM,5,21
FITEM,5,-23
CM,_Y,AREA
ASEL, , , ,P51X
CM,_Y1,AREA
CHKMSH,'AREA'
CMSEL,S,_Y
!*
AMESH,_Y1
!*
CMDEL,_Y
CMDEL,_Y1

```

```

CMDEL,_Y2
!*
!/ZOOM,1,SCRN,-
0.863540,-0.330978,-
0.836903,-0.391848
!EPLLOT
!/AUTO, 1
!/REP
!/ZOOM,1,SCRN,-
0.852124,-0.334783,-
0.852124,-0.391848
!/AUTO, 1
!/REP
!/ZOOM,1,SCRN,-
0.760797,0.064674,-
0.699912,-0.022826
!/FOC, 1 ,,-0.300000,,1
!/REP,FAST
!/AUTO, 1
!/REP
FLST,5,4,4,ORDE,4
FITEM,5,23
FITEM,5,30
FITEM,5,37
FITEM,5,43
CM,_Y,LINE
LSEL, , , ,P51X
!*
CM,_Y1,LINE
CMSEL,,_Y
!*
CLRMSHLN
LESIZE,_Y1, , ,2,0.5,
CMDEL,_Y
CMDEL,_Y1
!*
FLST,5,4,4,ORDE,4
FITEM,5,67
FITEM,5,74
FITEM,5,79
FITEM,5,86
CM,_Y,LINE
LSEL, , , ,P51X
!*
CM,_Y1,LINE
CMSEL,,_Y
!*
CLRMSHLN
LESIZE,_Y1, , ,2,0.5,
CMDEL,_Y
CMDEL,_Y1
!*
MSHKEY,0
FLST,5,6,5,ORDE,4
FITEM,5,21
FITEM,5,-23

```

```

FITEM,5,34
FITEM,5,-36
CM,_Y,AREA
ASEL, , , ,P51X
CM,_Y1,AREA
CHKMSH,'AREA'
CMSEL,S,_Y
!*
AMESH,_Y1
!*
CMDEL,_Y
CMDEL,_Y1
CMDEL,_Y2
!*
!SAVE, Oulton_EM,db,
MSHKEY,0
CM,_Y,AREA
ASEL, , , , 24
CM,_Y1,AREA
CHKMSH,'AREA'
CMSEL,S,_Y
!*
AMESH,_Y1
!*
CMDEL,_Y
CMDEL,_Y1
CMDEL,_Y2
!*
!/ZOOM,1,SCRN,-
0.886372,-0.330978,-
0.855930,-0.372826
MOPT,AMESH,DEFA
MOPT,QMESH,MAIN
MOPT,VMESH,DEFA
MOPT,TIMP,1
MOPT,PYRA,ON
MOPT,SPLIT,1
MSHKEY,0
MSHMID,0
MSHPATTERN,0
KEYW,ACCEPT,0
!*
MSHA,0,2D
MSHA,1,3D
!*
MSHKEY,0
CM,_Y,AREA
ASEL, , , , 24
CM,_Y1,AREA
CHKMSH,'AREA'
CMSEL,S,_Y
!*
!*
ACLEAR,_Y1
AMESH,_Y1
!*

```

```

CMDEL,_Y
CMDEL,_Y1
CMDEL,_Y2
!*
! EPLOT
! /AUTO, 1
! /REP
FLST,5,1,4,ORDE,1
FITEM,5,62
CM,_Y,LINE
LSEL,, ,P51X
!*
CM,_Y1,LINE
CMSEL,,_Y
LESIZE,_Y1, , ,60,1,
CMDEL,_Y
CMDEL,_Y1
!*
MSHKEY,0
CM,_Y,AREA
ASEL, , , , 24
CM,_Y1,AREA
CHKMSH,'AREA'
CMSEL,S,_Y
!*
AMESH,_Y1
!*
CMDEL,_Y
CMDEL,_Y1
CMDEL,_Y2
!*
! SAVE, Oulton_EM,db,
FLST,5,2,4,ORDE,2
FITEM,5,59
FITEM,5,61
CM,_Y,LINE
LSEL, , , ,P51X
!*
CM,_Y1,LINE
CMSEL,,_Y
!*
CLRMSHLN
LESIZE,_Y1, , ,19,1,
CMDEL,_Y
CMDEL,_Y1
!*
FLST,5,1,4,ORDE,1
FITEM,5,60
CM,_Y,LINE
LSEL, , , ,P51X
!*
CM,_Y1,LINE
CMSEL,,_Y
!*
CLRMSHLN
LESIZE,_Y1, , ,22,1,

```

```

CMDEL,_Y
CMDEL,_Y1
!*
MSHKEY,0
CM,_Y,AREA
ASEL, , , , 24
CM,_Y1,AREA
CHKMSH,'AREA'
CMSEL,S,_Y
!*
AMESH,_Y1
!*
CMDEL,_Y
CMDEL,_Y1
CMDEL,_Y2
!*
MSHKEY,0
CM,_Y,AREA
ASEL, , , , 24
CM,_Y1,AREA
CHKMSH,'AREA'
CMSEL,S,_Y
!*
AMESH,_Y1
!*
CMDEL,_Y
CMDEL,_Y1
CMDEL,_Y2
!*
FLST,5,2,4,ORDE,2
FITEM,5,24
FITEM,5,31
CM,_Y,LINE
LSEL, , , ,P51X
!*
CM,_Y1,LINE
CMSEL,,_Y
LESIZE,_Y1, , ,1,1,
CMDEL,_Y
CMDEL,_Y1
!*
!*
MSHKEY,0
CM,_Y,AREA
ASEL, , , , 24
CM,_Y1,AREA
CHKMSH,'AREA'
CMSEL,S,_Y
!*
AMESH,_Y1
!*
CMDEL,_Y
CMDEL,_Y1
CMDEL,_Y2
!*
/UI,MESH,OFF

```

```

MOPT,AMESH,DEFA
MOPT,QMESH,DEFA
MOPT,VMESH,DEFA
MOPT,TIMP,1
MOPT,PYRA,ON
MOPT,SPLIT,1
MSHKEY,0
MSHMID,0
MSHPATTERN,0
KEYW,ACCEPT,0
!*
MSHA,0,2D
MSHA,1,3D
!*
MSHKEY,0
MSHAPE,1,3d
MSHKEY,0
CM,_Y,AREA
ASEL, , , , 24
CM,_Y1,AREA
CHKMSH,'AREA'
CMSEL,S,_Y
!*
AMESH,_Y1
!*
CMDEL,_Y
CMDEL,_Y1
CMDEL,_Y2
!*
! /ZOOM,1,SCRN,-
0.882567,-0.319565,-
0.852124,-0.350000
! /AUTO, 1
! /REP
GPLOT
! /ZOOM,1,SCRN,-
0.905399,-0.228261,-
0.897788,-0.273913
! /FOC, 1, 0.300000,,,1
! /REP,FAST
! /AUTO, 1
! /REP
MOPT,AMESH,MAIN
MOPT,QMESH,DEFA
MOPT,VMESH,DEFA
MOPT,TIMP,1
MOPT,PYRA,ON
MOPT,SPLIT,1
MSHKEY,0
MSHMID,0
MSHPATTERN,0
KEYW,ACCEPT,0
!*
MSHA,1,2D
MSHA,1,3D
!*

```

```

MSHKEY,0
FLST,5,3,5,ORDE,2
FITEM,5,21
FITEM,5,-23
CM,_Y,AREA
ASEL,, , ,P51X
CM,_Y1,AREA
CHKMSH,'AREA'
CMSEL,S,_Y
!*
AMESH,_Y1
!*
CMDEL,_Y
CMDEL,_Y1
CMDEL,_Y2
!*
!/ZOOM,1,SCRN,-
0.863540,-0.350000,-
0.840708,-0.422283
!/AUTO, 1
!/REP
!/ZOOM,1,SCRN,-
0.821682,-0.038043,-
0.795045,-0.098913
!/AUTO, 1
!/REP

! APLOT
! EPLT
/PREP7
FLST,3,15,5,ORDE,2
FITEM,3,25
FITEM,3,-39
AGEN, ,P51X, , ,0.1, , , ,1
!/REPLT
CSYS,1
FLST,3,24,5,ORDE,2
FITEM,3,1
FITEM,3,-24
CSYS,1
AGEN,6,P51X, , ,0.60, , ,0
! EPLT

! ERASE
! APLOT
! EPLT
FLST,5,2568,2,ORDE,16
FITEM,5,75
FITEM,5,-83
FITEM,5,100
FITEM,5,-119
FITEM,5,136
FITEM,5,-159
FITEM,5,176
FITEM,5,-203
FITEM,5,220

FITEM,5,-251
FITEM,5,268
FITEM,5,-284
FITEM,5,633
FITEM,5,-736
FITEM,5,1144
FITEM,5,-3477
ESEL,S, , ,P51X
CM,rotor,ELEM
/PREP7
FLST,3,144,5,ORDE,4
FITEM,3,1
FITEM,3,-24
FITEM,3,40
FITEM,3,-159
CSYS,0
AGEN, ,P51X, , , -0.2, , , ,1
!/REPLT
ALLSEL,ALL
!/REPLT
! SAVE, temp, ,
FLST,3,15,5,ORDE,2
FITEM,3,25
FITEM,3,-39
AGEN, ,P51X, , , -0.1, , , ,1
!/REPLT
! SAVE, temp,db,
CSYS,1
FLST,3,15,5,ORDE,2
FITEM,3,25
FITEM,3,-39
AGEN,8,P51X, , ,0.45, , ,0
!/REPLT
! EPLT

NUMMRG,ALL,1e-005, ,
FLST,5,2904,2,ORDE,8
FITEM,5,543
FITEM,5,-632
FITEM,5,737
FITEM,5,-901
FITEM,5,1036
FITEM,5,-1143
FITEM,5,3478
FITEM,5,-6018
ESEL,S, , ,P51X
CM,stator,ELEM

! EPLT
ALLSEL,ALL
!/REPLT
CMSEL,S,ROTOR
!/REPLT
CMPL
GPLOT
ALLSEL,ALL

!/REPLT
FLST,5,144,5,ORDE,4
FITEM,5,1
FITEM,5,-24
FITEM,5,40
FITEM,5,-159
ASEL,S, , ,P51X
!/REPLT
! APLOT
CM,rotor,AREA
ALLSEL,ALL
!/REPLT
FLST,5,120,5,ORDE,4
FITEM,5,25
FITEM,5,-39
FITEM,5,160
FITEM,5,-264
ASEL,S, , ,P51X
!/REPLT
CM,stator,AREA
ALLSEL,ALL
!/REPLT

! APLOT
/PREP7
!*
UIMP,1,ENTH, , , ,
UIMP,1,HF, , , ,
UIMP,1,QRATE, , , ,
UIMP,1,VISC, , , ,
UIMP,1,SONC, , , ,
UIMP,1,MURX, , , ,1,
UIMP,1,MGXX, , , ,
UIMP,1,RSVX, , , ,
UIMP,1,PERX, , , ,
!*
*SET,N,87
*SET,I,0.024
*SET,b,0.0069999
*SET,a,I*b

! APLOT
ESLA,S
FLST,5,64,5,ORDE,40
FITEM,5,25
FITEM,5,-29
FITEM,5,33
FITEM,5,35
FITEM,5,-36
FITEM,5,160
FITEM,5,-164
FITEM,5,168
FITEM,5,170
FITEM,5,-171
FITEM,5,175
FITEM,5,-179

```

```

FITEM,5,183
FITEM,5,185
FITEM,5,-186
FITEM,5,190
FITEM,5,-194
FITEM,5,198
FITEM,5,200
FITEM,5,-201
FITEM,5,205
FITEM,5,-209
FITEM,5,213
FITEM,5,215
FITEM,5,-216
FITEM,5,220
FITEM,5,-224
FITEM,5,228
FITEM,5,230
FITEM,5,-231
FITEM,5,235
FITEM,5,-239
FITEM,5,243
FITEM,5,245
FITEM,5,-246
FITEM,5,250
FITEM,5,-254
FITEM,5,258
FITEM,5,260
FITEM,5,-261
ASEL,S,,P51X
!/REPLOT
ESLA,S
ESEL,ALL
ESLA,S
CM,force,ELEM
CMPLOT,FORCE
ALLSEL,ALL
! EPLOT

! APLOT
CMSEL,S,ROTOR
!/REPLOT
/PREP7
FLST,3,144,5,ORDE,4
FITEM,3,1
FITEM,3,-24
FITEM,3,40

```

```

FITEM,3,-159
CSYS,0
AGEN,,P51X,,0.2,,,,,1
!/REPLOT
ALLSEL,ALL
!/REPLOT
!*
UIMP,1,ENTH,,,,
UIMP,1,HF,,,,
UIMP,1,QRATE,,,,
UIMP,1,VISC,,,,
UIMP,1,SONC,,,,
UIMP,1,MURX,,1,
UIMP,1,MGXX,,,,
UIMP,1,RSVX,,,,
UIMP,1,PERX,,,,
!*
NUMCMP,ALL
FLST,2,8,4,ORDE,8
FITEM,2,89
FITEM,2,345
FITEM,2,380
FITEM,2,415
FITEM,2,450
FITEM,2,485
FITEM,2,520
FITEM,2,554
DL,P51X,,AZ,0,
!*
!*
FMAGBC,'FORCE'
! APLOT

! APLOT
/SOLU
FINISH
/POST1
!*
RSYS,1
! AVRES,2
AVPRIN,0
!*
FINISH
/SOLU
FINISH

```

```

/PREP7
!*
UIMP,1,ENTH,,,,
UIMP,1,HF,,,,
UIMP,1,QRATE,,,,
UIMP,1,VISC,,,,
UIMP,1,SONC,,,,
UIMP,1,MURX,,1,
UIMP,1,MGXX,,,,
UIMP,1,RSVX,,,,
UIMP,1,PERX,,,,
!*
!*
UIMP,1,ENTH,,,,
UIMP,1,HF,,,,
UIMP,1,QRATE,,,,
UIMP,1,VISC,,,,
UIMP,1,SONC,,,,
UIMP,1,MURX,,1,
UIMP,1,MGXX,,,,
UIMP,1,RSVX,,,,
UIMP,1,PERX,,,,
!*
!*
! MPLIST,ALL,,,EVLТ
!*
MPDELE,ALL,1,1,1,
!*
UIMP,1,ENTH,,,,
UIMP,1,HF,,,,
UIMP,1,QRATE,,,,
UIMP,1,VISC,,,,
UIMP,1,SONC,,,,
UIMP,1,MURX,,1,
UIMP,1,MGXX,,,,
UIMP,1,RSVX,,,,
UIMP,1,PERX,,,,
!*

CSYS,1
! APLOT
! SAVE,

LGWRITE,oulton_EM,lgw.,
COMMENT

```

## Appendix C Moment of Inertia Calculation for the 8/6 SRM Rotor

The moment of inertia  $J$  of the 8/6 SRM rotor is composed of three parts:  $J_1$  of the rotor shaft,  $J_2$  of the rotor core lamination (hollow cylinder part) and  $J_3$  of six rotor poles, as shown in Fig.C.1. The dimensions and material properties of the rotor are listed in Appendix A.

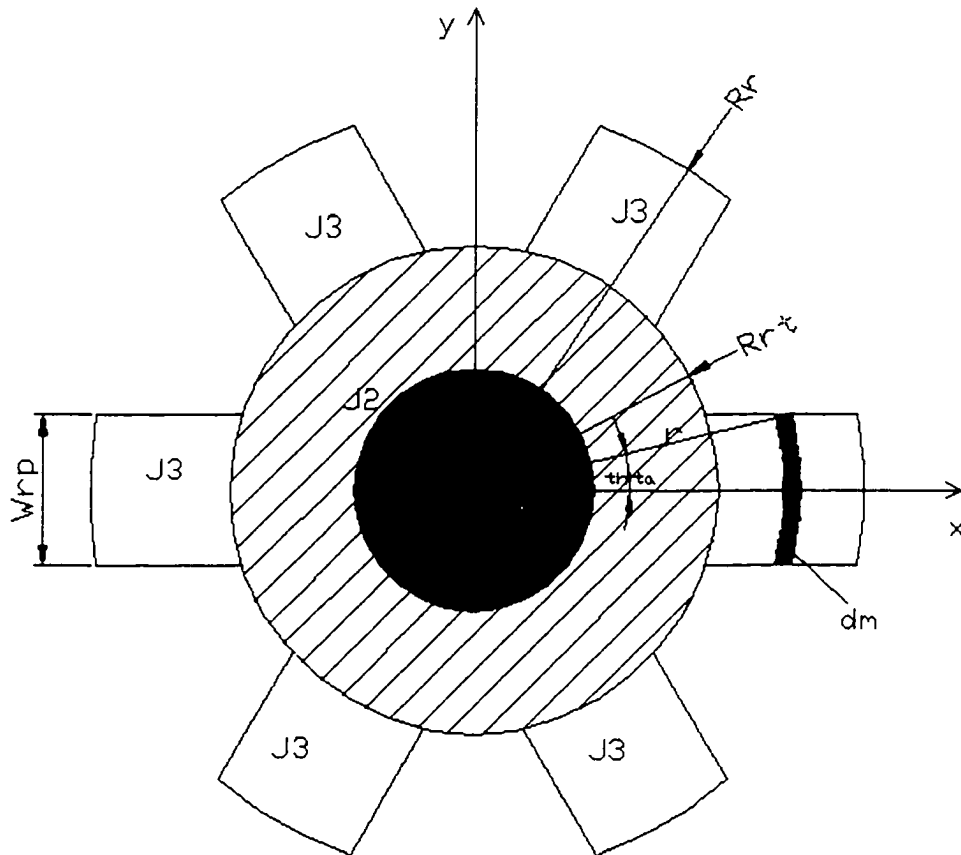


Fig.C.1 Moment of Inertia Calculation

$$J = J_1 + J_2 + J_3 \quad (C-1)$$

$$J_1 = \frac{1}{2} M_1 R_{sh}^2 = \frac{1}{2} \rho_{Fe} (\pi R_{sh}^2 L_{sh}) R_{sh}^2 = 0.00022639 (kg \cdot m^2) \quad (C-2)$$



$$J_2 = \frac{1}{2} \rho_{Fe} \pi L_{st} (R_{ri}^4 - R_{sh}^4) = 0.01458378 (\text{kg} \cdot \text{m}^2) \quad (\text{C-3})$$

$$\begin{aligned}
J_3 &= 6 \int_{R_n}^{R_r} r^2 dm \\
&= 6 \int_{R_n}^{R_r} r^2 \rho_{Fe} dV \\
&= 6 \int_{R_n}^{R_r} r^2 \rho_{Fe} L_{st} dS \\
&= 6 \rho_{Fe} L_{st} \int_{R_n}^{R_r} r^2 dS \\
&= 6 \rho_{Fe} L_{st} \int_{R_n}^{R_r} r^2 \cdot \pi [(r + dr)^2 - r^2] \frac{2\theta}{2\pi} \\
&= 6 \rho_{Fe} L_{st} \int_{R_n}^{R_r} r^2 \cdot 2r dr \cdot \theta \\
&= 12 \rho_{Fe} L_{st} \int_{R_n}^{R_r} r^3 \cdot \sin^{-1} \left( \frac{W_{rp}}{2r} \right) dr \\
&= 12 \rho_{Fe} L_{st} \cdot \left\{ \frac{1}{16} W_{rp}^4 \left[ 4 \frac{r^4 \sin^{-1} \left( \frac{W_{rp}}{2r} \right)}{W_{rp}^4} + \frac{2}{3} \frac{r^3 \sqrt{1 - \frac{W_{rp}^2}{4r^2}}}{W_{rp}^3} + \frac{1}{3} \frac{\sqrt{1 - \frac{W_{rp}^2}{4r^2}}}{W_{rp}} \right] \right\} \Bigg|_{r=R_n}^{r=R_r} \\
&= 0.003535 (\text{kg} \cdot \text{m}^2)
\end{aligned} \quad (\text{C-3})$$

$$J = J_1 + J_2 + J_3 = 0.00522 (\text{kg} \cdot \text{m}^2) \quad (\text{C-4})$$

## Appendix D Phase Winding Resistance Measurement for the 8/6 SRM

Resistance of the phase winding of the 8/6 Oulton SRM is measured. DC voltages are applied on the phase windings from terminals 1~2 (Phase A and B), 2~3 (Phase B and C), 3~4 (Phase C and D) and 4~1 (Phase D and A). Dc currents are recorded and average resistance of each two phase windings are calculated. They are shown in Table D.1.

Table D.1 Measurement of Phase Winding Resistance

1~2			3~4		
voltage(V)	current(A)	resistance(ohm)	voltage(V)	current(A)	resistance(ohm)
6.98	4.75	1.469474	7.16	4.81	1.488565
13.26	9	1.473333	10.17	6.83	1.489019
22.24	14.91	1.491616	14.94	10	1.494
29.2	19.2	1.520833	22.83	15	1.522
10.1	6.59	1.532625	30.33	19.67	1.541942
	average	1.497576		average	1.507105
2~3			4~1		
voltage(V)	current(A)	resistance(ohm)	voltage(V)	current(A)	resistance(ohm)
7.18	4.99	1.438878	7.8	5.36	1.455224
10.02	6.97	1.43759	10.12	6.95	1.456115
14.16	9.8	1.444898	14.87	10.18	1.460707
22.16	15.21	1.456936	21.99	14.92	1.473861
29.77	19.75	1.507342	29.13	19.45	1.497686
	average	1.457129		average	1.468719

The resistance of each phase winding is  $R=0.741316(\Omega)$ .

## Appendix E Matlab Code Used in SRM Operation Simulation Model

Code for main simulation model, including initialization of parameters.

```
% run this program to begin the transient simulation

close all;
clear all;

% Initialization

global angle_fire angle_extin I_base

V_dclink = 250; % volts, DC-link voltage
R = 0.741; % ohm, phase resistance
J = 0.00522; % kg*m^2, rotor inertia
Tl = 0.0; % N*m, no-load torque
f = 0.008; % friction ratio

% current band
I_base = 7;

angle_fire = 7; % firing angle
angle_extin = 22.5; % extinguishing angle

% data transformation for look-up tables

transform;

% run simulation

sim('current_sim');
```

Code for “Matlab Function angle\_B”

```
function thita_B = f(u)

% angle_B

% define variables based on input vector u of width 1

thita_B = u(1);

thita_B = thita_B - 15;

if thita_B < 0

    thita_B = thita_B + 60;

end
```

### Code for “Matlab Function switch\_B”

```
function V_applied = f(u)

% switch_B

global angle_fire angle_extin I_base I_band

% define variables based on input vector u of width 3

I_phase = u(1);
V_dclink = u(2);
angle_B = u(3);
V_applied = 0;

if I_phase >= I_base

    V_applied = - V_dclink;

else

    if (angle_B >= angle_fire) & (angle_B <= angle_extin)

        V_applied = V_dclink;

    else

        if angle_B >= angle_extin

            V_applied = -V_dclink;

        end

    end

end

if I_phase < 0

    V_applied = 0;

end
```

## Appendix F Equivalent Mass Density Calculation: Matlab Code

```
% This program is used for the calculation of equivalent density of the tooth for
% Delphi Square Motor, which will be used in FE analysis of stator resonant frequency

clear all;

L_stack = 0.046 % length of the pole (same as stator stack length)
H_pole = 0.0289-0.0182 % height of the pole
W_pole = 0.0182*sin((45-36.5)/180*pi)*2 % width of the pole
V_pole = L_stack * H_pole * W_pole % volume of the pole

density_steel = 7.8*1000 % density of steel
f_stack = 0.935 % stacking factor of stator lamination
% generally it is 0.92~0.95
m_pole = density_steel * f_stack * V_pole % mass of one pole

N_turn = 44 % number of turns of winding per pole
density_copper = 8.9*1000 % density of copper
length_copper = 0.056

R_oh = 0.01 % radius of winding overhang
L_copper = 0.056 % length of copper
L_turn = 2 * pi * R_oh + 2 * L_copper % length of each turn
D_barewire = 0.0008 % bare wire diameter of A.W.G. 18 copper wire
% with wire diameter of 1.024mm

A_turn = pi * (D_barewire/2)^2

m_turn = density_copper * L_turn * A_turn % mass of each turn

m_coil = N_turn * m_turn % mass of the coil

M_e = m_pole + m_coil % equivalent mass per pole

Density_e = (m_pole + m_coil)/V_pole % equivalent density for the pole
```

## Appendix G ANSYS Code for Resonant Frequency Determination

The ANSYS program for resonant frequency determination of the square motor (stator with windings) is listed as follows.

```

/BATCH
!/COM,ANSYS RELEASE
5.7 UP20001208
21:06:49 06/03/2002
/FILNAME,GM_Square,0
/TITLE,GM Square Motor
Vibration Analysis with
Windings
!*
/NOPR
/PMETH,OFF,0
KEYW,PR_SET,1
KEYW,PR_STRUC,1
KEYW,PR_THERM,0
KEYW,PR_FLUID,0
KEYW,PR_ELMAG,0
KEYW,MAGNOD,0
KEYW,MAGEDG,0
KEYW,MAGHFE,0
KEYW,MAGELC,0
KEYW,PR_MULTI,0
KEYW,PR_CFD,0
/GO
!*
!/COM,
!/COM,Preferences for GUI
filtering have been set to
display:
!/COM, Structural
!*
CSYS,1
DSYS,1
/REP7
!*
ET,1,PLANE42
!*
ET,2,SOLID45
!*
MPTEMP,,,,,,,,
MPTEMP,1,0
MPDATA,DENS,1,,14000
MPTEMP,,,,,,,,
MPTEMP,1,0
MPDE,EX,1
MPDE,EY,1
MPDE,EZ,1
MPDE,NUXY,1
MPDE,NUYZ,1
MPDE,NUXZ,1
MPDE,PRXY,1
MPDE,PRYZ,1
MPDE,PRXZ,1
MPDE,GXY,1
MPDE,GYZ,1
MPDE,GXZ,1
MPDATA,EX,1,,2.07e+11
MPDATA,PRXY,1,,0.3
!*CSET,1,2, 1,2,
MPCOPY,,1,2
TBCOPY,ALL,1,2
!*
MPTEMP,,,,,,,,
MPTEMP,1,0
MPDE,DENS,2
MPDATA,DENS,2,,78000
K,1,0,0,,
K,2,0.030,0,,
K,3,0.0345,0,,
K,2,0.03,0,,
K,4,0.0182,6.5,,
K,5,0.0182,23.5,,
K,6,0.0182,36.5,,
K,7,0.0182,45,,
K,8,0.029,45,,
K,9,0.04879,45,,
DSYS,1
!/REPLOTT
DSYS,1
!/REPLOTT
DSYS,0
!/REPLOTT
K,10,0.02889,39.657,,
K,11,0.02889,28.343,,
K,12,0.02889,9.657,,
K,12,0.03,7.6891,,
K,13,0.03,7.6891,,
K,12,0.02889,9.657,,
K,14,0.03,22.311,,
K,15,0.03,30,,
K,16,0.03,37.689,,
K,17,0.03984,30,,
! klist,all,,coord
DSYS,1
! klist,all,,coord
K,11,0.02889,20.343,,
DSYS,0
!/REPLOTT
LSTR, 7, 8
LSTR, 8, 9
LSTR, 9, 17
LSTR, 17, 3
LSTR, 3, 2
LSTR, 4, 12
LSTR, 5, 11
LSTR, 6, 10
LSTR, 8, 10
LSTR, 11, 12
LSTR, 15, 17
!*
LARC,7,6,1,0.0182,
!*
LARC,5,4,1,0.0182,
!*
LARC,16,15,1,0.03,
!*
LARC,15,14,1,0.03,
!*
LARC,13,2,1,0.03,
FLST,3,2,3
FITEM,3,10
FITEM,3,16
BSPLIN, ,P51X
FLST,3,2,3
FITEM,3,14
FITEM,3,11
BSPLIN, ,P51X
FLST,3,2,3
FITEM,3,12
FITEM,3,13
BSPLIN, ,P51X

```

FLST,2,4,4	CMDELE,_Y1	CM,_Y1,LINE
FITEM,2,1	!*	CMSEL,,_Y
FITEM,2,8	! /PNUM,KP,0	!*
FITEM,2,9	! /PNUM,LINE,0	LESIZE,_Y1,, ,4, , , , ,1
FITEM,2,12	! /PNUM,AREA,0	!*
AL,P51X	! /PNUM,VOLU,0	FLST,5,2,4,ORDE,2
FLST,2,4,4	! /PNUM,NODE,0	FITEM,5,2
FITEM,2,7	! /PNUM,TABN,0	FITEM,5,-3
FITEM,2,10	! /PNUM,SV AL,0	CM,_Y,LINE
FITEM,2,6	! /NUMBER,0	LSEL, , , ,P51X
FITEM,2,13	!*	CM,_Y1,LINE
AL,P51X	! /PNUM,MAT,1	CMSEL,,_Y
FLST,2,6,4		!*
FITEM,2,2	!*	LESIZE,_Y1,, ,5, , , , ,1
FITEM,2,3	! APLOT	!*
FITEM,2,11		FLST,5,1,4,ORDE,1
FITEM,2,14	!*	FITEM,5,4
FITEM,2,17	FLST,5,5,4,ORDE,4	CM,_Y,LINE
FITEM,2,9	FITEM,5,9	LSEL, , , ,P51X
AL,P51X	FITEM,5,12	CM,_Y1,LINE
FLST,2,8,4	FITEM,5,14	CMSEL,,_Y
FITEM,2,11	FITEM,5,-16	!*
FITEM,2,4	CM,_Y,LINE	LESIZE,_Y1,, ,9, , , , ,1
FITEM,2,15	LSEL, , , ,P51X	!*
FITEM,2,10	CM,_Y1,LINE	
FITEM,2,18	CMSEL,,_Y	/PREP7
FITEM,2,19	!*	MSHKEY,0
FITEM,2,16	LESIZE,_Y1,, ,2, , , , ,1	FLST,5,2,5,ORDE,2
FITEM,2,5	!*	FITEM,5,1
AL,P51X	FLST,5,2,4,ORDE,2	FITEM,5,-2
FLST,5,2,5,ORDE,2	FITEM,5,10	CM,_Y,AREA
FITEM,5,1	FITEM,5,13	ASEL, , , ,P51X
FITEM,5,-2	CM,_Y,LINE	CM,_Y1,AREA
CM,_Y,AREA	LSEL, , , ,P51X	CHKMSH,'AREA'
ASEL, , , ,P51X	CM,_Y1,LINE	CMSEL,S,_Y
CM,_Y1,AREA	CMSEL,,_Y	!*
CMSEL,S,_Y	!*	AMESH,_Y1
!*	LESIZE,_Y1,, ,3, , , , ,1	!*
CMSEL,S,_Y1	!*	CMDELE,_Y
AATT, 1, , 1, 0	FLST,5,3,4,ORDE,2	CMDELE,_Y1
CMSEL,S,_Y	FITEM,5,17	CMDELE,_Y2
CMDELE,_Y	FITEM,5,-19	!*
CMDELE,_Y1	CM,_Y,LINE	GPlot
!*	LSEL, , , ,P51X	
FLST,5,2,5,ORDE,2	CM,_Y1,LINE	FLST,2,5,4,ORDE,5
FITEM,5,3	CMSEL,,_Y	FITEM,2,10
FITEM,5,-4	!*	FITEM,2,15
CM,_Y,AREA	LESIZE,_Y1,, ,1, , , , ,1	FITEM,2,-16
ASEL, , , ,P51X	!*	FITEM,2,18
CM,_Y1,AREA	FLST,5,6,4,ORDE,4	FITEM,2,-19
CMSEL,S,_Y	FITEM,5,1	LCCAT,P51X
!*	FITEM,5,5	MSHKEY,0
CMSEL,S,_Y1	FITEM,5,-8	CM,_Y,AREA
AATT, 2, , 1, 0	FITEM,5,11	ASEL, , , , 4
CMSEL,S,_Y	CM,_Y,LINE	CM,_Y1,AREA
CMDELE,_Y	LSEL, , , ,P51X	CHKMSH,'AREA'

```

CMSEL,S,_Y
!*
AMESH,_Y1
!*
CMDELE,_Y
CMDELE,_Y1
CMDELE,_Y2
!*
GPLOT

MOPT,AMESH,ALT2
MOPT,QMESH,MAIN
MOPT,VMESH,ALTE
MOPT,TIMP,1
MOPT,PYRA,ON
MOPT,SPLIT,1
MSHKEY,0
MSHMID,0
MSHPATTERN,0
KEYW,ACCEPT,0
!*
MSHAPE,0,2D
MSHAPE,1,3D
!*
FLST,5,1,4,ORDE,1
FITEM,5,2
CM,_Y,LINE
LSEL,, , ,P51X
CM,_Y1,LINE
CMSEL,,_Y
!*
LESIZE,_Y1, , ,6, , , , ,1
!*
MSHKEY,0
CM,_Y,AREA
ASEL, , , , 3
CM,_Y1,AREA
CHKMSH,'AREA'
CMSEL,S,_Y
!*
AMESH,_Y1
!*
CMDELE,_Y
CMDELE,_Y1
CMDELE,_Y2
!*
FLST,2,3,4,ORDE,3
FITEM,2,9
FITEM,2,14
FITEM,2,17
LCCAT,P51X
MSHKEY,0
MSHAPE,1,3d
MSHKEY,0
CM,_Y,AREA
ASEL, , , , 3

```

```

CM,_Y1,AREA
CHKMSH,'AREA'
CMSEL,S,_Y
!*
ACLEAR,_Y1
AMESH,_Y1
!*
CMDELE,_Y
CMDELE,_Y1
CMDELE,_Y2
!*
NUMCMP,ALL

FLST,3,4,5,ORDE,2
FITEM,3,1
FITEM,3,-4
AGEN,2,P51X, , ,0,45, , ,0
CSYS,0
FLST,3,4,5,ORDE,2
FITEM,3,5
FITEM,3,-8
ARSYM,X,P51X, , , ,0,0
CSYS,1
FLST,2,4,5,ORDE,2
FITEM,2,1
FITEM,2,-4
ADELE,P51X, , ,1
FLST,2,4,5,ORDE,2
FITEM,2,1
ACLEAR,P51X
FLST,2,4,5,ORDE,2
FITEM,2,1
ADELE,P51X, , ,1

GPLOT
FLST,2,6,4,ORDE,2
FITEM,2,14
FITEM,2,-19
LDELE,P51X, , ,1
FLST,3,8,5,ORDE,2
FITEM,3,5
FITEM,3,-12
AGEN, ,P51X, , , ,0,45, , , ,1
GPLOT
FLST,3,8,5,ORDE,2
FITEM,3,5
FITEM,3,-12
ARSYM,X,P51X, , , ,0,0
CSYS,0
FLST,3,8,5,ORDE,2
FITEM,3,5
FITEM,3,-12
ARSYM,X,P51X, , , ,0,0

```

```

FLST,3,16,5,ORDE,2
FITEM,3,1
FITEM,3,-16
ARSYM,Y,P51X, , , ,0,0
GPLOT
NUMMRG,ALL,0.000001, ,
,LOW
NUMCMP,ALL

FINISH
/SOLU
!*
ANTYPE,2
!*
MODEOPT,LANB,50
EQSLV,SPAR
MXPAND,50, , ,0
LUMPM,0
PSTRES,0
!*
MODEOPT,LANB,50,20,2200
0, ,OFF, , ,2

! /PNUM,KP,0
! /PNUM,LINE,0
! /PNUM,AREA,0
! /PNUM,VOLU,0
! /PNUM,NODE,0
! /PNUM,TABN,0
! /PNUM,SV,0
! /NUMBER,1
!*
! /PNUM,MAT,1
! /REPLOT
!*
! APLOT

! /RGB,INDEX,100,100,100,
0
! /RGB,INDEX, 80, 80,
80,13
! /RGB,INDEX, 60, 60,
60,14
! /RGB,INDEX, 0, 0, 0,15
! /REPLOT

MOPT,AMESH,DEFA
MOPT,QMESH,DEFA
MOPT,VMESH,DEFA
MOPT,TIMP,1
MOPT,PYRA,ON
MOPT,SPLIT,1
MSHKEY,0
MSHMID,0

```



```

MSHPATTERN,0
KEYW,ACCEPT,0
!*
MSHAPE,0,2D
MSHAPE,1,3D
!*

TYPE, 2
EXTOPT,ESIZE,10,0,
EXTOPT,ACLEAR,0
!*
EXTOPT,ATTR,1,1,1
!*
FLST,2,32,5,ORDE,2
FITEM,2,1
FITEM,2,-32
CSYS,0
VEXT,P51X, , ,0,0,0.0456,,,
!/VIEW, 1 ,1,2,3
!/ANG, 1
!/REP,FAST

NUMMRG,ALL,1e-006, ,
,LOW

```

```

NUMCMP,ALL

/PREP7
MPTEMP,,,,,,,,
MPTEMP,1,0
MPDE,EX,1
MPDE,EY,1
MPDE,EZ,1
MPDE,NUXY,1
MPDE,NUYZ,1
MPDE,NUXZ,1
MPDE,PRXY,1
MPDE,PRYZ,1
MPDE,PRXZ,1
MPDE,GXY,1
MPDE,GYZ,1
MPDE,GXZ,1
MPDATA,EX,1,,1.513E+011
MPDATA,PRXY,1,,0.3
MPTEMP,,,,,,,,
MPTEMP,1,0
MPDE,EX,2
MPDE,EY,2
MPDE,EZ,2

```

```

MPDE,NUXY,2
MPDE,NUYZ,2
MPDE,NUXZ,2
MPDE,PRXY,2
MPDE,PRYZ,2
MPDE,PRXZ,2
MPDE,GXY,2
MPDE,GYZ,2
MPDE,GXZ,2
MPDATA,EX,2,,1.513E+011
MPDATA,PRXY,2,,0.3
! SAVE, GM_Square_3D.db.
!/COM,ANSYS RELEASE
5.7 UP20001208
23:06:29 08/05/2002
/SOLU
!/STATUS,SOLU
SOLVE
!
LGWRITE,GM_Square,lgw.,
COMMENT

```